# DYNAMICAL MEAN FIELD THEORIES AND THE ANDERSON LOCALIZATION

#### BY SERGEY PANKOV

A dissertation submitted to the
Graduate School—New Brunswick
Rutgers, The State University of New Jersey
in partial fulfillment of the requirements
for the degree of
Doctor of Philosophy
Graduate Program in Physics and Astronomy
Written under the direction of
Professor Gabriel Kotliar
and approved by

New Brunswick, New Jersey
October, 2003

ABSTRACT OF THE DISSERTATION

Dynamical Mean Field theories and the

**Anderson Localization** 

by Sergey Pankov

Dissertation Director: Professor Gabriel Kotliar

We investigate extended dynamical mean field theory (EDMFT) of the interacting

Bose-Fermi system using quasiclassical approximation on the impurity solver. We

compare semiclassical results to the exact Quantum Monte Carlo (QMC) solution

and find a good agreement in a range of parameters. Taking the classical limit we

prove that the transition to the ordered phase is of the first order in any dimension

below four. Using the functional formulation of EDMFT we derive a criterion for

the instability of the disordered phase.

We explain how DMFT and extended DMFT approximations can be formu-

lated in the parquet equation language. A natural extension, based on the parquet

formalism, is proposed to incorporate nonlocal particle particle and particle hole

fluctuations.

We also revisited Anderson localization problem and clarified few unclear as-

pects.

ii

# Acknowledgements

I am grateful to Prof. Gabi Kotliar for his guidance and support throughout the years of my graduate study. I am indebted to him for sharing with me his invaluable experience. I cannot overstate his role in my decision to continue to pursue the career of a physicist. It was a pleasure and privilege to work with him.

Special thanks to Vlad Dobrosavljevic, working and discussing physics with him was a truly exciting experience. I am also thankful to him for his thorough and critical reading of my dissertation.

I thank Antoine Georges and Serge Florens. I enjoyed collaborating with them during my stay in Santa Barbara.

I thank Masud Haque and Indranil Paul for many enriching discussions and productive collaboration.

I thank many faculty members, postdocs and graduate students whom I met in the Physics Department at Rutgers, and from whom I learned much. Among them: Piers Coleman, Lev Ioffe, Andrew Millis, Natan Andrei, Alexander Zamolodchikov, Michael Stephen, Ping Sun, Chris Hooley, Giulio Biroli, Gennady Chitov, Achim Rosch, R. Chitra, Kristjan Haule, Victor Udovenko, Andrea Perali, Andrei Lopatin, Revaz Ramazashvili, Rossen Roussev, John Hopkinson, Nayana Shah, Carlos Bolech, Sarma Kancharla, Panayotis Kevrekidis, Ivan Skachko, Sahana Murthey, Edouard Boulat, Pankaj Mehta, Vitaly Podzorov.

I thank many other people in the department who helped me in different ways, among them: Kathy Dimeo, Misha Gershenson, Yuri Khavine, Anatoly Morozov, Dima Fradkin, Giga Gabadadze, Vadim Brazhnikov, Joel Shapiro, Mark Croft, Ruth Bennett.

I thank scientists from outside Rutgers University, with whom I had many useful discussions: Subir Sachdev, Qimiao Si, Hilbert von Lhneysen, Vaclav Janis, Alexander Lichtenstein, Silke Biermann.

I would like to thank other people from outside Rutgers University, whose support and participation was absolutely essential in my graduate journey: Roman Rafikov, Mikhail Polianski, Timur Shutenko, Sergey Kiselev, Alexander Tumanov, Aleksey Ershov, Andrei Onischenko, Olexei Motrunich, Akakii Melikidze, Ilia Nemenman, Valery Miftakhov, Mikhail Voropaev and many others.

I wish to express my warmest gratitude to my parents and my sister for their unwavering support.

I thank the many people, whom I accidentally have not named here.

And last, but not the least, my upmost thanks goes to to Leela Hebbar, for her help, patience, and love.

# Dedication

To my parents

# Table of Contents

$\mathbf{A}$	ostra	${f ct}$	ii
A	cknov	vledgements	iii
D	edica	tion	v
Li	st of	Figures	ix
1.	Intr	$\operatorname{oduction}$	1
2.	Intr	oduction to DMFT	5
	2.1.	Diagram resummation method	5
	2.2.	Hubbard model	8
		2.2.1. Weak coupling expansion	8
		2.2.2. Cumulant expansion	9
	2.3.	Electron phonon interaction, broken symmetry included	10
	2.4.	Heisenberg Magnet	11
3.	EDI	MFT	13
	3.1.	Introduction	13
	3.2.	Model and semiclassical approximation	15
	3.3.	3D phonons	22
		3.3.1. Weak coupling	24
		3.3.2. Strong coupling	24
		3.3.3. Intermediate coupling	27
	3.4.	2D phonons	27

4.	Fun	ctional approach to EDMFT	34
	4.1.	Intro to functional formulation of the EDMFT	34
	4.2.	Ordered Phase and Critical Temperature	37
	4.3.	Numerical analysis	41
	4.4.	Instability analysis	50
<b>5.</b>	Par	quet EDMFT	55
	5.1.	Dynamical Mean Field Theories in the Parquet Formalism $\ \ldots \ \ldots$	55
	5.2.	Parquet theory	56
	5.3.	DMFT and EDMFT approximations	57
	5.4.	EDMFT2	59
	5.5.	Super-conducting fluctuations	61
6.	And	lerson localization	63
	6.1.	Introduction	63
	6.2.	Phenomenon of the Anderson localization	65
	6.3.	Overview of numerical results	68
	6.4.	General Approach	75
	6.5.	Toy Model	79
	6.6.	Anderson Model	83
	6.7.	Integral Equation Reduction	87
	6.8.	Comparison of NSM, TM and AM	89
7.	Con	iclusion	92
Aı	pen	dix A. EDMFT	94
	A.1.	Critical Temperature	94
	A.2.	Order of the phase transition	96
	A.3	Quantum phase transition	97

Appendix B. Parquet EDMFT	101	
B.1. Definitions	101	
B.2. Exact parquet theory	104	
B.3. Two parquet scheme equivalence	107	
Appendix C. Anderson Localization	110	
C.1. Anderson model equation	110	
C.2. Green's function distribution function	112	
C.3. Real part of the Green's function, Cauchy distribution	113	
C.4. Fourier Laplace transormed integral equation	114	
C.5. Variational method	117	
C.6. $C(x)$ function	118	
C.7. Limits of the integral equation kernel	121	
C.8. Integral equation reduction	122	
References		
Vita	197	

# List of Figures

2.1.	An example of the DMFT approximation, restricting site indices,	
	applied to a two point diagram $C_{ij}$ . Indices $k, l, m, n$ are summed	
	independently	6
2.2.	The diagram shown in $\operatorname{Fig}(2.1)$ is modified: one line reducible block	
	is substituted with $G_1(l)$	7
2.3.	The diagram from $\operatorname{Fig}(2.2)$ is modified further, illustrating step 2)	8
3.1.	$d=3.$ Effective phonon frequency $\omega^*$ as a function of $\lambda^2/\omega_0^2$ at	
	$\omega_1 = 0.0, 0.1, 0.2, 0.3$ . Comparison to QMC	23
3.2.	$d=3.$ Weak coupling $\lambda=.2.$ Comparison to QMC. a) The bare	
	phonon greens function. b) The imaginary part of the electron self	
	energy with the spectral function in the inset. $\omega_1=0.1,0.2,0.3.$ .	25
3.3.	$d=3.$ Strong coupling. $\lambda=.8.$ a) Bare phonon greens function.	
	b) Imaginary part of the electron self energy with the spectral	
	function in the inset. $\omega_1 = 0.1, 0.2, 0.3, 0.4$	26
3.4.	$d=3.$ Intermediate coupling $\lambda=.4.$ Comparison to QMC. a)	
	Bare phonon greens function. b) Imaginary part of the electron	
	self energy with the spectral function in the inset. $\omega_1 = 0.0, 0.2, 0.4$ .	28
3.5.	$d=2$ . Effective phonon frequency $\omega^*$ as a function of $\lambda^2/\omega_0^2$ at	
	$\omega_1 = 0.0, 0.05, 0.1, 0.15, 0.2 \dots \dots \dots \dots \dots \dots \dots \dots \dots$	29
3.6.	$d=2$ . Weak coupling. $\lambda=.2$ . a) The bare phonon greens	
	function. b) The imaginary part of the electron self energy with	
	the spectral function in the inset. $\omega_1 = 0.0, 0.1, 0.2, 0.3, \dots$	30

3.7.	$d=2$ . Intermediate coupling. $\lambda=.4$ . a) The bare phonon greens	
	function. b) The imaginary part of the electron self energy with	
	the spectral function in the inset. $\omega_1 = 0.0, 0.1, 0.2, 0.3, 0.4$	31
3.8.	$d=2$ . Strong coupling. $\lambda=.8$ . a) The bare phonon greens	
	function. b) The imaginary part of the electron self energy with	
	the spectral function in the inset. $\omega_1 = 0.0, 0.1, 0.2, 0.3, 0.4$	32
3.9.	$d=2.$ Bare phonon greens function. $\lambda=.2,.3,.4,.8$	33
4.1.	Diagrammatic expansion of $\Phi_1$ up to the second order. $\Sigma$ and $U$	
	are denoted by a cross and a dot respectively	36
4.2.	Diagrammatic expansion of $\Phi$ up to the first two orders in $U$	38
4.3.	Diagrammatic expansion of $m$ up to the first two orders in $U$ . A	
	thin line is the free phonon propagator $D_0$ , a thick line is the full	
	phonon propagator. A full dot stands for $m$	38
4.4.	Top to bottom: BL, EDMFT, exact solution, MFT; Critical $J_c$	
	(vertical axis) vs nearest neighbors number $z$ (horizontal axis)	42
4.5.	Magnetization vs. temperature on a cubic lattice. There are three	
	branches at $3.96 < T < 4.45$ : $m_3 > m_2 > m_1 = 0$ , $m_1$ and $m_3$ are	
	physical solutions, while $m_2$ is not. Classical $\pm 1$ spin Ising model.	43
4.6.	Free energy evolution with $T$ . Free energy has a single minimum	
	(m=0) above $T=4.45$ ; at $T=4.45$ the solution bifurcates at	
	m = .45. There are free extrema at $3.96 < T < 4.45$ corresponding	
	to $0 = m1 < m2 < m3$ . As T approaches $T_c = 3.96$ , $m2$ merges	
	with $m1$	44
4.7.	Evolution of the free energy with temperature in the classical Ising	
	spin model. Curves, bottom to top, are plotted in the temperature	
	interval from 4.00 to 4.60 with the step 0.05. Curves are shifted	
	for convenience	45

4.8.	Soft spins, $-r = U = 1$ . Inverse temperature is plotted verses the	
	coordination number	46
4.9.	Soft spins, $-r = U = 3$ . Inverse temperature is plotted verses the	
	coordination number	47
4.10.	. Soft spins, $-r = U = 10$ . Inverse temperature is plotted verses the	
	coordination number	48
4.11.	. Soft spins, $-r = U = 300$ . Inverse temperature is plotted verses	
	the coordination number. This graph should be compared to the	
	classical spin limit, Fig.4.5	49
4.12.	. Diagrammatic expansions for $\Sigma$ and $\Sigma_{ph}$	52
5.1.	Ladder diagram, particle particle channels	61
5.2.	Ladder diagram, particle particle channels	62
6.1.	$\langle ImG \rangle_{typical}$ as a function of disorder strength $\gamma$	70
6.2.	Distribution of the onsite Green function $G = x + iy$ at the dis-	
	order strength $\gamma=.05$ obtained in a simulation for the Cauchy	
	distribution of disorder	70
6.3.	The same as above but at the disorder strength $\gamma=1$	71
6.4.	In this figure we plotted $\sqrt{\ln(P_y(y)/P_y^{max})}$ vs. y to check how well	
	$P_y$ may be fitted in Gaussian distribution. If $P_y$ were Gaussian,	
	then graph would be a straight line. Disorder strength $\gamma=.1$ $$	72
6.5.	In this figure we plotted $\sqrt{\ln(P_y(y)/P_y^{max})}$ vs. $\ln y$ to check how	
	well $P_y$ may be fitted in log-normal distribution. If $P_y$ were log=normal	l,
	then graph would be a straight line. Disorder strength $\gamma=.1$	73
6.6.	Contour plot of the function $P_{x,\ln y}/P_x(x)$ in variables $x$ and $\ln \eta =$	
	$\ln(yf(x));$ vertical and horizontal axis correspond to $x$ and $\ln\eta$ re-	
	spectively. Simulation done for: $m=3, \gamma=7.81 \ (\alpha=0.122),$	
	$N \equiv 10000$	74

6.7.	Solution of equation $Im\Lambda_z=0$ is plotted in $b,\nu$ axes, $z=\nu+ib$ ,	
	for the Anderson and toy models respectively	77
6.8.	Real eigenvalue $\Lambda(\gamma, \nu(b), b)$ is plotted as a function of $\nu$ for the	
	Anderson and toy models. In the first case eigenvalue is symmetric	
	function with respect to $\nu=1/2$ . Lower branch corresponds to	
	nonzero $b$ , it is a monotonically growing function of $b$ (for $b > 0$ ).	
	Two brunches merge at the minimum of the upper branch	78
6.9.	$P_{-\log(y)}$ at coord. number =10	81
A.1.	$1/N$ expansion of $\Gamma$ . All diagrams are of the order $1/N$	98
B.1.	Two-body diagram $\alpha$ . Legs 1 and 2 are incoming particles, legs 3	
	and 4 are outgoing particles. Diagrams $\bar{\alpha}$ and $\tilde{\alpha}$ are exchange of $\alpha$	
	and a flip of $\alpha$ respectively	102
B.2.	Five distinctive ways to connect two diagrams $\alpha$ and $\beta$	103
C.1.	Eigenfunction $C(x)$ for small values of $\gamma'$ ('w' on the plot)	119
C.2.	Function $C(\frac{\xi}{\gamma'})[2\ln\gamma' + \frac{1}{2}\ln(1+\frac{1}{\xi^2}) + \frac{1}{\xi}\arctan\frac{1}{\xi}]^{-1}$ is plotted for	
	large values of $\gamma'$ ('w' on the plot). If analytical expression given by	
	eq(6.39) is correct, than graphs should tend to asymptotic function	
	$2\xi/(\xi^2+1)$ (full line)	120

# Chapter 1

### Introduction

Rarely problems, arising in our quest for understanding the nature of the physical world, can be solved with complete mathematical rigour. The need arises for using some approximations, either in the choice of the physical models mimicing the real world, or in the methods of solving them, or both. It may be difficult to assess if a particular approximation (theory) not only makes the problem formally solvable, but also preserves the essence of the considered phenomenon, unless there is a parameter in the theory which becomes small (or large) in some limit. Such approximations are called controlled and are most appriciated in theoretical physics. The dynamical mean field theory (DMFT) is an example of a controlled theory, it becomes exact in the limit of large coordination number or dimensionality d. Different approximations are often complimentary, where one fails, another may be of great help. Therefore it is of paramount impotance to learn the strengths and limitations of each approach, and to know when each method can be applied. In this work we attempt to widen our understanding of the class of mean field theories, which are generecally referred to as dynamical mean field theories.

The development of the DMFT started with the pioneering work of Metzner and Vollhard, [1] who showed that in the limit of  $d \to \infty$  the physics of correlated fermions remains nontrivial provided the hopping matrix elements are properly scaled. They also showed that diagramatic calculations are greatly simplified and the self energy of the Hubbard model becomes local.

The next significant advancement was made when it was realized that the Hubbard model could be mapped exactly onto the Anderson impurity model [2] in the limit  $d = \infty$ , and that this method could be extended to a large number of other models. For the first time the Hubbard model could be studied in the whole range of the interaction strength, something the perturbation theory could not do. The perturbation theory was useful only in the weak or strong coupling limit and was breaking down at the intermediate coupling, where the Mott transition was taking place. The nontrivial picture of the transition was revealed, showing the formation of the resonans in the density of states at Fermi level and its destruction in the transition. The transition was found to be the first order at zero temperature.

Mapping to an impurity also permitted the use of many methods, available for treating Anderson impurity, in solving correlated systems on a lattice. Computing the Green's function from the local DMFT action exactly requires application of the Quantum Monte Carlo algorithms, which become exponentially costly at small temperature. Instead one can use an approximate scheme, like iterated perturbation theory (ITP) [2] or exact diagonalization method, as well as a number of analytic methods.

In the following, whenever we refer to DMFT, we imply the approximation which is exact in the limit  $d \to \infty$ , be it the impurity formulation, or a functional integral formulation, unless specified otherwise.

It was quickly understood that DMFT can be applied to many other models, like: periodic Anderson model [3], Kondo lattice [3], quantum spin glasses [4], Falikov Kimball model [5–7], Holstein model [8,9], etc. Later DMFT was extended to include longer range interactions [10, 11], for example in extended Hubbard model, hence the name of extended DMFT, or simply EDMFT. In its spirit EDMFT is quite similar to DMFT.

The DMFT is a controlled approximation, which is exact in the infinite d

limit. However the systems we study in practice are at most three dimensional, therefore it is desirable to build an extension near the exact infinite d limit. The extension should be accounting for 1/d corrections. Other than improving the quantitative results obtained with DMFT, this would be crucial for capturing some effects which are absent in a single site formulation, like d-wave superconductivity. The EDMFT attempts to include nonlocal collective excitations, but they are treated in the DMFT fashion and must be built into the Hamiltonian to begin with. It does not capture nonlocal particle hole or particle particle excitations. The alternative route is to consider a cluster embedded in a selfconsistent bath. Several cluster DMFT formulation has been proposed [12, 13] and there properties investigated [14–16]. Extension to just a  $2 \times 2$  cluster already captures d-wave superconductivity features of the 2D Hubbard model [17, 18].

Among recent sucesses of DMFT we can name a succeful combination of the DMFT with the local density approximation theory [19,20] (LDA) - realistic band structure calculation method, which was significantly improved by brining in the many body physics.

Much effort was put in combining DMFT and the disorder. A common approach in treating the disorder is to introduce n replicas and take the limit  $n \to 0$  after integrating out the disorder. This proved to be useful for studying glassy physics. This approach is applicable for interacting problem as well [21] including DMFT formulation [22], but it proved to be of little help in capturing correctly the physics of strong localization. This might be due to the lack of understanding of the applicability of the replica trick [23]. An alternative to the replica trick is the supersymmetry approach [24, 25], but it is applicable to noninteracting systems only. One therefore has to turn to uncontrolled but successful methods like statistical DMFT [26] or typical medium theory [27] (TMT) which do incorporate disorder and interaction in DMFT setting and allow the description of the Anderson transition.

In our work, in addition to exploring the EDMFT, we study different features of the Anderson localization, understanding of which should be useful in any attempt to combine the DMFT and disorder.

The outline of the dissertation is as follows. In chapter 2 we show how DMFT and EDMFT equations can be derived for a number of models by resumming nonlocal diagrams. In chapter 3 we consider a semiclassical approximation on EDMFT (which can be considered as a choice of an impurity solver) to study electron phonon problem. The results are compared to QMC approach of the Ref. [28]. In chapter 4 we consider a functional approach to DMFT, which is formulated as a local approximation on the Baym-Kadanoff functional [29]. We compute the free energy functional in the classical limit and perform an instability analysis of the symmetrical phase, clarifying the computation of susceptibilities in a very general DMFT setting. In the following chapter 5 we present yet another way of viewing the DMFT approximation, using the parquet equation formalism. We attempt to extend the local approximation to account for nonlocal particle particle and particle hole excitations. In chapter 6 we investigate the Anderson localization problem, making an accent on undestanding the correlation between the real and imaginary parts of the Green's function in the vicinity of the transition.

# Chapter 2

#### Introduction to DMFT

### 2.1 Diagram resummation method

There exist many ways of deriving DMFT equations. In this section we present one of them, where momentum dependent parts of diagrams are resummed and an impurity action with self consistently determined parameters is used to compute local correlation functions. This method is quite universal, we imply it to derive both DMFT and EDMFT equations, in both symmetrical and ordered phases, using both weak coupling expansion and cumulant expansion formalism.

We consider a graphical representation of a perturbation theory of a model under consideration. The perturbation theory will be either built around the Gaussian free theory which permits the use of the Wick's theorem, or around the atomic limit. In the first case we expand in the local interaction and call it the weak coupling expansion, in the second case we expand in the nonlocal matrix element and call it the cumulant expansion. Each graph representing a term in the perturbative expansion is made of vertices and lines. There can be more than one kind of vertices and lines. We assume that the graphical representation is chosen in such a way, that each line represent a nonlocal object, like a propagator or a long range interaction, while a vertex represent a local object, like local interaction or bare cumulant in a cluster. In other words, a site index assigned to each vertex, and those indices are independent in the exact perturbation theory. The DMFT approximation imposes constraints on this indices, by requiring some lines to be local. It can be formulated concisely: if a vertex in a diagram can

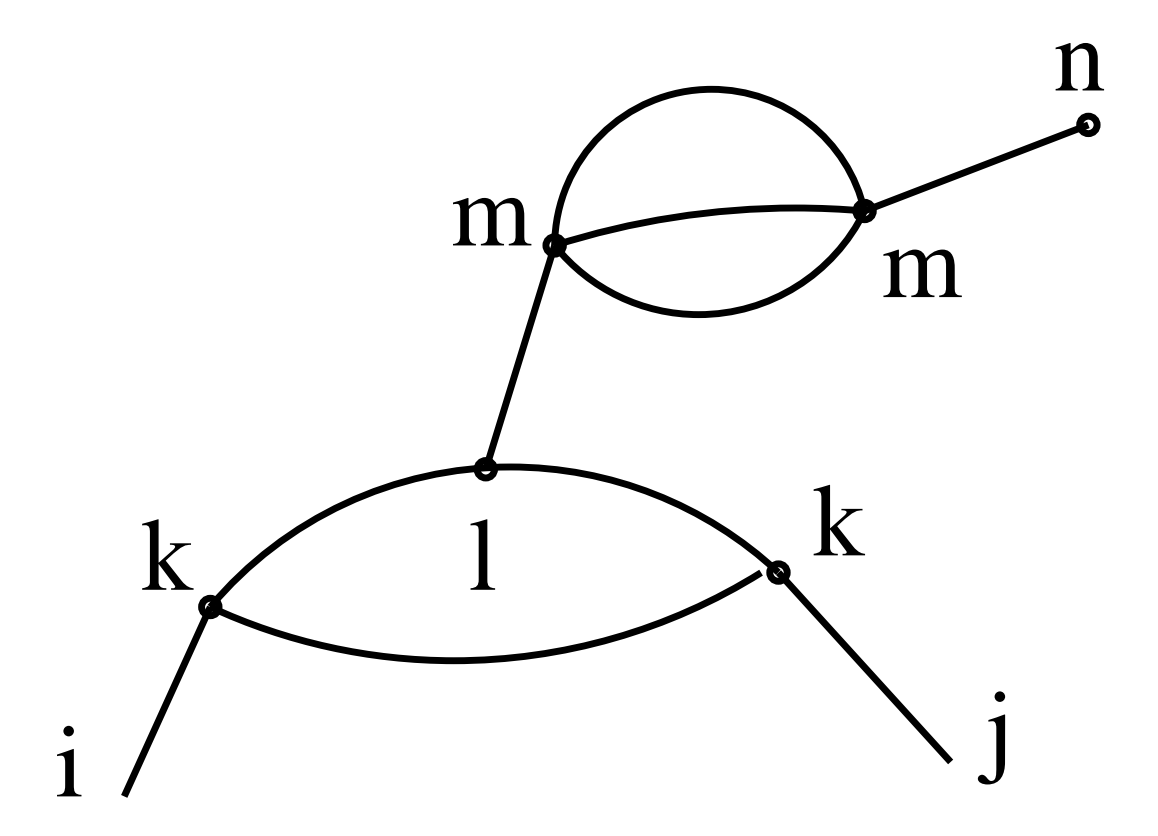


Figure 2.1: An example of the DMFT approximation, restricting site indices, applied to a two point diagram  $C_{ij}$ . Indices k, l, m, n are summed independently.

be separated from the diagram by cutting one or two (necessarily so) lines, then those lines are taken to be nonlocal. All other lines are taken to be local. An example is given in Fig.(2.1).

To map a lattice model onto a local impurity model we resum nonlocal blocks in diagrams according to the rules:

- 1) Every block which can be separated by a single cut is substituted with a local bond  $G_1^a(i)$ , (see Fig.(2.2)).
- 2) Every block which requires two cuts is substituted with a bond  $G_2^{ab}(ij)$ , (see Fig.(2.3)).
  - 3) Steps 1) and 2) applied until no nonlocal insertions left.

Upper indices in  $G_1^a$  and  $G_2^{ab}$  denote the types of the lines that are being cut in the substitution. We also note that the result of a diagram reduction according to steps (1-3) is unique. Moreover, if we consider a diagram representing a local

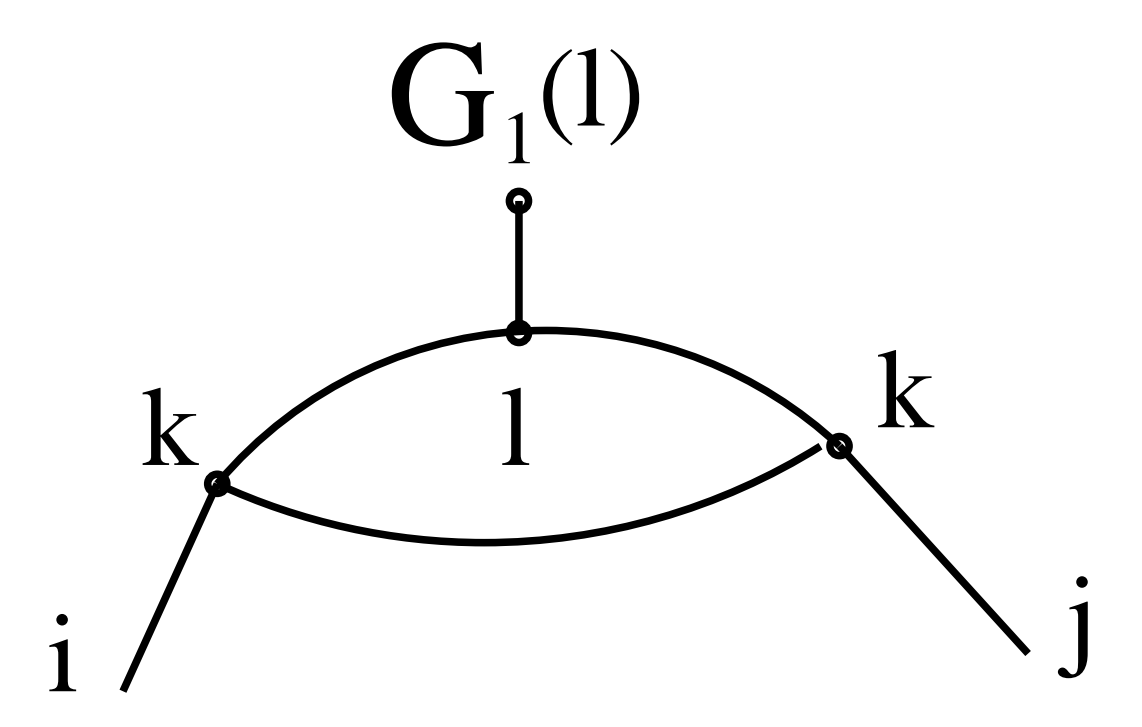


Figure 2.2: The diagram shown in Fig(2.1) is modified: one line reducible block is substituted with  $G_1(l)$ .

correlation function  $C_i$  or  $C_{ij}$  then the reduced graph includes only local  $G_1$  and  $G_2$ .

The next step is to construct a local impurity action. First we separate local and nonlocal terms in the lattice action  $S_{lat} = S_{loc} + S_{nonloc}$ , then we write the impurity action in the form  $S_{imp} = S_{loc} + \tilde{S}$ , where  $\tilde{S}$  has the same structure as  $S_{nonloc}$ . It is clear that the same procedure, namely resumming one-line and two-line reducible blocks and substituting them with  $G_{1imp}^a$  and  $G_{2imp}^{ab}$  can be done on graphs generated in the perturbative expansion corresponding to the local action  $S_{imp}$ . If, by choosing appropriately parameters in  $\tilde{S}$ , we could insure that

$$G_1(i) = G_{1imp}$$

$$G_2(ii) = G_{2imp}$$
(2.1)

then all local lattice quantities would be equal to corresponding impurity model quantities. Below we illustrate the described approach on specific examples. In the following sections we apply the resummation method to different models.

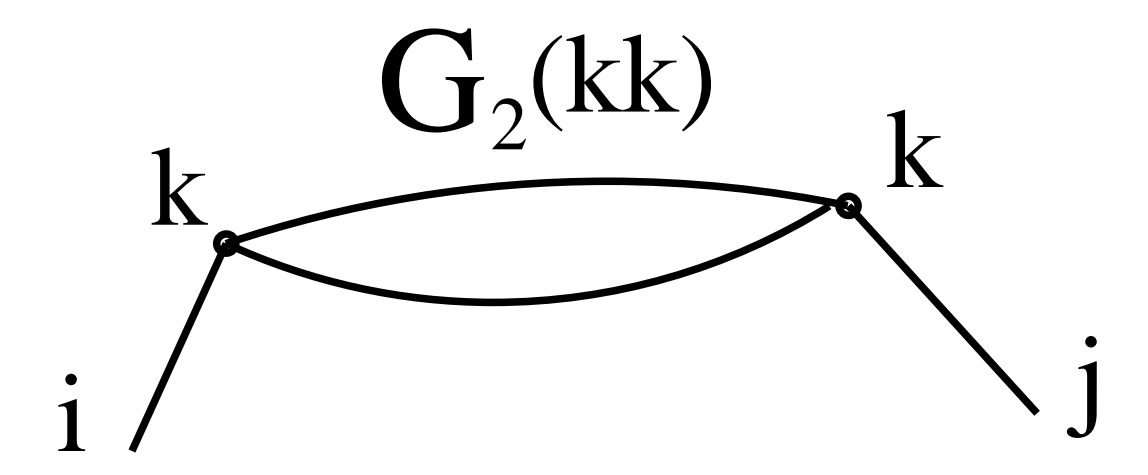


Figure 2.3: The diagram from Fig(2.2) is modified further, illustrating step 2)

#### 2.2 Hubbard model

The Hubbard model Hamiltonian reads:

$$H = \sum_{ij} t_{ij} c_{i\sigma}^{\dagger} c_{j\sigma} + U \sum_{i} n_{i\uparrow} n_{i\downarrow}$$
 (2.2)

#### 2.2.1 Weak coupling expansion

In this section we derive DMFT equations for the Hubbard model using usual weak coupling expansion. Feynman diagrams rules assign U to each vertex and  $G_0(ij)$  to each line. To be able to compare  $G_2$  and  $G_{2imp}$  we have to express them in terms of an irreducible (and hence local) part. In this case it is self energy:

$$G_2(ii) = G_0(ii) + \sum_j G_0(ij)\Sigma G_0(ji) + \dots = [(G_0^{-1} - \Sigma)^{-1}]_{ii}$$
 (2.3)

The impurity action reads:

$$S_{imp} = -\sum_{\sigma} \int d\tau d\tau' c_{\sigma}^{\dagger}(\tau) G_{0\sigma imp}^{-1}(\tau - \tau') c_{\sigma}(\tau) + U \int d\tau n_{\uparrow}(\tau) n_{\downarrow}(\tau) \qquad (2.4)$$

Similarly to Eq.(2.3) we obtain for the impurity model:

$$G_{2imp} = G_{0imp} + G_{0imp} \Sigma G_{0imp} + \dots = (G_{0imp}^{-1} - \Sigma)^{-1}$$
 (2.5)

we do not make any difference between  $\Sigma_i$  and  $\Sigma_{imp}$ , since, as we mentioned before, local parts must coincide if Eqs.(2.1) are satisfied. The last step is to relate a local correlation function to  $G_2$ . In this case it is trivial:

$$G_2 = G (2.6)$$

Combining Eqs(2.1, 2.3, 2.5, 2.6) we derive the selfconsistency equation, which in momentum space reads:

$$G = \sum_{q} (G_{0q}^{-1} - G_{0imp}^{-1} + G^{-1})^{-1}$$
(2.7)

In the next section we will derive same equation using cumulant expansion.

#### 2.2.2 Cumulant expansion

In the cumulant expansion formalism each vertex with n legs represents a bare cumulant  $M_n^0(i) = \langle c_i c_i^{\dagger} \rangle_{S_{loc}}$  and each line represent the hopping matrix element  $t_{ij}$ .  $G_2$  can be expressed in terms of  $t_{ij}$  and renormalized cumulant  $M_2$ :

$$G_2(ii) = t_{ii} + \sum_{i} t_{ij} M_2 t_{ji} + \dots = [(t^{-1} - M_2)^{-1}]_{ii}$$
 (2.8)

The impurity action reads:

$$S_{imp} = \sum_{\sigma} \int d\tau c_{\sigma}^{\dagger}(\tau) (\frac{\partial}{\partial \tau} - \mu) c_{\sigma}(\tau)$$

$$+ U \int d\tau n_{\uparrow}(\tau) n_{\downarrow}(\tau) + \sum_{\sigma} \int d\tau d\tau' c_{\sigma}^{\dagger}(\tau) \Delta(\tau - \tau') c_{\sigma}(\tau)$$
(2.9)

We wrote the action in the form  $S_{imp} = S_{loc} + \tilde{S}$ , where first two terms belongs to  $S_{loc}$  and the third term belong to  $\tilde{S}$ . For  $G_{2imp}$  we obtain:

$$G_{2imp} = -\Delta + \Delta M_2 \Delta + \dots = -(\Delta^{-1} + M_2)^{-1}$$
 (2.10)

local correlation function G relates to  $G_2$  via:

$$G = -\langle cc^{\dagger} \rangle = -M_2 - M_2 G_2 M_2 \tag{2.11}$$

Solving Eqs(2.1, 2.8, 2.10, 2.11) we arrive to Eq.(2.7) again, with  $G_{0imp}^{-1} = i\omega + \mu - \Delta(i\omega)$ .

#### 2.3 Electron phonon interaction, broken symmetry included

In this section we derive EDMFT equations in the ordered phase, where the phonon field acquires non zero expectation value. We could use with equal ease either the cumulant or weak coupling expansion, and we choose the second method.

Interacting electron-phonon Hamiltonian reads:

$$H = -\sum_{ij,\sigma} (t_{ij} - \mu) c_{i\sigma}^{\dagger} c_{j\sigma} + \sum_{i} \frac{p_i^2}{2M} - \sum_{ij} \frac{J_{ij}}{2} x_i x_j + \sum_{i\sigma} \lambda x_i c_{i\sigma}^{\dagger} c_{i\sigma}$$
 (2.12)

The corresponding action reads:

$$S = -\sum_{ij\sigma\omega_n} c_{i\sigma}^{\dagger}(i\omega_n) G_{0\ ij}^{-1}(i\omega_n) c_{j\sigma}(i\omega_n) + \frac{1}{2} \sum_{ij\Omega_n} x_i(i\Omega_n) D_{0\ ij}^{-1}(i\Omega_n) x_j(i\Omega_n) + \lambda \sum_{i\sigma\Omega_n} x_i(i\Omega_n) n_{i\sigma}(i\Omega_n)$$

$$(2.13)$$

where

$$G_0^{-1}{}_{ij}(i\omega_n) = (i\omega + \mu)\delta_{ij} + t_{ij}$$

$$D_0^{-1}{}_{ij}(i\Omega_n) = -\Omega_n^2 M \delta_{ij} - J_{ij}$$
(2.14)

A line a Feynman diagram represents either a free electron propagator  $G_0(i\omega)$  (a solid line) or a free phonon propagator  $D_0(i\Omega)$  (a dashed line). The coupling constant  $\lambda$  is assigned to a vertex. For  $G_1^{ph}$  we find:

$$G_1^{ph} = \lambda \sum_{j\sigma\omega} D_{0ij}(0) G_{jj\sigma}(i\omega)$$
 (2.15)

For  $G_2$  we find similarly to the previous section:

$$G_2^{el}(ii) = [(G_0^{-1} - \Sigma_{el})^{-1}]_{ii}$$

$$G_2^{ph}(ii) = [(D_0^{-1} - \Sigma_{ph})^{-1}]_{ii}$$
(2.16)

The impurity action reads:

$$S_{imp} = \sum_{\sigma} \int d\tau d\tau' \left\{ -c_{\sigma}^{\dagger}(\tau) G_{0\sigma \ imp}^{-1}(\tau - \tau') c_{\sigma}(\tau) + x(\tau) D_{0}^{-1}(\tau - \tau') x(\tau') \right\}$$
$$+ \lambda \sum_{\sigma} \int x(\tau) n_{\sigma}(\tau) - h \int d\tau x(\tau)$$
(2.17)

We write  $G_1$  and  $G_2$  for the impurity model:

$$G_{1imp}^{ph} = \lambda D_{0imp}(0) \left[ \sum_{\sigma\omega} G_{\sigma imp}(i\omega) + h \right]$$

$$G_{2imp}^{el} = \left[ (G_{0imp}^{-1} - \Sigma_{el})^{-1} \right]$$

$$G_{2imp}^{ph} = \left[ (D_{0imp}^{-1} - \Sigma_{ph})^{-1} \right]$$
(2.18)

 $G_1$  and  $G_2$  are trivially related to the correlators:

$$G_1^{ph} = m = \langle x \rangle$$
 
$$G_2^{el} = G$$
 
$$G_2^{ph} = D$$
 (2.19)

Solving Eqs(2.1, 2.15, 2.16, 2.18, 2.19) we find selfconsistency equations:

$$G = \sum_{q} (G_{0q}^{-1} - G_{0imp}^{-1} + G^{-1})^{-1}$$

$$D = \sum_{q} (D_{0q}^{-1} - D_{0imp}^{-1} + D^{-1})^{-1}$$

$$h = m(D_{0q=0}^{-1} - D_{0imp}^{-1})$$
(2.20)

# 2.4 Heisenberg Magnet

The last example we consider is the Heisenberg Magnet:

$$H = \frac{1}{2} \sum_{ij} J_{ij} S_i S_j \tag{2.21}$$

Here we must use the cumulant expansion. The derivation of DMFT equations in this case is almost identical to the case of the Hubbard model, which we already considered, so we summarize results. The lattice and impurity actions read:

$$S_{lat} = \int d\tau \sum_{i} S_{B}[S_{i}(\tau)] + \frac{1}{2} \sum_{ij} J_{ij} S_{i}(\tau) S_{j}(\tau)$$

$$S_{imp} = \int d\tau S_{B}[S(\tau)] + \frac{1}{2} S(\tau) \chi_{0imp}^{-1}(\tau - \tau') S(\tau')$$
(2.22)

For  $G_2$ ,  $G_{2imp}$  and the correlation function  $\chi = \langle SS \rangle$  we find:

$$G_2(ii) = -[(\hat{J}^{-1} + M_2)^{-1}]_{ii}$$

$$G_{2imp} = -[(\chi_{0imp} + M_2)^{-1}]_{ii}$$
(2.23)

and

$$\chi = M_2 + M_2 G_2 M_2 \tag{2.24}$$

The bare cumulant  $M_2^0$  is defined here as  $\langle SS \rangle_{S_{loc}}$ . From Eqs.(2.22-2.24) we obtain selfconsistency condition:

$$\chi = \sum_{q} (J_q - \chi_{0imp}^{-1} + \chi^{-1})^{-1}$$
 (2.25)

# Chapter 3

#### **EDMFT**

#### 3.1 Introduction

The dynamical mean field theory has been very successful in unraveling non perturbative problems such as the Mott metal to insulator transition [30]. In spite of its many successes, this technique has several limitations resulting from its single site character and from the lack of feedback of the non local collective excitations on the one particle spectra. Several approaches are being pursued to extend the scope of the DMFT method. In this chapter we explore an extension of the DMFT method (EDMFT) [10,11] which maintains a local self energy while incorporating feedback effects of the charge and spin dynamics in the one electron properties. This method gives rise to quantum impurity problems with fermionic and bosonic baths that need to be solved self consistently. This method has already been applied to wide class of models, such as the spin fermion model [31], fermions interacting with long range (Coulomb) electron-electron interaction [32], electron-phonon systems [28] and frustrated magnets [33].

The EDMFT equations are more involved than the conventional DMFT equations because they involve a solution of a self consistency problem in an additional bosonic sector and only recently a full numerical analysis of the self consistency conditions of EDMFT were carried out [28]. The interpretation of the EDMFT instabilities is also not as straightforward as in DMFT because bosonic and fermionic propagators involve very different regions of momentum space, and a formulation of EDMFT for ordered phases was only obtained recently [29].

In this chapter we develop the EDMFT approach further by analyzing several aspects of this method: a) We implement a semiclassical technique for its solution [34–36] and compare its results to the earlier QMC study [28] to test its accuracy. We show that the analytic treatment is in satisfactory agreement with exact (QMC) results in the high temperature regime of the three dimensional model and provides analytic expressions for various physical quantities. b) We extend this study to the case of 2-dimensional phonons, which had not been treated in ref [28]. We demonstrate that in the 2-dimensional case the EDMFT treatment at finite temperatures, if it produces an ordering transition it is necessarily of the first order. This analysis applies to a very general class of models including those used in ref [31].

We also analyze the EDMFT equations in the ordered phase [29], for a simple spin model. This analysis clarifies the the strengths and the limitations of the EDMFT approach, in a very simple setting.

The chapter is organized as follows. In section 3.2 we write the Fermion Boson model and the extended DMFT equations. We then describe the semiclassical strategy for their analysis in both weak and strong electron-phonon coupling. In section 3.3 we present results of solving the saddle point equations for 3D phonons coupled to electrons in different regimes and discuss the agreement with results in QMC approach. In section 3.4 we describe the results for 2D phonons. If the electrons are fully integrated out, the semiclassical treatment of EDMFT has to reduce to a mean field theory in classical statistical mechanics. In section 4.2 we compare EDMFT with other classical mean field treatments such as the Weiss mean field approach and the Bloch Langer method [37]. The stability analysis of the EDMFT theory is carried out in an appendix 4.4.

#### 3.2 Model and semiclassical approximation

The model under consideration is described by the lattice Hamiltonian:

$$H = H_{el} + H_{ph} + H_{el-ph} (3.1)$$

where

$$H_{el} = -\sum_{ij,\sigma} t_{ij} c_{i\sigma}^{\dagger} c_{j\sigma} \tag{3.2}$$

$$H_{ph} = \sum_{i} \frac{p_i^2}{2M} - \sum_{ij} \frac{J_{ij}}{2} x_i x_j \tag{3.3}$$

$$H_{el-ph} = \sum_{i\sigma} \lambda x_i (c_{i\sigma}^{\dagger} c_{i\sigma} - \frac{1}{2}) \tag{3.4}$$

The first term describes free electrons,  $c_{i\sigma}^{\dagger}$  ( $c_{i\sigma}$ ) creates (annihilates) an electron with spin  $\sigma$  on a site i. The second term describes nonlocal (dispersive) phonons,  $x_i$  and  $p_i$  are canonical variables. The last term couples the fermionic and the bosonic degrees of freedom. We consider a half filled system of fermions.

The second term could alternatively be written as:

$$H_{ph} = \sum_{q} \omega_q (a_q^{\dagger} a_q + \frac{1}{2}) \tag{3.5}$$

where  $a_q$ ,  $a_q^{\dagger}$  are related to the phonon field by  $x_q = (2M\omega_q)^{-\frac{1}{2}}(a_q + a_{-q}^{\dagger})$  and  $\omega_q^2 = J_q/M$ . Dispersion (momentum dependence) of the boson frequency  $\omega_q$  stems from nonlocal character of  $J_{ij}$ . The local limit of  $J_{ij}$  corresponds to the Holstein model [38], so the model under consideration is an extension of the Holstein model to dispersive phonons.

The extended DMFT equations for this model [28] are a set of equations for Weiss functions  $G_{0\sigma}^{-1}(i\omega_n)$  and  $D_0^{-1}(i\omega_n)$ :

$$G_{\sigma}[G_0, D_0](i\omega_n) = \sum_{q} \left[ i\omega_n - t_q + G_{\sigma}[G_0, D_0]^{-1}(i\omega_n) - G_{0\sigma}^{-1}(i\omega_n) \right]^{-1}$$
 (3.6)

$$D[G_0, D_0](i\omega_n) = \sum_{q} \left[ M(i\omega_n)^2 - J_q + D[G_0, D_0]^{-1}(i\omega_n) - D_0^{-1}(i\omega_n) \right]^{-1}$$
 (3.7)

where full Green's functions  $G_{\sigma}(i\omega_n)$  and  $D(i\omega_n)$  are expressed through  $G_{0\sigma}^{-1}(i\omega_n)$  and  $D_0^{-1}(i\omega_n)$  in terms of the effective impurity action:

$$S_{eff} = \sum_{\omega_n, \omega_m, \sigma} c_{\sigma}^{\dagger} (i\omega_n + i\omega_m) \left( G_{0\sigma}^{-1} (i\omega_n) \delta_{0, \omega_m} + \lambda x (i\omega_m) \right) c_{\sigma} (i\omega_n) - \frac{1}{2} D_0^{-1} (i\omega_m) x^2 (i\omega_m)$$

$$(3.8)$$

$$G_{\sigma}(i\omega_n) = \frac{\int \mathcal{D}[c_{\sigma}^{\dagger}, c_{\sigma}, x] c_{\sigma}(i\omega_n) c_{\sigma}^{\dagger}(i\omega_n) e^{-S_{eff}[c_{\sigma}^{\dagger}, c_{\sigma}, x]}}{\int \mathcal{D}[c_{\sigma}^{\dagger}, c_{\sigma}, x] e^{-S_{eff}[c_{\sigma}^{\dagger}, c_{\sigma}, x]}} = \langle c_{\sigma}(i\omega_n) c_{\sigma}^{\dagger}(i\omega_n) \rangle_{S_{eff}}$$
(3.9)

$$D_{\sigma}(i\omega_n) = -\langle x^2(i\omega_n)\rangle_{S_{eff}}$$
(3.10)

Eqs(3.6-3.10) in general have to be solved numerically. In many cases though, a number of approximations reducing numerical work but preserving a physical content of the problem are possible. One of the approximations is in using a model density of states (DOS) for fermions and bosons, so that momentum summations in EDMFT equations could be performed analytically. It is convenient to chose semicircular electron DOS:

$$\rho_{el}(\epsilon) = \frac{2}{\pi W^2} \sqrt{W^2 - \epsilon^2} \tag{3.11}$$

where W is the electron band halfwidth. The particular choice of semicircular electron DOS is qualitatively unimportant since we consider half filled electron band. For phonons, on the contrary, the shape of the phonon band near the

bottom is crucial for temperatures smaller than the phonon band width. For d-dimensional phonons the bottom of the band has  $e^{\frac{d-2}{2}}$  singularity. That is why to represent 3d and 2d phonons we chose semicircular and stepfunctionlike phonon DOS respectively:

$$3d \qquad \rho_{ph}(\epsilon) = \frac{2}{\pi\omega_1^2} \sqrt{\omega_1^2 - (\epsilon - \omega_0)^2}$$
 (3.12)

$$2d \rho_{ph}(\epsilon) = \frac{1}{2\omega_1} \theta(\omega_1^2 - (\epsilon - \omega_0)^2) (3.13)$$

After replacing the summations over the wave vector by integrations over energy, Eq(3.6) and Eq(3.7) read:

$$G_{\sigma}(i\omega_n) = \int d\epsilon \frac{\rho_{el}(\epsilon)}{\zeta - \epsilon}$$
 (3.14)

$$D(i\omega_n) = \int d\epsilon \frac{\rho_{ph}(\epsilon)}{\xi^2 - \epsilon^2}$$
 (3.15)

where  $\zeta = i\omega_n + G_{\sigma}^{-1}(i\omega_n) - G_{0\sigma}^{-1}(i\omega_n)$ ,  $\xi^2 = M(i\omega_n)^2 + D^{-1}(i\omega_n) - D_0^{-1}(i\omega_n)$ ; density of states  $\rho(\epsilon) \equiv \frac{dq}{d\epsilon_q}$ . For electron  $\rho_{el}(\epsilon)$  and phonon  $\rho_{ph}(\epsilon)$  DOS respectively  $\epsilon_q = t_q$  and  $\epsilon_q^2 = J_q$ . For DOS defined in Eqs(3.11- 3.13) integrations over energy in Eqs(3.14,3.15) yield:

$$G_{\sigma}(i\omega_n) = \frac{2}{W^2} \left( \zeta - s\sqrt{\zeta^2 - W^2} \right) \tag{3.16}$$

where  $s=\text{sgn}[\text{Im}\zeta]$ .

$$3d D(i\omega_n) = \frac{1}{\xi\omega_1^2} (2\xi + \sqrt{(\xi - \omega_0)^2 - \omega_1^2} - \sqrt{(\xi + \omega_0)^2 - \omega_1^2}) (3.17)$$

$$2d D(i\omega_n) = \frac{1}{4\xi\omega_1} \ln\left[\frac{(\xi + \omega_1)^2 - \omega_0^2}{(\xi - \omega_1)^2 - \omega_0^2}\right] (3.18)$$

We consider here a semiclassical treatment of the problem. In its most general form, the approach has been described in ref [34], and is an application of the

saddle point method. We use a more limited form of this method that consists of evaluating Eqs(3.9,3.10) by a saddle point technique. It can be viewed as a combination of two separate approximations: the static approximation (equivalent to the phonon mass  $M \to \infty$  limit) and a saddle point analysis of the EDMFT equations in the static approximation.

The approach of treating the collective excitations as classical, while the electrons are treated fully quantum mechanically, goes back to the Hubbard approximation [39]. It was pointed out that a static approximation of the impurity model coupled with the DMFT self consistency conditions indeed gives a solution closely related to Hubbard's [40]. This approach has been used extensively in refs [35,36] in DMFT studies of the Holstein model. From the DMFT studies of the Mott transition [30], we know that this approach becomes insufficient in the correlated metallic regime at very low temperatures, where a quasiparticle feature forms in addition to the spectral features produced in the semiclassical approximation. It is worth pointing out, that improvements of the static or of the saddle point approximation [34], will not remedy this shortcoming, which requires a non perturbative resummation of instanton events. Still, we show here that this simple analysis is able to reproduce all the trends of the solution of the EDMFT equations by the more expensive QMC method [28].

The EDMFT equations in the static approximation Eqs(3.9,3.10) reduce to:

$$G(i\omega_n) = \int dx P(x) \frac{1}{G_0^{-1}(i\omega_n) + \lambda x}$$
(3.19)

$$D = -\beta \int dx P(x)x^2 \tag{3.20}$$

where

$$P(x) = \frac{1}{N} \exp\left(g \sum_{n \ge 0} \ln\left(1 - G_0(i\omega_n)^2 \lambda^2 x^2\right) - \frac{\beta}{2} D_0^{-1} x^2\right)$$
(3.21)

Eqs(3.19-3.21) have to be solved together with Eqs(3.6, 3.7). In the static limit only the zero phonon frequency survives, so we drop frequency index for the phonon correlation functions  $D_0$  and D. In Eqs(3.19-3.21) and everywhere below we consider x being the phonon field amplitude, it is related to its Fourier transform as  $x = \beta^{-\frac{1}{2}} x_{\omega_m=0}$ . We consider no symmetry breaking in the electron spin channel, so we dropped the spin index; factor g (equal 2 for spin one-half) in the Eq(3.21) appears from trace over the spin index. N normalizes P(x) to unity. P(x) is the probability distribution function of the phonon field amplitude x.

We now evaluate Eqs(3.19-3.21) in the saddle point approximation in the variable x. There are two limits, weak and strong coupling. In the weak coupling the saddle point is at x = 0, and in the strong coupling there are two equivalent saddle points at  $x = \pm x_0 \neq 0$ . Deriving the saddle point equations we explicitly use semicircular electron DOS, Eqs(3.11,3.16). The relation between the bare and full Green's functions is especially simple in this case:

$$G_0(i\omega_n)^{-1} = i\omega_n - t^2 G(i\omega_n)$$
(3.22)

where t = W/2. Everywhere below in the chapter energy is measured in units of t. In this chapter we restrict ourselves to the particle-hole symmetric case.

In the weak coupling regime in the saddle point approximation, which includes Gaussian fluctuations of x around zero, semiclassical EDMFT equations Eqs(3.19-3.21) read:

$$\tilde{G}(\tilde{G} + \omega)^3 - (\tilde{G} + \omega)^2 + \alpha^2 = 0 \tag{3.23}$$

$$D_0^{-1} - D^{-1} = -T \sum_{n \ge 0} \frac{2g\lambda^2}{(\tilde{G} + \omega_n)^2}$$
 (3.24)

where  $\tilde{G} = iG(i\omega_n)$  and  $\alpha^2 = \lambda^2 |D|T = -\lambda^2 T \int d\epsilon \rho_{ph}(\epsilon) [D^{-1} - D_0^{-1} - \epsilon^2]^{-1}$ , so  $\alpha^2$  is solved for the phonon self energy thus making the system of the saddle point equations closed.

In the strong coupling regime we consider two saddle points  $x = \pm x_0$ . We discard fluctuations around these points (so  $|D| = \beta x_0^2$ ), since nontrivial information is contained in the fact that we have two saddle points, and not in the Gaussian fluctuations, like it was in the case of weak coupling. EDMFT equations Eqs(3.19-3.21) now read:

$$\tilde{G}(\tilde{G} + \omega)^2 - (\tilde{G} + \omega) + \tilde{G}\alpha^2 = 0 \tag{3.25}$$

$$D_0^{-1} = -T \sum_{n>0} \frac{2g\lambda^2}{(\tilde{G} + \omega_n)^2 + \lambda^2 T D}$$
 (3.26)

Weak coupling equations Eqs(3.23,3.24) are a saddle point expansion up to the first order in small parameter  $\lambda^2 DT$ , and strong coupling equations Eqs(3.25,3.26) - up to the first order in large parameter  $\lambda^2 D/T$ . These equations have overlapped regions of applicability, provided  $T \ll 1$ . This allows us to combine weak and strong coupling equations into a unique set of equations, controlled by the small parameter T:

$$\tilde{G}(\tilde{G} + \omega)^2 - (\tilde{G} + \omega) + \tilde{G}\alpha^2 = 0 \tag{3.27}$$

$$D_0^{-1} - D^{-1} = -2g\lambda^2 T \sum_{n \ge 0} \frac{\tilde{G}}{\tilde{G} + \omega_n}$$
 (3.28)

These are our final semiclassical EDMFT equations. They are exact in the limit  $MT^2 \gg \omega_0^2$ ,  $T \ll 1$ . For 3d and 2d phonons Eqs(3.27,3.28) have to be solved together with Eq(3.17,3.18), where  $\xi^2 = D^{-1} - D_0^{-1}$ . Saddle point equations Eqs( 3.27,3.28) are very simple, they can be solved for D and  $D_0$  with minimal numerical efforts. Lhs part of Eq(3.27) is a third degree polynomial, so electron

Green's function can be written as an elementary function determined by a single parameter  $\alpha^2$  which is a function of phonon self energy and bare parameters of the model.

In the limits of small and large  $\alpha^2$  (or  $\lambda$ ) Eqs.(3.27,3.28) are solved completely for self energies:

 $\alpha \ll 1$ 

$$\Sigma_{el}(i\omega_n) = \left(-\frac{\omega_n}{2} + \sqrt{1 + (\frac{\omega_n}{2})^2}\right)\alpha^2$$
 (3.29)

$$\Sigma_{ph} = -\frac{4g}{3\pi}\lambda^2 \tag{3.30}$$

Moreover, in the dispersionless case  $\alpha^2 = \lambda^2 T/(\omega_0^2 - \frac{4g}{3\pi}\lambda^2)$ . This expression is valid everywhere except for the small region  $\Delta\lambda \sim \omega_0 T$  below  $\lambda_c \sim \omega_0$ . We consider here a disordered phase solution. In d=3 the disorder solution becomes unstable at  $\lambda \sim \omega_0 - \omega_1$  while it remains stable for all coupling in d=2. The self energies in the strong coupling regime  $\alpha \gg 1$  are given by:

$$\Sigma_{el}(i\omega_n) = \frac{\alpha^2}{\omega_n} \tag{3.31}$$

$$\Sigma_{ph} = -\frac{g\lambda^2}{2\alpha} \tag{3.32}$$

In the strong coupling the phonon field distribution function is split in two peaks.  $2x_0$ , the peak separation is given by  $x_0 = -g\lambda D_0/2$ ,  $D = -\beta x_0^2$ . In the dispersionless case  $\alpha^2 = (\frac{g}{2}\lambda^2/\omega_0^2)^2$ , this is valid when  $\lambda \gg \omega_0$ . This is completely similar to the previous analysis [36].

In d=3 the instability to the ordered phase occurs already at small  $\omega_1 \sim \frac{\omega_0^3}{\beta g^2} \frac{1}{\lambda^2}$ , so  $D_0$  stays practically unrenormalized.

In d=2 at  $\omega_1 \sim \frac{\omega_0^3}{\beta g^2} \frac{1}{\lambda^2}$  the system enters a regime when the phonon energy is exponentially small:

$$\Sigma_{ph} - (\omega_0 - \omega_1)^2 \approx 2\omega_1 \exp\left[-\beta g \frac{\omega_1}{\omega_0^3} \lambda^2\right]$$
 (3.33)

In the limit  $T \to 0$  one readily obtains the polaron formation condition, which happens at intermediate  $(\lambda_c \sim \omega_0)$  coupling:

$$-\frac{4g}{3\pi}\lambda_c^2 D_0 = 1 (3.34)$$

where  $D_0 = \omega_0^{-2}$  in the dispersionless case, but has to be found numerically for interacting phonons.

#### 3.3 3D phonons

In this section we compare our semiclassical solution to the exact QMC results [28]. The saddle point equations we derived are exact when  $(2\pi T)^2 M \omega_0^{-2} \gg 1$  and  $Tt^{-1} \ll 1$ . The QMC results [28] however, were obtained for  $(2\pi T)^2 M \omega_0^{-2} \approx 2.5$  and  $Tt^{-1} \approx 0.13$ . We want to show, that even in these cases when the parameters controlling the saddle point equations are relatively close to 1, the semiclassical solution, even without including the refinements outlined in ref [34] not only captures all the qualitative trends of the exact solution, but in many instances is quantitatively close to it.

We study the case of 3-dimensional phonons. We use the same parameters as in the ref [28]: inverse temperature  $\beta = 8$ , the phonon band is centered at  $\omega_0 = .5$ , electrons have double spin degeneracy g = 2 and hopping amplitude t = 1, phonon mass M = 1. The electron band is half filled. To model 3d phonons semicircular DOS Eq.(3.12) is used. We present the solution of Eqs(3.27,3.28) and Eq(3.17).

In every figure in this section we plot both our and QMC curves. Our results are plotted using solid or dashed lines only, without symbols. QMC graphs are presented using dotted lines and always with symbols.

A local instability, starting from the disordered phase, takes place within EDMFT when as discussed in ref [28] the effective phonon frequency  $\omega^* =$ 

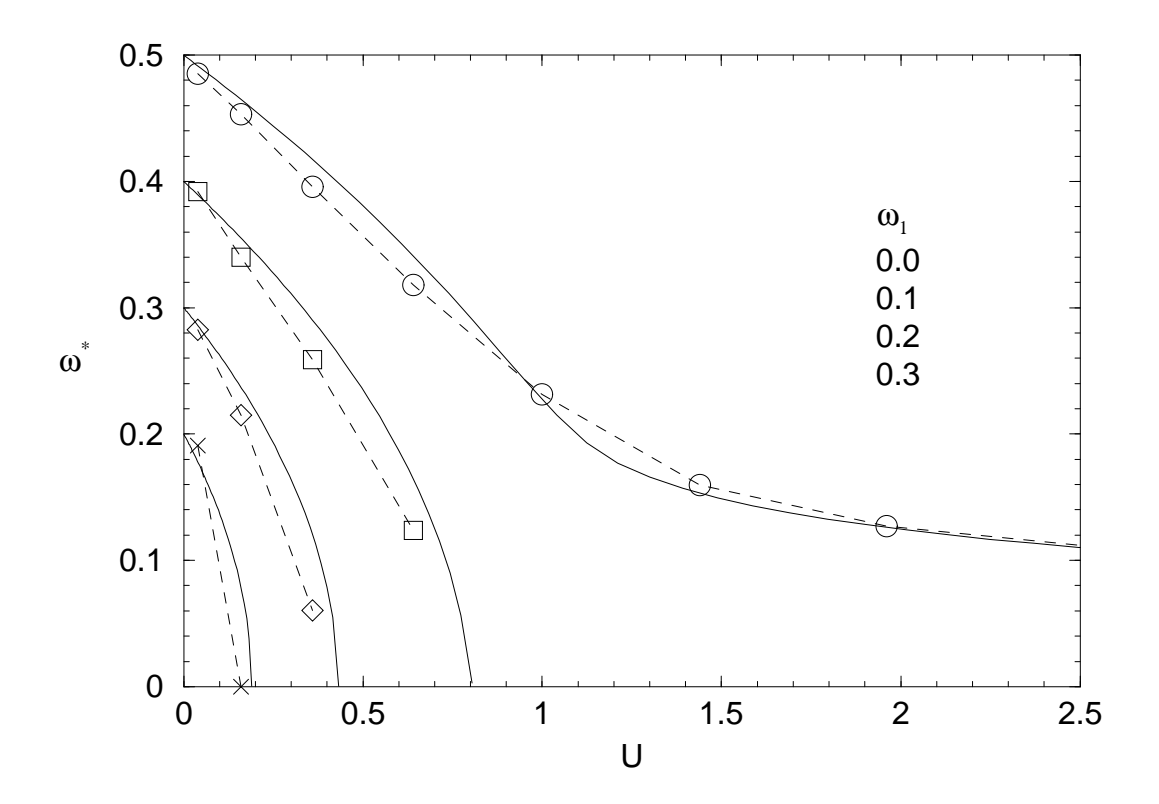


Figure 3.1: d=3. Effective phonon frequency  $\omega^*$  as a function of  $\lambda^2/\omega_0^2$  at  $\omega_1=0.0,0.1,0.2,0.3$ . Comparison to QMC.

 $\sqrt{(\omega_0-\omega_1)^2+\Pi}$ , given by the pole in the phonon Green's function, becomes equal to zero. The phonon mode softening for different values of the phonon dispersion are shown in Fig.(3.1).  $\omega^*$  is plotted versus the quantity characterizing the effective interaction:  $U=\lambda^2/\omega_0^2$ . The effective electron-electron interaction, mediated by phonons is given by  $U_{eff}=\lambda^2 D_0$  evaluated at zero frequency. When the phonon dispersion vanishes  $U_{eff}=U$ . The upper curve in Fig.(3.1) corresponds to the dispersionless case.

On the other hand, we find this is not the best way to detect an instability to an ordered phase and we discuss in the appendix an alternative way to compute within EDMFT the phonon self energy which retains momentum dependence.

The equations in section 3.2 do not include the possibility of the phonon field symmetry breaking. They need to be modified to describe long range ordering [29], and we implement this in section 4.2. A well known property of mean

field theories is that they allow the analytic continuation of mean field solutions beyond the parameter regime where they are stable. This was very fruitful in the understanding of the paramagnetic Mott insulating phase which is unstable to ferromagnetism [30]. As was done by QMC in ref [28], we study the continuation of the EDMFT equations beyond paramagnetic phase. It may hopefully be understood as a metastable phase. This requires some care since the instability to a charge ordered phase is signaled by a singularity appearing in the integrand in Eq(3.15) and this instability causes D to acquire an imaginary part. As in ref [28], we take the principal part of the integrand setting to zero the imaginary part of  $D_0$  in every numerical iteration loop which allow us to compare our results with the results of QMC.

#### 3.3.1 Weak coupling

The finite dispersion treated within DMFT renormalizes  $D_0$  (see Fig.(3.2.a)). Since the effective electron electron interaction is proportional to  $D_0$ , the electron self energy is enhanced as well (see Fig.(3.2.b)). While the features of the exact solution are qualitatively well reproduced in the semiclassical approach, it lacks quantitative agreement. The weak coupling is the worst case. The quantitative agreement is better for intermediate and strong coupling.

# 3.3.2 Strong coupling

In the strong coupling regime as dispersion increases,  $D_0$  renormalizes downward (see Fig(3.3.a)), together with the electron self energy (see Fig.(3.3.b)). For the strong coupling the quantitative agreement with QMC is very good.

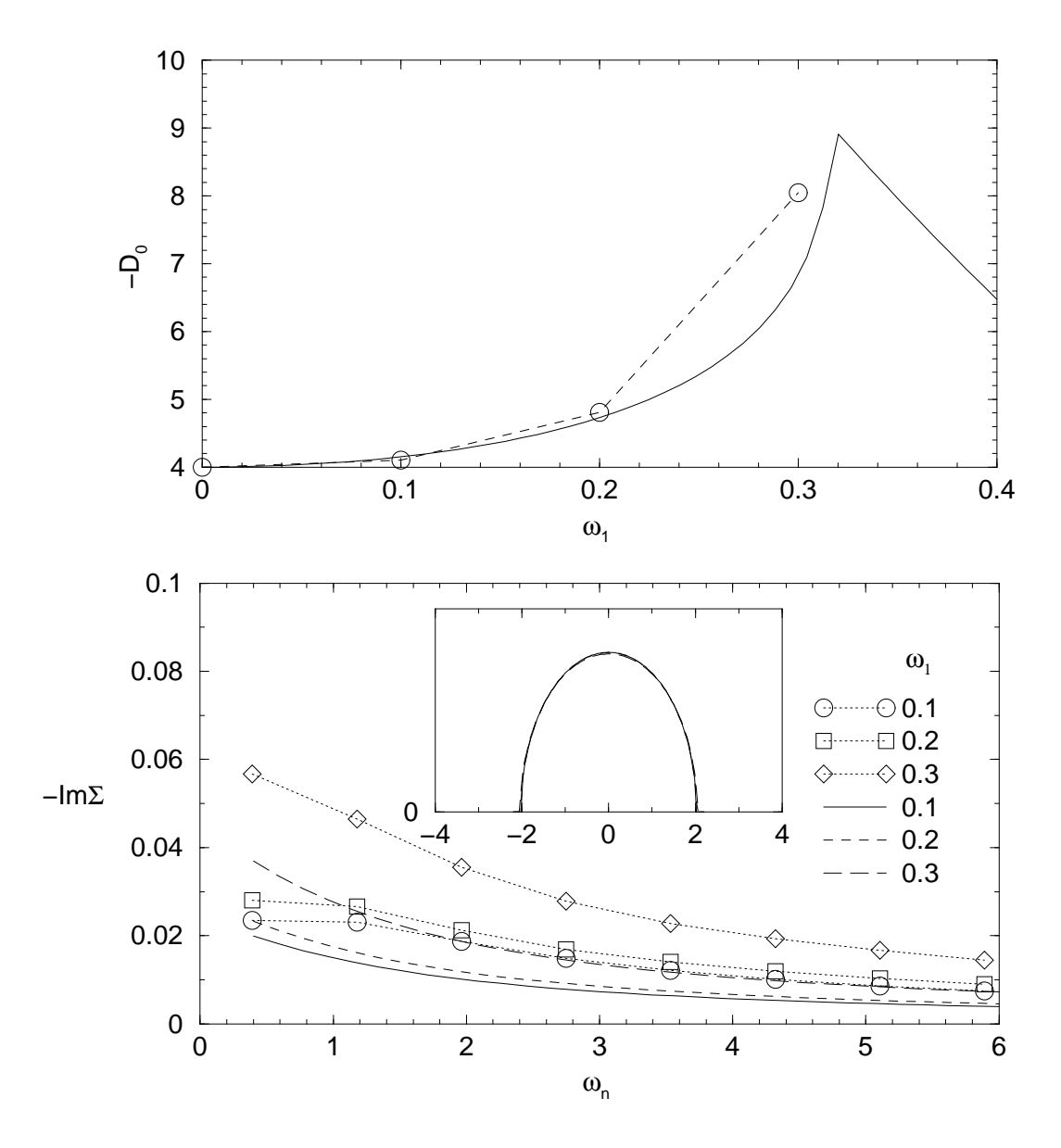


Figure 3.2: d=3. Weak coupling  $\lambda=.2$ . Comparison to QMC. a) The bare phonon greens function. b) The imaginary part of the electron self energy with the spectral function in the inset.  $\omega_1=0.1,0.2,0.3$ .

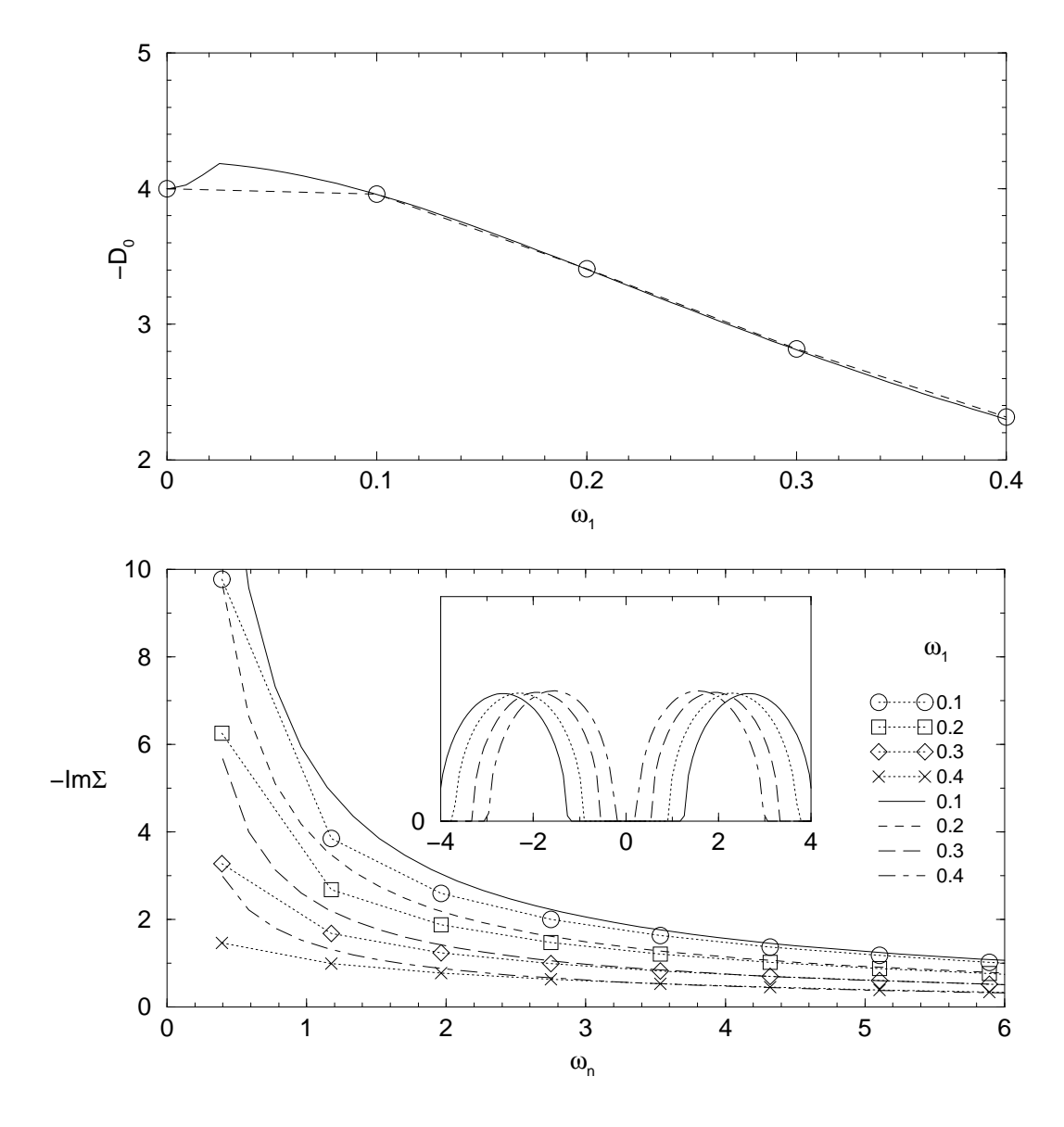


Figure 3.3: d=3. Strong coupling.  $\lambda=.8$ . a) Bare phonon greens function. b) Imaginary part of the electron self energy with the spectral function in the inset.  $\omega_1=0.1,0.2,0.3,0.4$ 

#### 3.3.3 Intermediate coupling

At intermediate coupling system is in a crossover between weak and strong coupling regimes. As  $\omega_1$  increases, effective electron-electron interaction first becomes stronger,  $D_0$  and electron self energy increases, like at weak coupling. At  $\omega_1 = \omega^*$  behavior changes on reverse, the picture is similar to strong coupling case. This is illustrated in Fig.(3.4.a) and Fig.(3.4.b).

#### 3.4 2D phonons

In the previous section we calculated various functions at different parameters in 3D case. The saddle point approximation is exact in the limit of infinite mass M and zero temperature T. At finite M and T the applicability of the method in a wide region of parameters was established in the previous section by comparison to QMC data. In this section we study 2D phonon case (Eqs(3.27,3.28) and Eq(3.18)) in the same range of parameters.

Unlike the 3d case, the 2d disorder solution is locally stable, and we focus on this solution in this section. As we will show in section 4.2 EDMF in dimensions d < 4, gives rise to a first order transition at a critical coupling strength. We study the disordered state solution continued along the second order transition branch, which is skipped in the first order transition.

In the EDMFT approach, d = 2, appears as a lower critical dimension for finite temperature second order transition. This result describes accurately the situation with order parameters possessing a continuous symmetry, but it is a spurious consequence of the inability of a local approximation to generate spatial anomalous dimensions in the cases where order breaks a discrete symmetry.

First we illustrate the exponential softening of the collective mode: in Fig.(3.5) we plot effective frequency  $\omega^*$  versus U. The Fig.(3.5) should be compared to Fig.(3.1) (3D case). In the latter the curves hit U axis, what implies a second

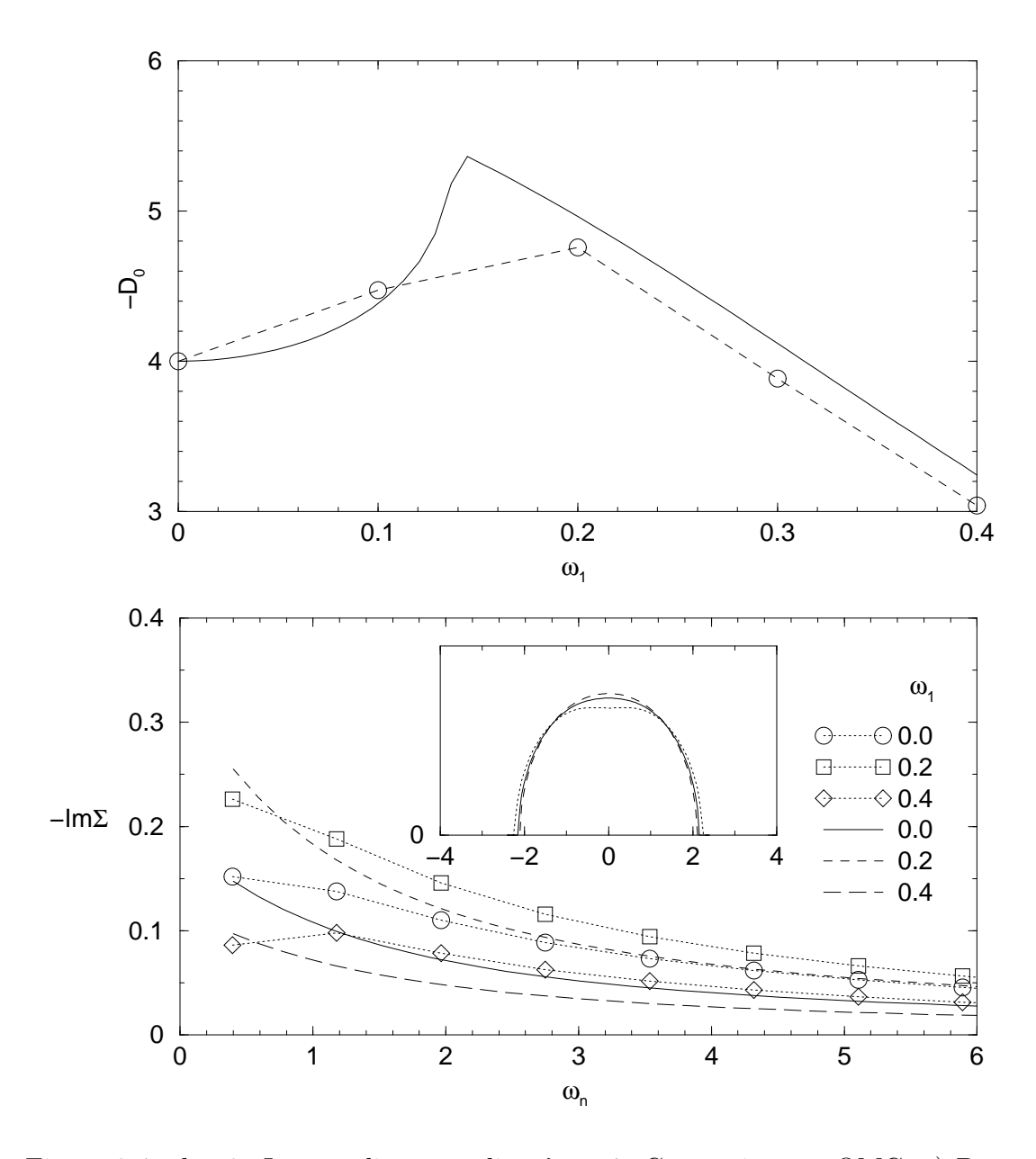


Figure 3.4: d=3. Intermediate coupling  $\lambda=.4$ . Comparison to QMC. a) Bare phonon greens function. b) Imaginary part of the electron self energy with the spectral function in the inset.  $\omega_1=0.0,0.2,0.4$ .

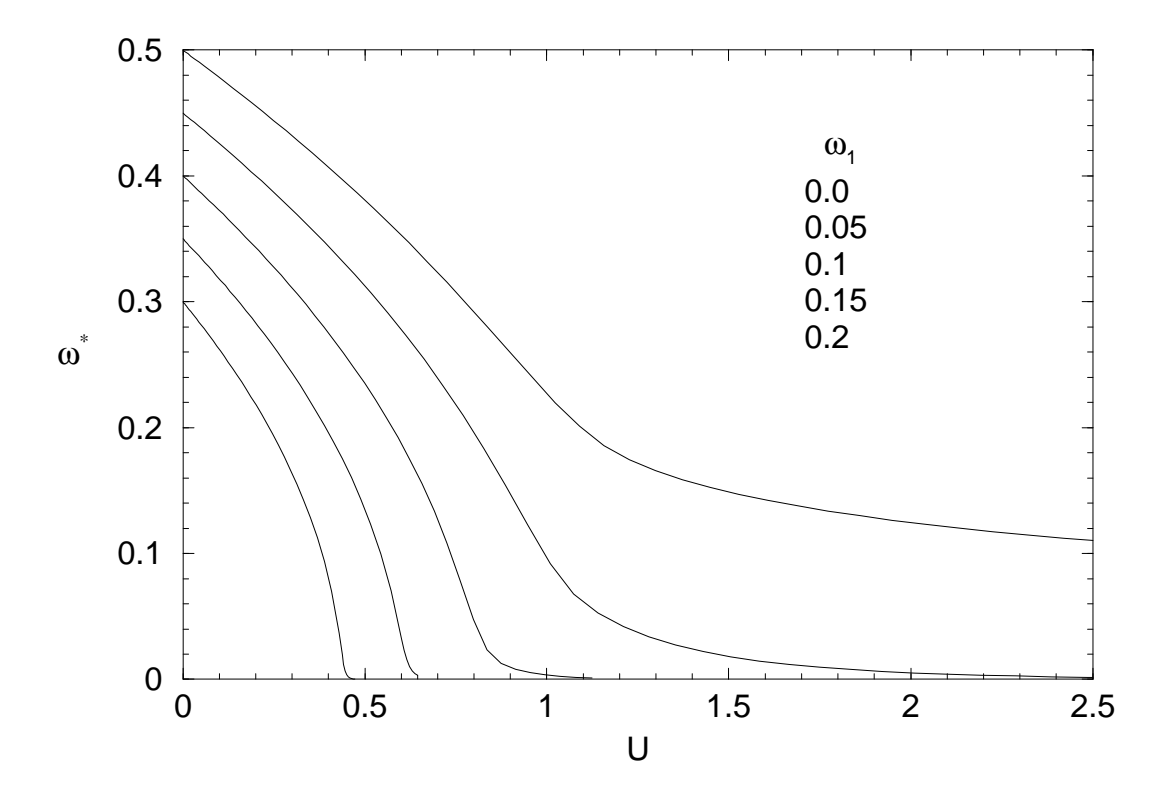


Figure 3.5: d=2. Effective phonon frequency  $\omega^*$  as a function of  $\lambda^2/\omega_0^2$  at  $\omega_1=0.0,0.05,0.1,0.15,0.2$ 

order transition. In Fig.(3.5) the curves rather gradually approach U axis, never crossing it.

Phonons generate effective electron-electron interaction  $\sim \lambda^2 D_0$ , so we are especially interested in  $D_0$  behavior. We investigate 2D system for similar sets of parameters as we did in 3D case.

We obtained the following plots in weak, intermediate and strong coupling regimes:

The behavior of 2D system is very similar to that of 3D system before the energy of the phonon mode vanishes. In all cases  $D_0$  gets renormalized, as the dispersion, and consequently the effective interaction, increases. The electron self energy enhances correspondingly. The only difference is the rate of  $D_0$  renormalization in the weak, strong and intermediate coupling.  $D_0$  renormalizes faster at larger  $\lambda$  (see Fig.(3.9)), since electrons are stronger coupled to phonons.

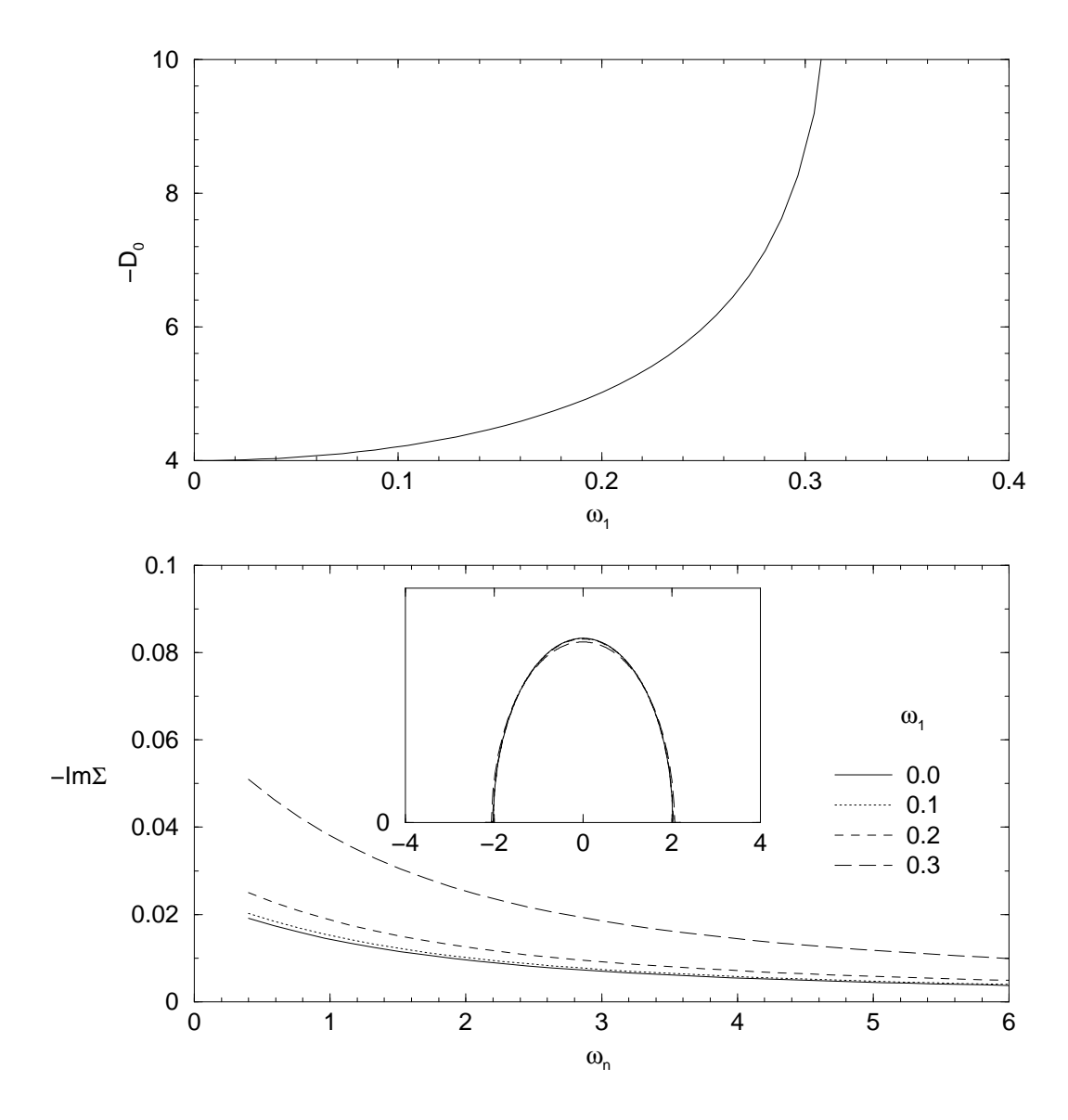


Figure 3.6: d=2. Weak coupling.  $\lambda=.2$ . a) The bare phonon greens function. b) The imaginary part of the electron self energy with the spectral function in the inset.  $\omega_1=0.0,0.1,0.2,0.3$ .

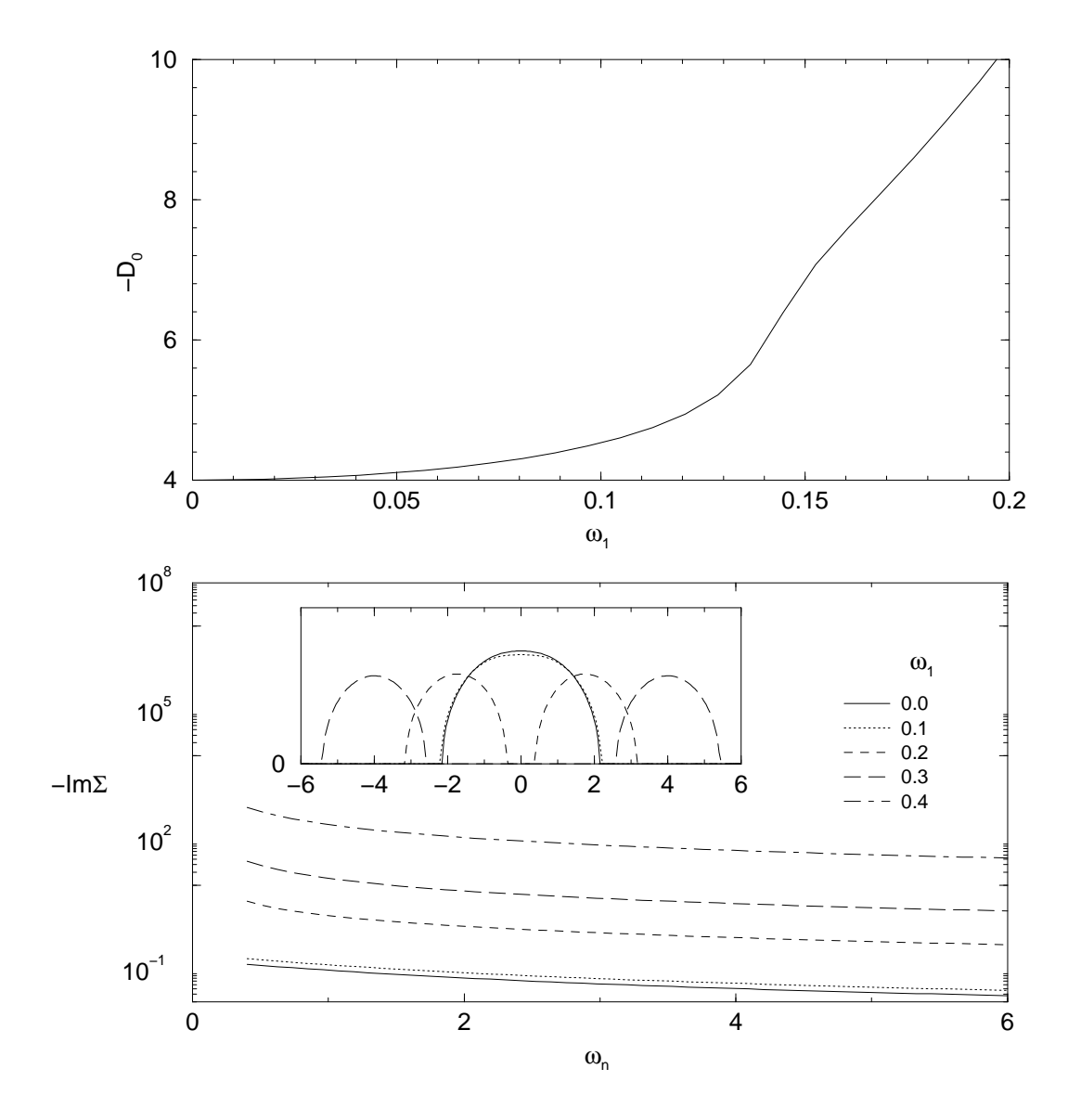


Figure 3.7: d=2. Intermediate coupling.  $\lambda=.4$ . a) The bare phonon greens function. b) The imaginary part of the electron self energy with the spectral function in the inset.  $\omega_1=0.0,0.1,0.2,0.3,0.4$ 

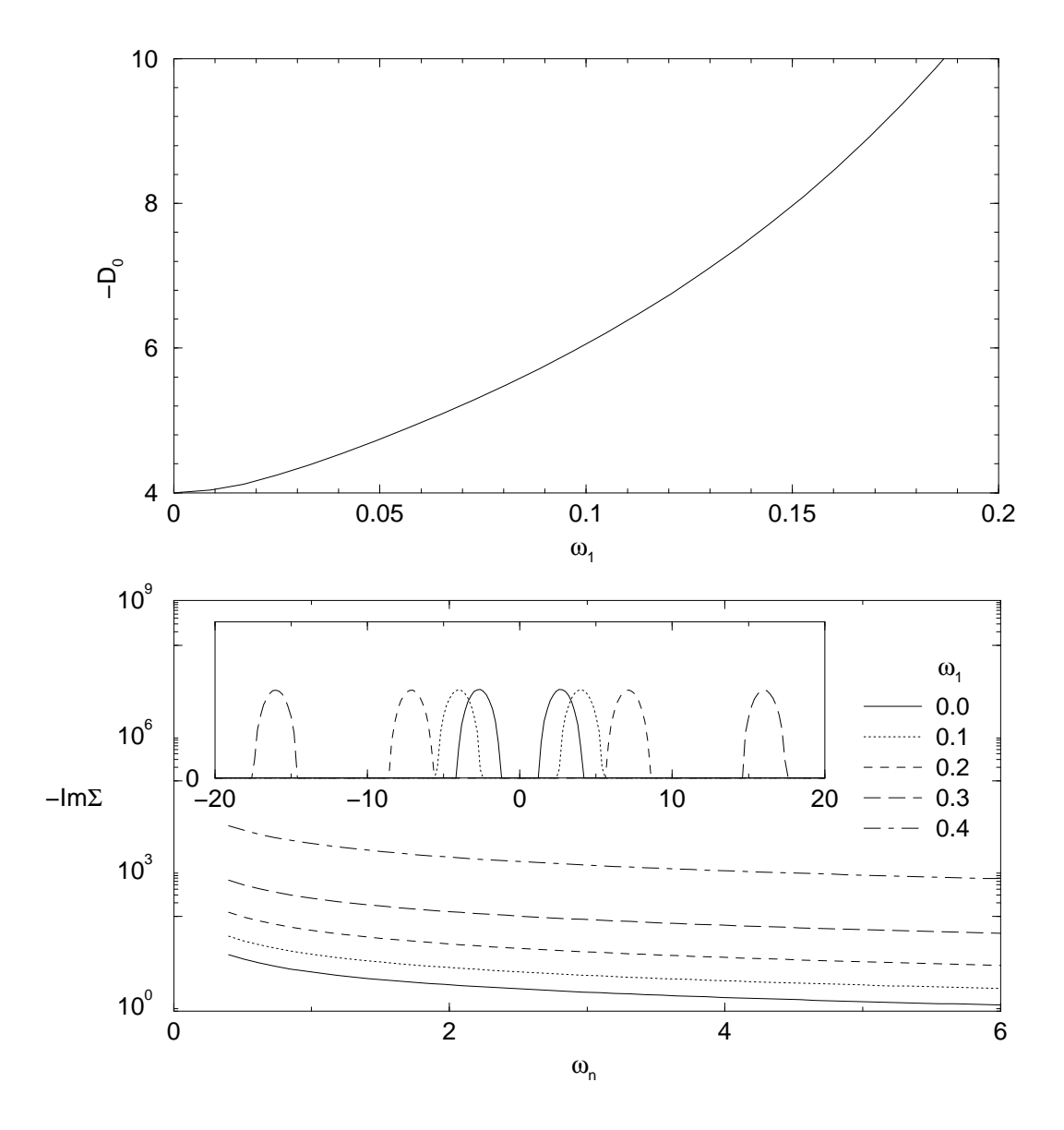


Figure 3.8: d=2. Strong coupling.  $\lambda=.8$ . a) The bare phonon greens function. b) The imaginary part of the electron self energy with the spectral function in the inset.  $\omega_1=0.0,0.1,0.2,0.3,0.4$ 

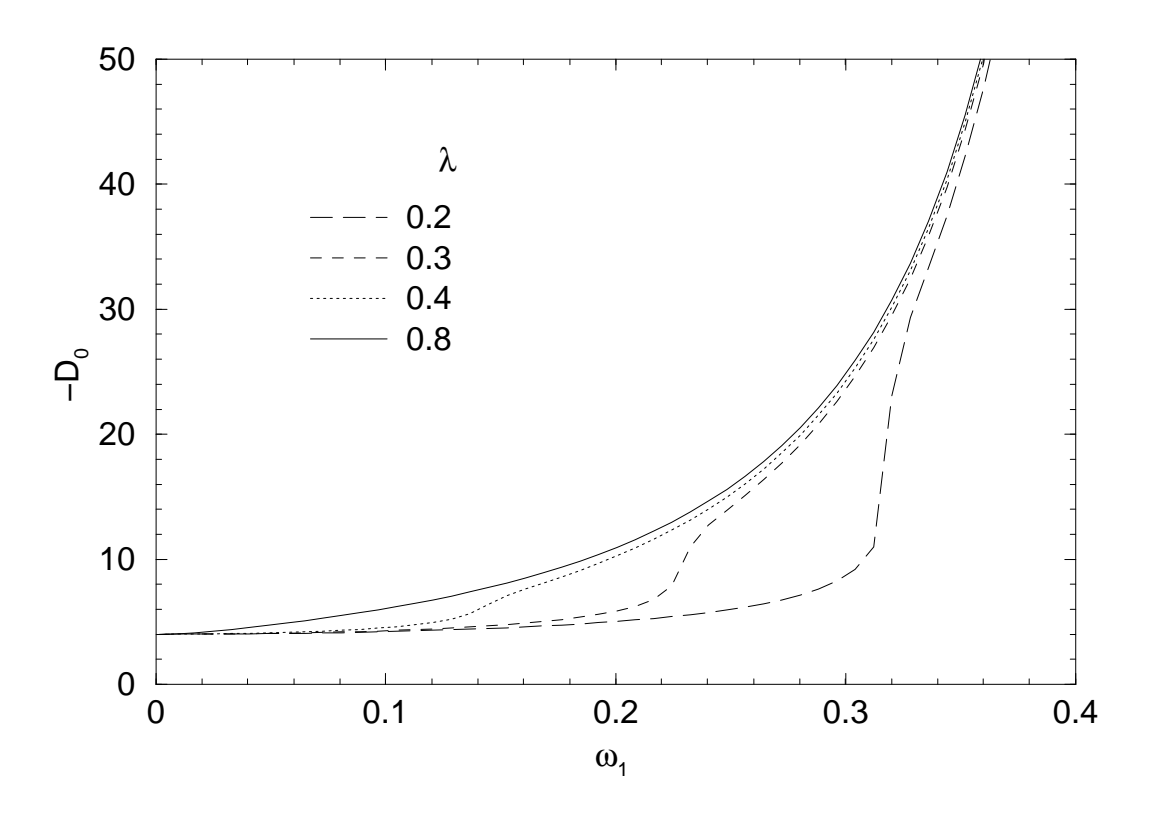


Figure 3.9: d=2. Bare phonon greens function.  $\lambda=.2,.3,.4,.8$ 

# Chapter 4

# Functional approach to EDMFT

#### 4.1 Intro to functional formulation of the EDMFT

In this chapter we adopt a different point of view on DMFT, we will consider it as a local approximation on the free energy functional. The history of using free energy functionals for formulating various approximations goes back to the work of Baym and Kadanoff [41], after whom those functionals are named. The functional approach is a convenient tool to systematize and compare different approximations. It also guarantees that a given approximation is going to preserve certain conservation laws and certain sum rules.

The Baym Kadanoff functional can be written in terms of variables which are important for a current problem. One first inserts in the action the source fields coupled to those variables and then perform the Legender transformation with respect to these variables. We illustrate this in detail below, using as an example  $\phi^4$  theory. The source dependent action reads:

$$S[\phi] = \frac{1}{2}D_0^{-1}\phi^2 + \frac{U}{4!}\phi^4 + \frac{J}{2}\phi^2$$
 (4.1)

where  $D_0^{-1}$  is the free theory propagator, U is the repulsive interaction and J/2 is the source field. The summation over the space and time coordinates is understood in Eq.(4.1), but is omitted for simplicity. The partition function of the system is given by:

$$Z = \int \mathcal{D}\phi e^{-S[\phi]} \tag{4.2}$$

The integration in Eq.(4.2) is performed over different field configurations. The

free energy is defined as:

$$W = -\ln Z \tag{4.3}$$

The source dependent free energy is a generating functional for correlation functions:

$$D = \langle \phi^2 \rangle = 2 \frac{\delta W}{\delta J} \tag{4.4}$$

The Baym Kadanoff functional is defined as a Legendre transform:

$$\Gamma_{BK} = W - \frac{1}{2}JD \tag{4.5}$$

It is easy to check that the variation with respect the propagator is equal to the source field:

$$\frac{\delta\Gamma}{\delta D} = -\frac{1}{2}J\tag{4.6}$$

We see that at stationarity the source field must vanish and the functional becomes the exact free energy of the system. The propagator and the source filed D and J are related to each other through Eq.(4.4). This relations has to be inverted and the functional has to be written in terms of the correlation functions D only, before it can be of any use. The inversion can be done order by order in U. We will do it in a slightly different way. Let us write the Dyson equation:

$$J = D^{-1} - D_0^{-1} + \Sigma \tag{4.7}$$

where  $\Sigma$  is the self energy. Using this equation we cast the action in a slightly different form:

$$S[\phi] = \frac{1}{2}D^{-1}\phi^2 + \frac{\Sigma}{2}\phi^2 + \frac{U}{4!}\phi^4$$
 (4.8)

Now the Baym Kadanoff functional can be written as:

$$\Gamma_{BK} = -\frac{1}{2} \ln D + \frac{1}{2} D(D_0^{-1} - D^{-1}) - \frac{1}{2} \Sigma D - \Phi_1$$
 (4.9)

where the functional  $\Phi_1$  is the sum of all vacuum graphs constructed from the propagator D and two and four point vertices  $\Sigma$  and U respectively. The diagrammatic representation of the functional  $\Phi_1$  up to the second order is depicted in

$$\mathbf{\Phi}_1 = \mathbf{\Phi} + \mathbf{\Phi}$$

Figure 4.1: Diagrammatic expansion of  $\Phi_1$  up to the second order.  $\Sigma$  and U are denoted by a cross and a dot respectively

the Fig.4.1: The second graph in Fig.4.1 cancels the term  $-\Sigma D$  in Eq.(4.9). One can understand that in the all other graphs the vertex  $\Sigma$  acts like a counterterm for two particle reducible (2PR) insertions, which are constructed from U vertex, by canceling those insertions in each order. We demonstrate this explicitly by computing the symmetry factors for the diagrams shown in Fig.4.1:

$$\Phi_1 = -\frac{1}{8}U - \frac{1}{2}\Sigma D + \frac{1}{48}\Sigma D + \frac{1}{4}\Sigma^2 D^2 + \frac{1}{4}U\Sigma D^3 + \frac{1}{16}U^2 D^2 + \dots$$
 (4.10)

The self energy expansion to the second order reads:

$$\Sigma = -\frac{U}{2}D + \frac{1}{6}U^2D^3 \tag{4.11}$$

From Eq.(4.10) and Eq.(4.11) we find that the last three terms in  $\Phi_1$  indeed cancel out in first two orders. Eventually only two particle irreducible graphs (2PI) are left in  $\Phi_1$  and  $\Gamma_{BK}$  can be written as:

$$\Gamma_{BK} = -\frac{1}{2} \ln D + \frac{1}{2} D(D_0^{-1} - D^{-1}) + \Phi$$
 (4.12)

where  $\Phi$  includes all 2PI vacuum graphs taken with an overall minus sign. In a similar way one can derive the free energy functional for other theories, including those with broken symmetries.

#### 4.2 Ordered Phase and Critical Temperature

We now turn to the generalization of the EDMFT equations to the ordered phase [29]. For simplicity we will consider a classical model. This is justified, since in the semiclassical limit we can always integrate out the electrons, reducing EDMFT equations to classical mean field equations. For instance tracing out the electrons and performing a static approximation in the electron-phonon field leaves us with an action of the form ( neglecting terms of order  $\phi^6$  and higher):

$$S[\phi] = \sum_{i} \frac{r}{2} \phi_i^2 + \frac{U}{4} \phi_i^4 - \sum_{ij} \phi_i \frac{J_{ij}}{2} \phi_j = S_{loc}[\phi] - \sum_{ij} \phi_i \frac{J_{ij}}{2} \phi_j$$
 (4.13)

To extend the EDMFT approach to the ordered phase it is useful to write down the Baym Kadanoff functional for the action,

$$\Gamma[m, D] = -\frac{1}{2} \operatorname{Tr} \log D + \frac{1}{2} \operatorname{Tr} (D_0^{-1} - D^{-1}) D + \frac{1}{2} m D_0^{-1} m + \Phi[m, D]$$
 (4.14)

 $\Phi$  is a sum of all two particle irreducible diagrams constructed from phonon Green's functions D, phonon field expectation value m and four legged interaction vertex -3!U. We could also say that  $\Phi$  is a sum of all two particle irreducible diagrams constructed from phonon Green's functions D and four, three, two legged vertices plus the first diagram shown in figure (4.2), which contains no propagators. The vertices yield factors of -3!U, -3!Um,  $-3Um^2$  and  $-\frac{1}{4}Um^4$  for four, three, two and zero legged vertices respectively. Each diagram in  $\Phi$  has an extra -1 factor.

In the Fig(4.2) we drew first and second order (in U) diagrams entering  $\Phi$ . The extended DMFT equations in the ordered phase are derived by making the local approximation on  $\Phi$  in the Baym Kadanoff functional and solving the stationary conditions for the magnetization and the local propagator resulting from the stationarity of Eq.(4.14) after this local approximation is made. In the local approximation the leading terms in a perturbative expansion in the quartic

Figure 4.2: Diagrammatic expansion of  $\Phi$  up to the first two orders in U

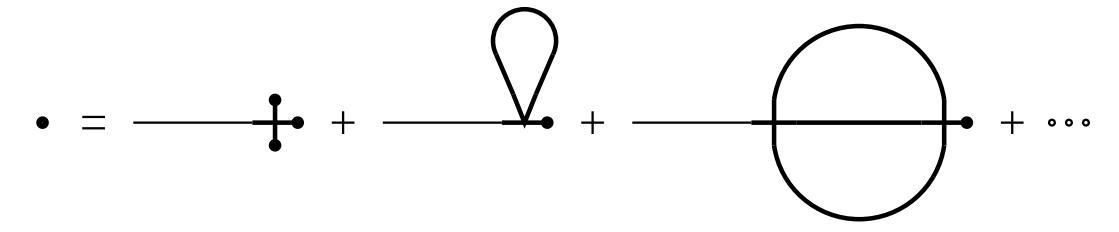


Figure 4.3: Diagrammatic expansion of m up to the first two orders in U. A thin line is the free phonon propagator  $D_0$ , a thick line is the full phonon propagator. A full dot stands for m.

coupling are given by 
$$\Phi = \frac{1}{4}Um^4 + \frac{3}{2}UDm^2 + \frac{3}{4}UD^2 - 3U^2D^3m^2 - \frac{3}{4}U^2D^4 + \dots$$

Stationarity of the functional in Eq.(4.14) would give exact equations for D and m. In the local approximation these equations reduce to EDMFT equations in zero magnetization and therefore generalize those to the ordered phase [29]. They are given by

$$m(r - J_{q=0}) + \frac{\delta\Phi}{\delta m} = 0$$

$$D = \sum_{q} [r - J_q + 2\frac{\delta\Phi}{\delta D}]^{-1}$$
(4.15)

where only local graphs are included in  $\Phi$ . Diagram series equivalent to the first equation are shown in Fig.(4.3).

For the practical solution of the EDMFT Eqs.(4.15) , it is useful to follow the dynamical mean field procedure of introducing an impurity local effective action [2, 30] to sum up the graphs generated by the functional for  $\Phi$  and its functional derivatives  $\delta\Phi/\delta D$  and  $\delta\Phi/\delta m$  in terms of the cavity fields h and  $\Delta$ . The effective action

$$S_{EDMFT}[\phi] = S_{loc}[\phi] - h\phi - \frac{\Delta}{2}\phi^2$$
(4.16)

generates the correct local quantities provided that the Weiss fields h and  $\Delta$  are chosen to obey the EDMFT self consistency conditions:

$$r - \Delta - D^{-1} = -2\frac{\delta\Phi}{\delta D} \tag{4.17}$$

$$h = -m(r - \Delta) - \frac{\delta\Phi}{\delta m} \tag{4.18}$$

Eqs.(4.15) and Eqs.(4.17,4.18) are a closed set of EDMFT equations, describing both ordered and disordered phase of the classical system Eq(4.13):

$$D = \sum_{q} [D^{-1} + \Delta - J_q]^{-1}$$
(4.19)

$$S_{EDMFT}[\phi] = S_{loc}[\phi] - m \left(J_{q=0} - \Delta\right) \phi - \frac{\Delta}{2} \phi^2$$
 (4.20)

$$m = \langle \phi \rangle_{S_{EDMET}} \tag{4.21}$$

$$D = \langle \phi^2 \rangle_{S_{EDMFT}} - m^2 \tag{4.22}$$

The equations above are consistent in describing the transition: magnetization vanishing in the ordered phase, and divergence of spin susceptibility across the transition do occur at the same critical temperature. This is not surprising, since the EDMFT equations can be derived from the approximation to the free energy functional. We will argue below that the magnetic ordering transition for d < 4 is actually the first order. This is an artifact of EDMFT, and one needs to compare free energy in different extrema to find a correct first order transition

temperature. For this purpose we show how free energy can actually be computed from the impurity model.

The source dependent impurity action reads:

$$S_{imp}[\phi] = S_{loc}[\phi] - (h + \tilde{h})\phi - \frac{1}{2}(\Delta + \tilde{\Delta})\phi^2$$
(4.23)

The corresponding Baym Kadanoff functional of the impurity model is a Legendre transform of the impurity free energy  $W_{imp}$ , which is performed with the fields  $-\tilde{h}$  and  $-\tilde{\Delta}$ :

$$\Gamma_{imp}[m, D] = W_{imp}[\tilde{h}, \tilde{\Delta}] + \tilde{h}m + \frac{1}{2}\tilde{\Delta}(D + m^2) = -\frac{1}{2}\log D + \frac{1}{2}D_{0imp}^{-1}D + \frac{1}{2}mD_{0imp}^{-1}m + \Phi[m, D]$$
 (4.24)

The local correlation functions D and m in the impurity model and in lattice EDMFT approximation are the same, so  $\Phi$  in Eq.(4.14) and Eq.(4.24) coincide. This allows us to express  $\Gamma$  in terms of the impurity free energy  $W_{imp}$ :

$$\Gamma = W_{imp}[\tilde{h}, \tilde{\Delta}] - \frac{1}{2} \text{Tr} \log D + \frac{1}{2} \text{Tr} (D_0^{-1} - D^{-1}) D + \frac{1}{2} \log D$$
$$- \frac{1}{2} (D_{0imp}^{-1} - D^{-1}) D + \frac{1}{2} m (D_{0k=0}^{-1} - D_0^{-1}) m + (h + \tilde{h}) m + \frac{1}{2} \tilde{\Delta} (D + m^2) \quad (4.25)$$

At the saddle point

$$\frac{\delta\Gamma}{\delta D} = \frac{1}{2} \left[ \sum_{k} (D_{0k=0}^{-1} - D_{k}^{-1}) + (D^{-1} - D_{0}^{-1}) \right] + \frac{1}{2} \tilde{\Delta}$$

$$\frac{\delta\Gamma}{\delta m} = m(D_{0k=0}^{-1} - D_{0}^{-1}) + h + \tilde{h}$$
(4.26)

at zero source fields we recover the EDMFT equations. At the stationarity the expression for the free energy in Eq.(4.25) simplifies to:

$$\Gamma = W_{imp} + \frac{1}{2} \sum_{k} \log(D^{-1} + \Delta - J_k) + \frac{1}{2} \log D + \frac{1}{2} (\Delta - J_{k=0}) m^2 + hm \quad (4.27)$$

This result is an extension of the free energy formula to the ordered phase [7].

When  $U \to \infty$ ,  $r \to -\infty$ , U/r = -1 the system, described by the action Eq(4.13) reduces to a classical Ising model with spin values  $\pm 1$ . In this limit the standard Weiss mean field equations

$$m = \tanh m J_{q=0} \tag{4.28}$$

can be compared with the EDMFT equations which now read:

$$m = \tanh m \left( J_{q=0} - \Delta \right)$$

$$1 - m^2 = \sum_{q} \left[ (1 - m^2)^{-1} + \Delta - J_q \right]^{-1}$$
(4.29)

We will also compare the EDMFT equations to an extension of mean field theory due to Bloch and Langer (BL) [37]:

$$M_1 = \int_{-\infty}^{+\infty} dx (2\pi G_2)^{-\frac{1}{2}} \exp\left[-\frac{(M_1 J_{q=0} - x)^2}{2G_2}\right] \tanh x \tag{4.30}$$

$$M_2 = \int_{-\infty}^{+\infty} dx (2\pi G_2)^{-\frac{1}{2}} \exp\left[-\frac{(M_1 J_{q=0} - x)^2}{2G_2}\right] (\cosh x)^{-2}$$
 (4.31)

$$G_2 = \sum_{q} \frac{J_q}{1 - J_q M_2} \tag{4.32}$$

where  $M_1$  is the magnetization. It can be shown that EDMFT counts (without overcounting) more terms in diagrammatic expansion of various physical quantities, like correlation function or free energy, than BL method does. One can also check that for the classical  $\pm 1$  spin model EDMFT gives a better estimate for  $T_c$  than BL method does.

# 4.3 Numerical analysis

We computed the critical temperature  $T_c$  for the Ising model on a Bethe lattice with finite coordination following the paramagnetic solution till it disappears

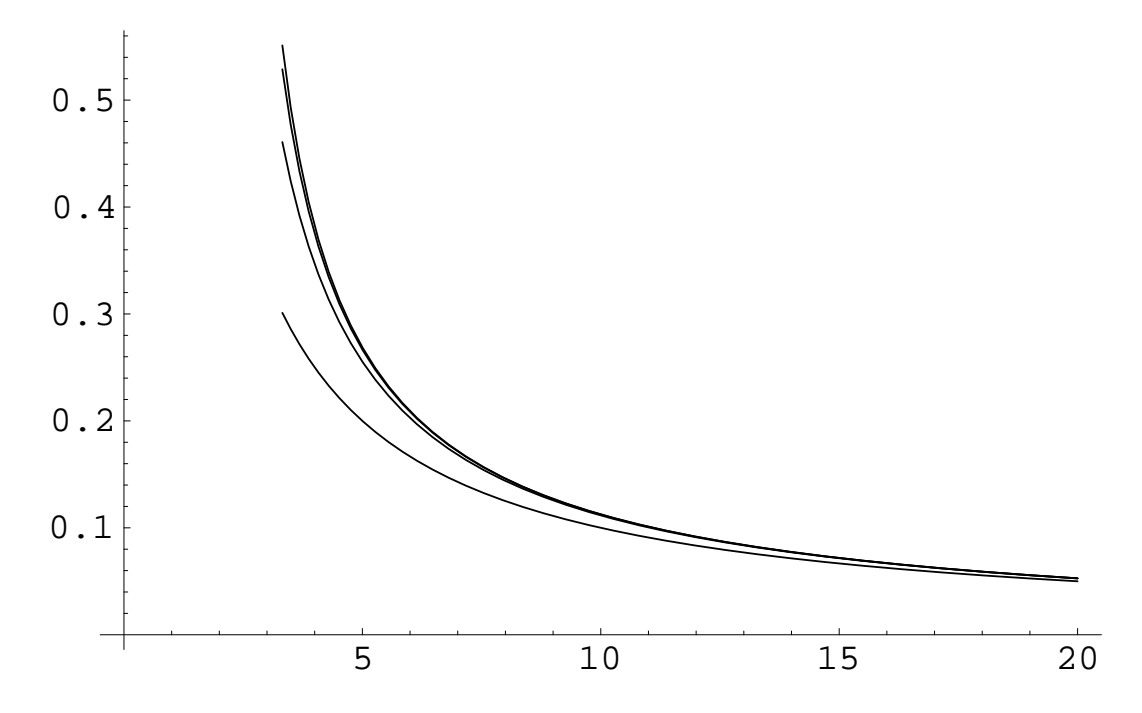


Figure 4.4: Top to bottom: BL, EDMFT, exact solution, MFT; Critical  $J_c$  (vertical axis) vs nearest neighbors number z (horizontal axis)

using the different approximations described in this section. The results are shown in Fig(4.4). The EDMFT result shows significant improvement over MFT, and is slightly better than BL method. Some more technical details comparing the approximation schemes are relegated to Appendix A.1.

In spite of the quantitative improvement of  $T_c$ , the order of the transition is incorrectly given by the EDMF approximation. In Fig(4.5) we present result of solving EDMFT equations for the simplest  $\pm 1$  spin model in d=3. We plotted magnetization as a function of temperature. At sufficiently low temperature the solution consists of three branches with magnetizations  $m_3 > m_2 > m_1 = 0$ . These branches are extrema of the free energy, which is shown schematically in Fig.(4.6).  $m_3$  and  $m_1$  correspond to local minima in the free energy, while  $m_2$  corresponds to a local maximum and is unphysical. The transition is clearly of the first order. The order of the transition does not change up to d=4.

The Fig.4.6 is only a caricature of the actual free energy, drawn out of scale to simplify the perception. The free energy in the limit of classical spins is given

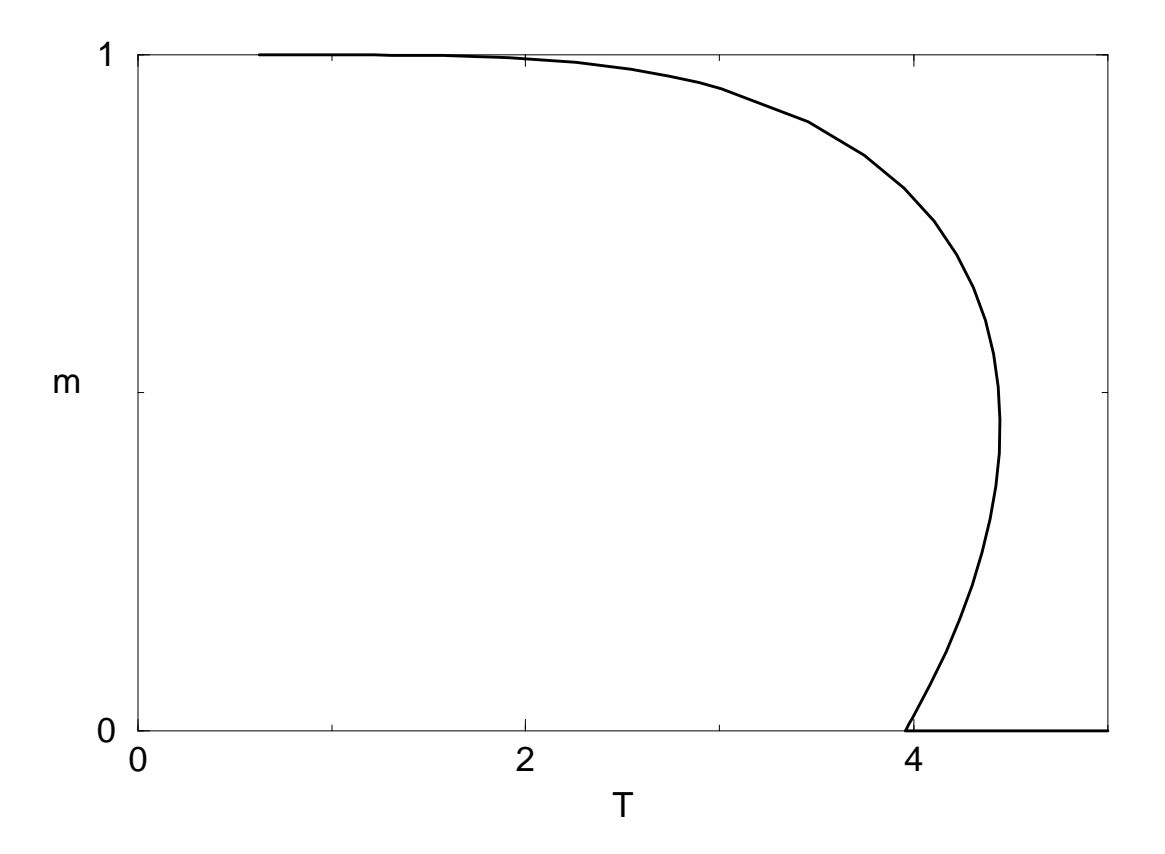


Figure 4.5: Magnetization vs. temperature on a cubic lattice. There are three branches at 3.96 < T < 4.45:  $m_3 > m_2 > m_1 = 0$ ,  $m_1$  and  $m_3$  are physical solutions, while  $m_2$  is not. Classical  $\pm 1$  spin Ising model.

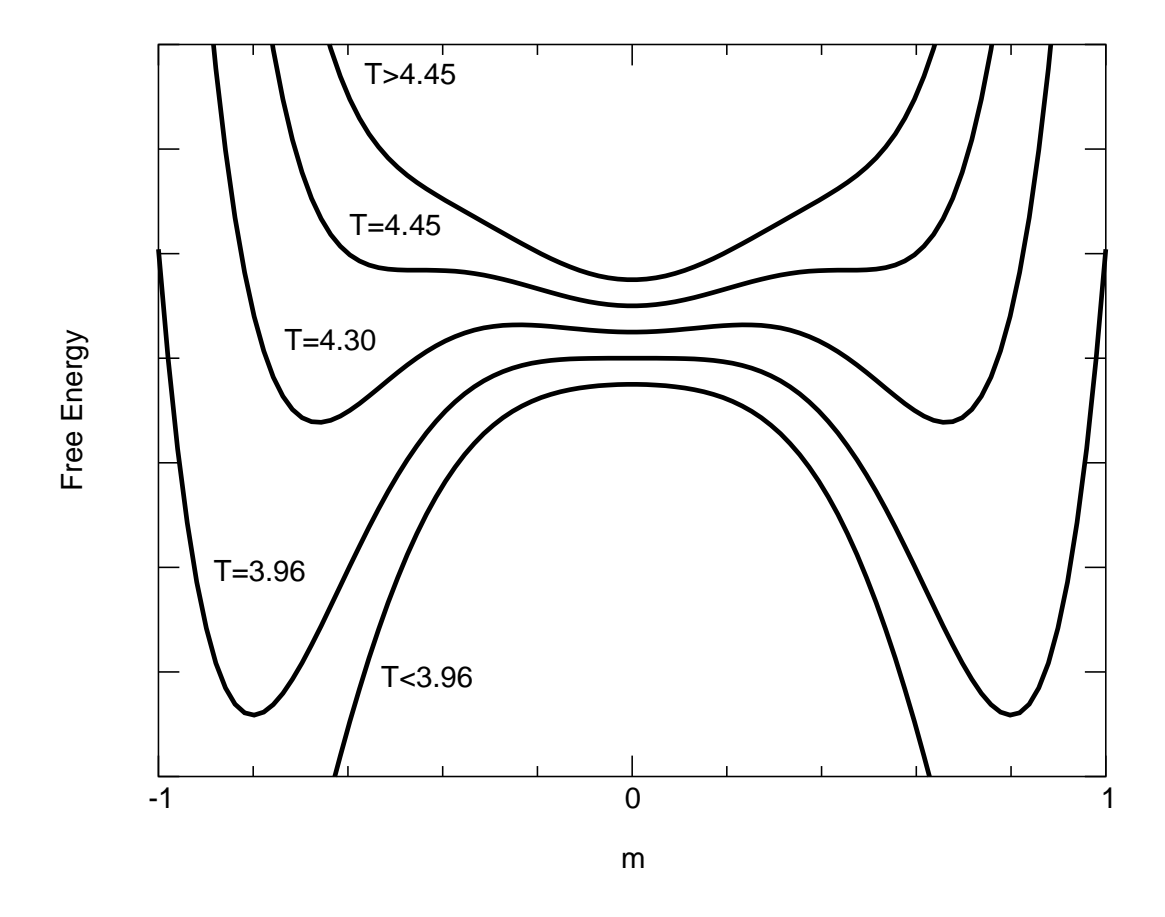


Figure 4.6: Free energy evolution with T. Free energy has a single minimum (m=0) above T=4.45; at T=4.45 the solution bifurcates at m=.45. There are free extrema at 3.96 < T < 4.45 corresponding to 0=m1 < m2 < m3. As T approaches  $T_c=3.96$ , m2 merges with m1.

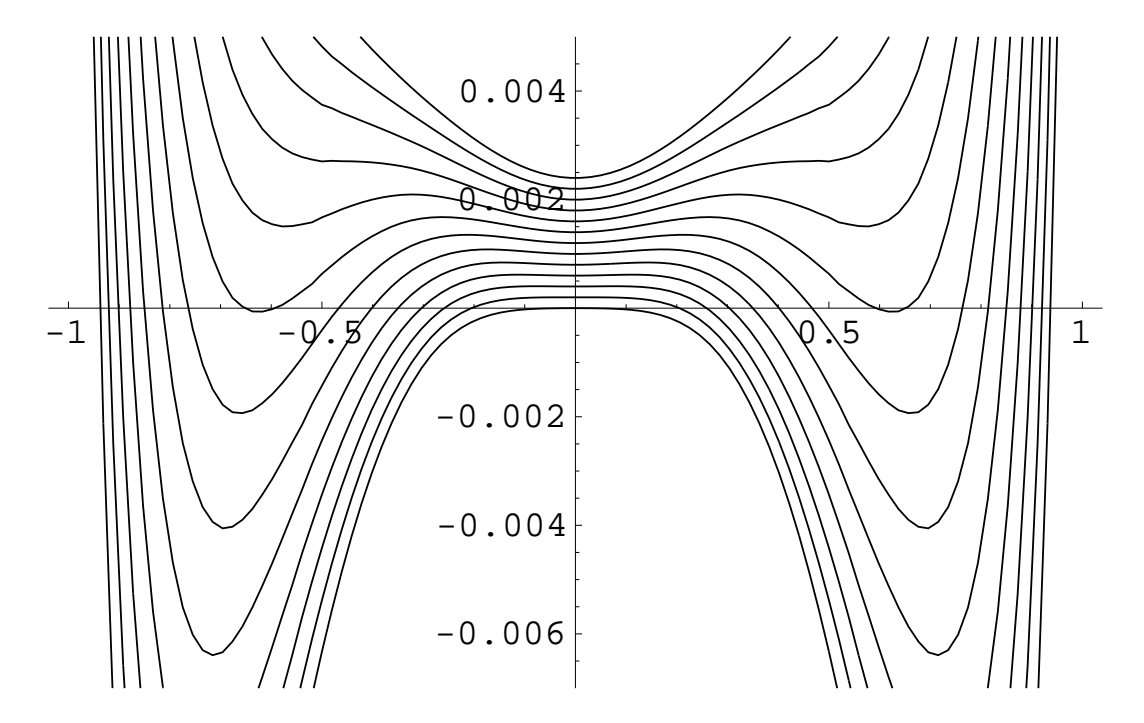


Figure 4.7: Evolution of the free energy with temperature in the classical Ising spin model. Curves, bottom to top, are plotted in the temperature interval from 4.00 to 4.60 with the step 0.05. Curves are shifted for convenience.

by:

$$\Gamma = \frac{1}{2} \sum_{k} \log((1 - m^2)^{-1} + \Delta - J_k) + \log(1 - m^2) + m \tanh^{-1} m - \frac{1}{2} \Delta (1 - m^2) - \frac{1}{2} J_{k=0} m^2 \quad (4.33)$$

In the Figure 4.7 we plotted free energy of the 3d classical Ising spin model solved in EDMFT setup. One can see how the triple minimum feature evolves across the transition, and that the extremal point indeed correspond to the solution of EDMFT equations, plotted in Fig. 4.5. The free energy curves corresponding to different temperatures are shifted for convenience, actual curves are more separated.

The inability of EDMFT to predict the correct order of the transition is related to the inability of a local theory to produce anomalous dimensions, and persists in quantum problems when the dynamical critical exponent and the dimensionality are such that they require the introduction of spatial anomalous dimensions.

# Critical T in the soft spin Ising model.

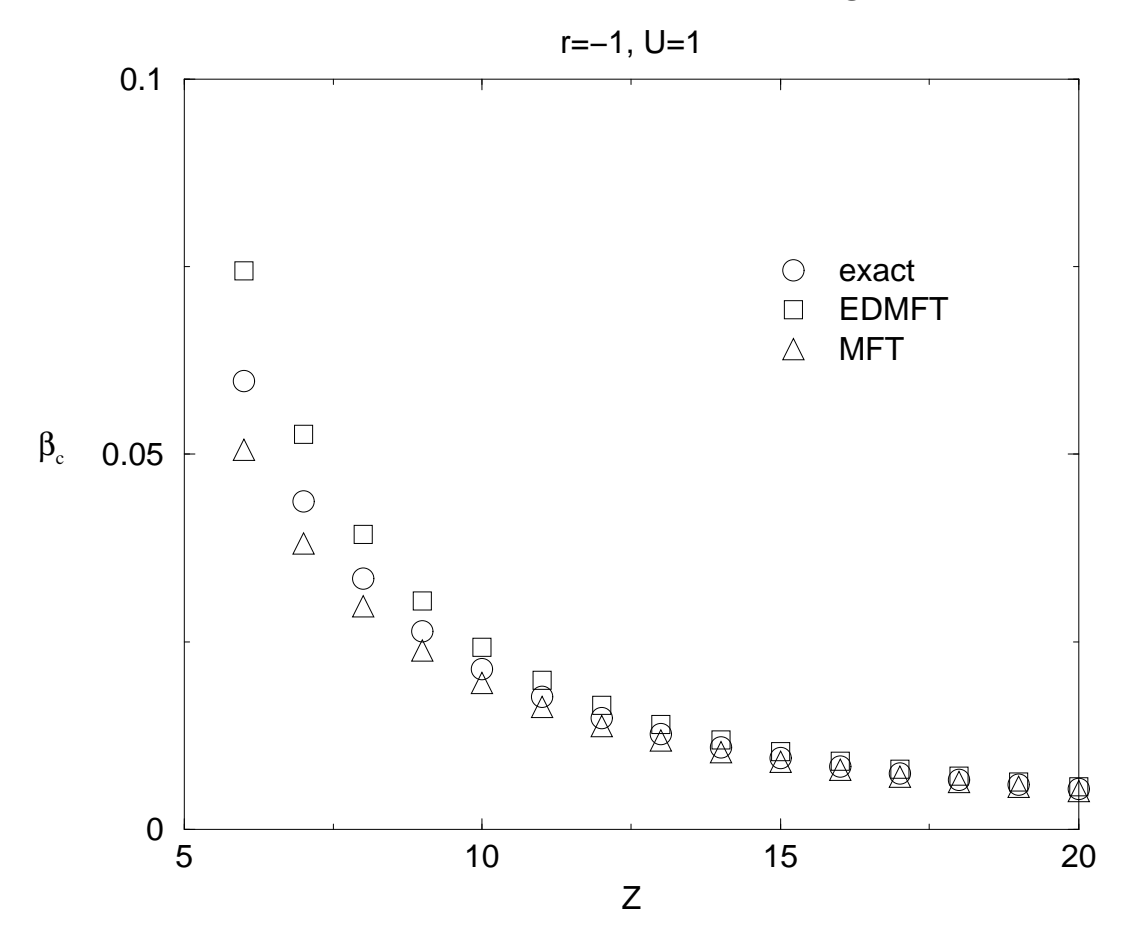


Figure 4.8: Soft spins, -r = U = 1. Inverse temperature is plotted verses the coordination number.

Details are given in Appendix A.2.

In the end of this section we present results of the solving soft spin EDMFT equations. The purpose of this is twofold: first we demonstrate that the limit of classical spins was taken correctly, and second, we would like to demonstrate the performance of EDMFT in comparison to MFT and exact solution. As can be seen form the set of figures Fig.4.8-Fig.4.11, for soft spins, in the regime  $r, U \approx J$ , EDMFT overestimate  $T_c$ , as much as MFT underestimates it. It is also obvious that in the limit  $r, U \gg J$  we recover the case of previously studied classical spins.

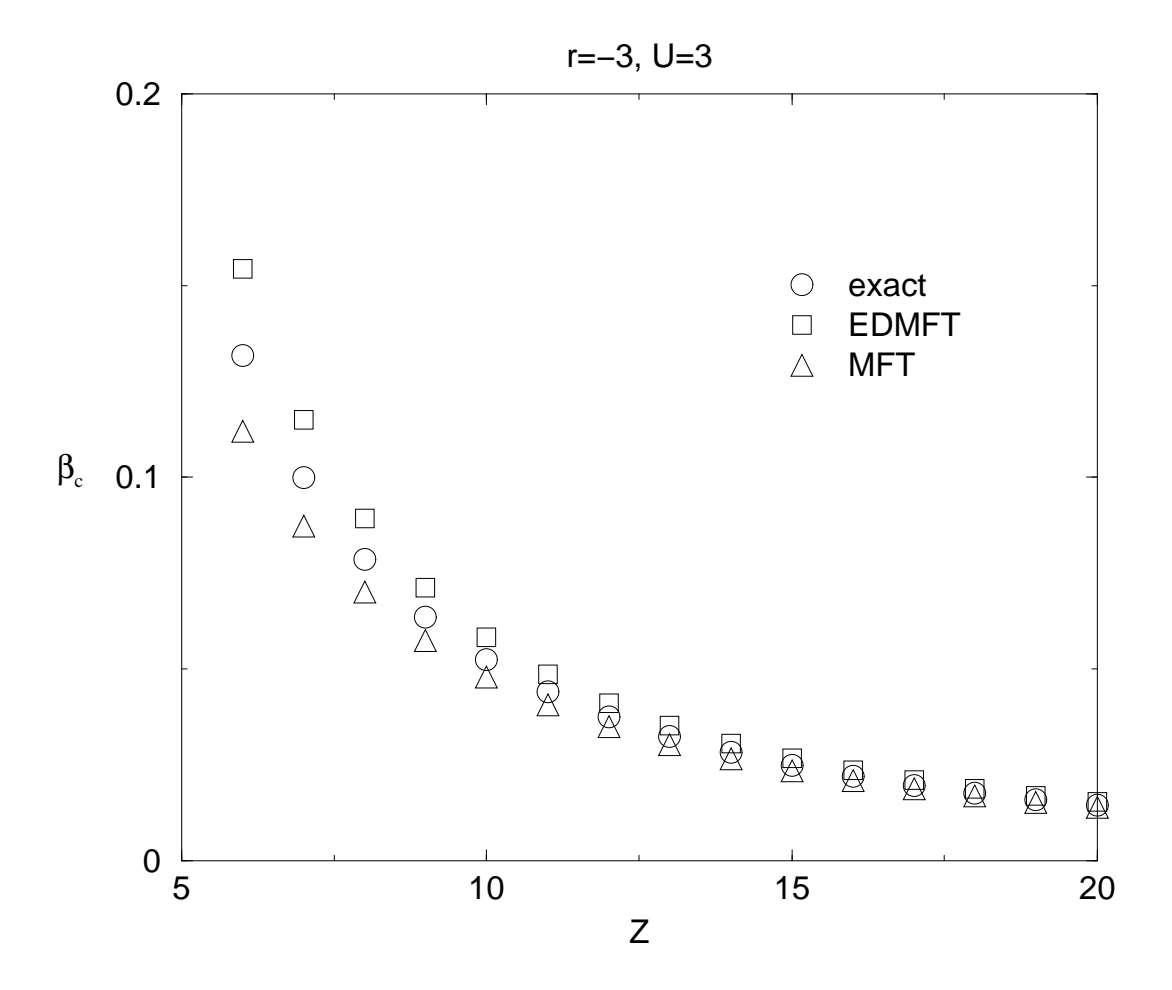


Figure 4.9: Soft spins, -r=U=3. Inverse temperature is plotted verses the coordination number.

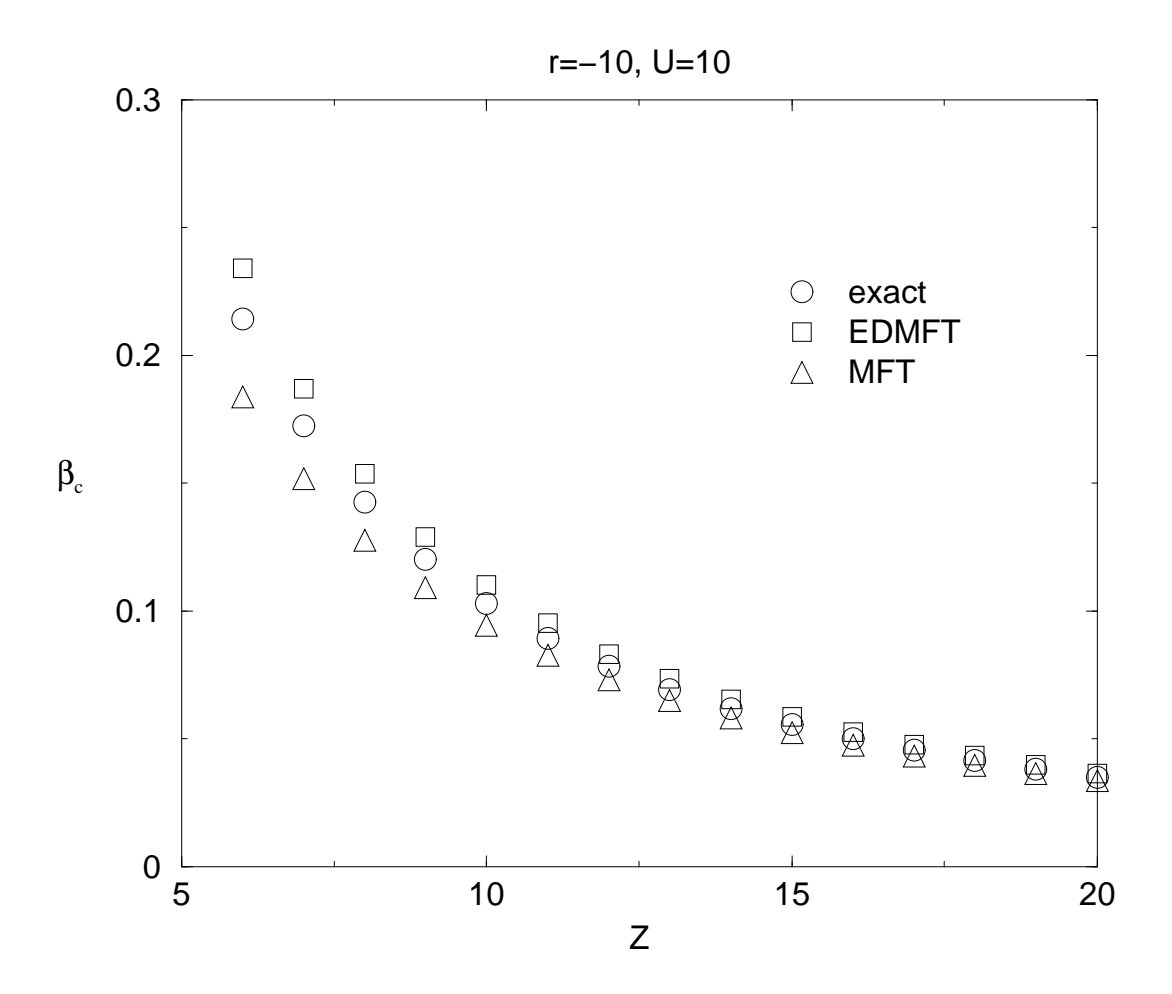


Figure 4.10: Soft spins, -r=U=10. Inverse temperature is plotted verses the coordination number.

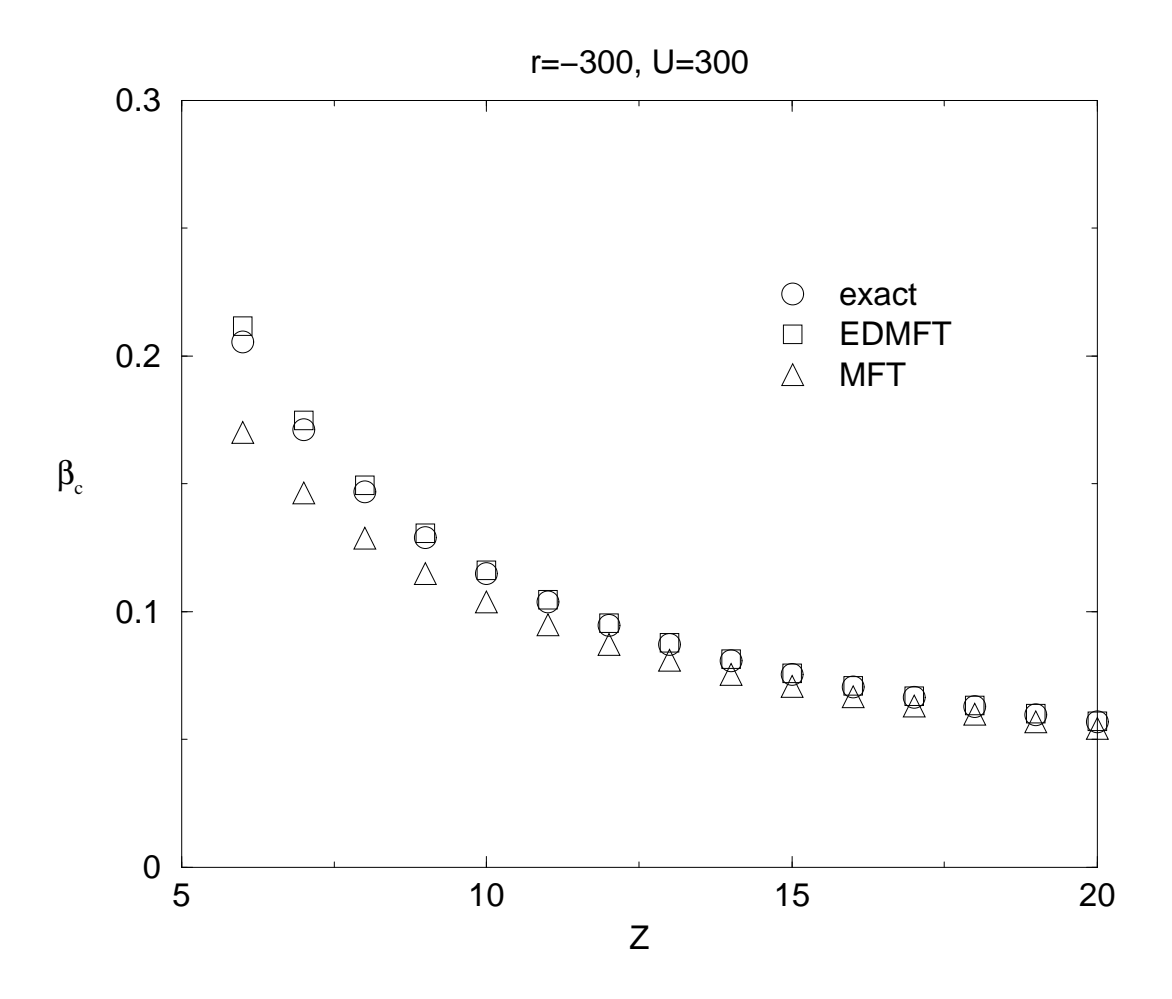


Figure 4.11: Soft spins, -r=U=300. Inverse temperature is plotted verses the coordination number. This graph should be compared to the classical spin limit, Fig.4.5

#### 4.4 Instability analysis

Let us consider a very general electron phonon Hamiltonian which describes an electron phonon system with electron-electron interaction (local or long range), electron-phonon interaction and phonon-phonon interaction (phonon unharmonicity). We can always use a Hubbard Stratonovich decoupling on electron-electron interaction, so we assume that information about long range electron-electron interaction is stored in the phonon dispersion and we will not write the long range interaction explicitly. We can introduce a source dependent action S where the sources are coupled to different fields. The free energy  $W = -\ln \int e^S$  is the generating functional for expectation values of those fields.

$$S = \int dx dx'$$

$$c_{\sigma}^{\dagger}(x) G_{0\sigma}^{-1}(x - x') c_{\sigma}(x') + \frac{1}{2} \phi(x) D_{0}^{-1}(x - x') \phi(x')$$

$$+ \delta(x - x') \left( U n_{\uparrow}(x) n_{\downarrow}(x) + V_{4} \phi^{4}(x) + \lambda \phi(x) c_{\sigma}^{\dagger}(x) c_{\sigma}(x) \right)$$

$$- J_{\sigma}(x, x') c_{\sigma}^{\dagger}(x) c_{\sigma}(x') - \frac{1}{2} \phi(x) K(x, x') \phi(x') - \delta(x - x') L(x) \phi(x) \quad (4.34)$$

x variable includes both space and time in the above formula and repeated indices imply summation. Expectation values of the fields coupled to the sources are given by:

$$G = \frac{\delta W}{\delta J}, \quad K = 2\frac{\delta W}{\delta K}, \quad m = \frac{\delta W}{\delta L},$$
 (4.35)

Exact Greens functions correspond to the limit of zero sources. To study phase transitions, like the transition when the phonon field acquires non zero expectation value, one needs to have the free energy as a functional of correlation functions only. Such a functional can be derived as a Legendre transform of the free energy:  $\Gamma = W - JG - K/2D - Lm$ . The sources J,K and L have to be solved for G,D and m. The functional  $\Gamma$  is called a Baym Kadanoff functional and

its stationary yields equations for zero source correlation functions. We present the functional without derivation:

$$\Gamma_{BK}[G, D, m] = \text{Tr} \log G - \text{Tr}(G_0^{-1} - G^{-1})G$$

$$-\frac{1}{2}\text{Tr} \log D + \frac{1}{2}\text{Tr}D_0^{-1}D + \frac{1}{2}mD_0^{-1}m + \Phi[G, D, m] \quad (4.36)$$

 $G_0$  and  $D_0$  are free fields of the action,  $\Phi$  functional is the sum of all two particle irreducible graphs constructed from the original bare interaction vertices, from vertices generated by shifting the phonon field by m and full correlation functions G and D.

The charge ordering instability can be studied by looking at the zero frequencymomentum phonon propagator behavior: the propagator diverges in a charge
density wave (CDW) transition. Alternatively one can study the transition from
the ordered side, by observing the order parameter vanishing (m in our case).
The two approaches should give consistent results. We will first show that this is
indeed the case in the exact theory, then we explain how a similar approach can
be applied in the EDMF theory.

Let us introduce some compact notations we are going to use.  $o_{\alpha}^{a}$  is a field operator of a kind at  $\alpha$  space-time point. a=G specifies an electron field operator and a=D specifies a phonon field operator.  $O_{\alpha\beta,\gamma\delta}^{ab}$  is a four point function, which is a subset of all connected diagrams in the perturbative expansion of  $\langle o_{\alpha}^{a\dagger} o_{\beta}^{a} o_{\delta}^{b\dagger} o_{\gamma}^{b} \rangle$ , rules for selecting the subset of diagrams depends on a particular operator. Multiplication of two operators is defined by:  $[O^{(1)}O^{(2)}]_{\alpha\beta,\gamma\delta} = \sum_{\mu\nu} O_{\alpha\beta,\mu\nu}^{(1)} O_{\mu\nu,\gamma\delta}^{(2)}$ . We are introducing three four point operators:1)  $\chi_{0}$  includes all graphs which enter skeleton graphs without interaction vertices. 2)  $\Sigma$  includes all 1D irreducible diagrams; 3)  $\Gamma$  includes all 2P irreducible diagrams. In our case reducibility of  $O_{\alpha\beta,\gamma\delta}$  is understood as disconnecting  $\alpha\beta$  part from  $\gamma\delta$  part. "1D irreducible" means "one particle irreducible with respect to cutting a phonon line". "2P irreducible"

Figure 4.12: Diagrammatic expansions for  $\Sigma$  and  $\Sigma_{ph}$ 

means "two particle irreducible".  $\chi_0$  is trivially expressed in terms of correlation functions:  $\chi_0^{GD} = \chi_0^{DG} = 0$ ,  $\chi_{0\alpha\beta,\gamma\delta}^{GG} = G_{\alpha\gamma}G_{\beta\delta}$  and  $\chi_{0\alpha\beta,\gamma\delta}^{DD} = D_{\alpha\gamma}D_{\beta\delta} + D_{\alpha\delta}D_{\beta\gamma}$ .

We can write out the following Dyson's equations for the components of  $\Sigma$  operator:

$$\Sigma^{GG} = \chi_0^{GG} + \chi_0^{GG} \Gamma^{GG} \Sigma^{GG} + \chi_0^{GG} \Gamma^{GD} \Sigma^{DG}$$

$$\Sigma^{GD} = \chi_0^{GG} \Gamma^{GG} \Sigma^{GD} + \chi_0^{GG} \Gamma^{GD} \Sigma^{DD}$$

$$\Sigma^{DG} = \chi_0^{DD} \Gamma^{DD} \Sigma^{DG} + \chi_0^{DD} \Gamma^{DG} \Sigma^{GG}$$

$$\Sigma^{DD} = \chi_0^{DD} + \chi_0^{DD} \Gamma^{DD} \Sigma^{DD} + \chi_0^{DD} \Gamma^{DG} \Sigma^{GD}$$

$$(4.37)$$

or we could simply write:

$$\Sigma = \chi_0 + \chi_0 \Gamma \Sigma \tag{4.38}$$

Solving for  $\Sigma$  we find:  $\Sigma = [\chi_0^{-1} - \Gamma]^{-1} = -(\partial^2 \Gamma_{BK})^{-1}$ . Second derivative  $\partial^2 \Gamma_{BK}$  is 2 x 2 matrix defined by:

$$(\partial^2 \Gamma_{BK})_{ab} = \frac{\partial^2 \Gamma_{BK}}{\partial C_a \partial C_b} \tag{4.39}$$

where C is a two component vector:  $C_G = G, C_D = D$ .

 $\Sigma$  matrix is related to the phonon self energy  $\Sigma_{ph}$  in a simple way, as can be seen from the diagrammatic series in Fig. (4.12).  $\Sigma$  comprises all four legged 1PI graphs, while  $\Sigma_{ph}$  comprises all two legged 1PI graphs. 2PI four legged block is nothing but  $\Gamma$ . Two horizontal lines represent a couple of correlation functions of the same kind, GG or DD, we assume that a summation runs over each couple of horizontal lines, while 2PI four legged blocks are understood as 2 x 2 matrices.

The first line is a diagrammatic analog of Eq.(4.38). The second line provides connection between  $\Sigma$  and  $\Sigma_{ph}$ . That can be written as:

$$\Sigma_{ph} = -\frac{\partial^2 \Phi}{\partial m \partial m} + \frac{\partial^2 \Phi}{\partial m \partial C_a} \Sigma^{ab} \frac{\partial^2 \Phi}{\partial C_b \partial m}$$

$$\tag{4.40}$$

or in a slightly different way:

$$\Sigma_{ph} = -\frac{\partial^2 \Phi}{\partial m \partial m} + \frac{\partial^2 \Gamma_{BK}}{\partial m \partial C} \left( \frac{\partial^2 \Gamma_{BK}}{\partial C \partial C'} \right)^{-1} \frac{\partial^2 \Gamma_{BK}}{\partial C' \partial m}$$
(4.41)

The condition for the CDW instability at wave vector q is:  $D_{0q}^{-1} - \Sigma_{ph} = 0$ .

We will reproduce the above result studying CDW transition from the ordered phase.  $\Gamma_{BK}$  is the free energy, so in the transition point

$$\frac{d^2\Gamma_{BK}}{dmdm} = 0\tag{4.42}$$

From the way  $\Gamma_{BK}$  is constructed it follows  $\partial \Gamma_{BK}/\partial C = 0$  and  $d\Gamma_{BK}/dm = \partial \Gamma_{BK}/\partial m$ . If we use  $d(\partial \Gamma_{BK}/\partial C)/dm = 0$  and Eq(4.42) we find:

$$\frac{\partial^2 \Gamma_{BK}}{\partial m \partial m} - \frac{\partial^2 \Gamma_{BK}}{\partial m \partial C} \left( \frac{\partial^2 \Gamma_{BK}}{\partial C \partial C'} \right)^{-1} \frac{\partial^2 \Gamma_{BK}}{\partial C' \partial m} = 0 \tag{4.43}$$

This equation is identical to Eq.(4.41) as should be in exact theory. In EDMFT approach we take the local approximation for the two particle irreducible graphs. All 2PI graphs in  $\Gamma_{BK}$  are contained by  $\Phi$ . So the condition for m vanishing is still given by Eq.(4.43) with  $\Phi$  being local. Alternatively we can use Eqs(4.38) where  $\Gamma^{ab} = \frac{\partial^2 \Phi}{\partial C_a \partial C_b}$  is local, in which case these two methods are equivalent. Let us consider the second method, when the transition is approached from the disordered phase.

The local  $\Gamma^{ab}$  can be computed using the impurity action of EDMF theory. For simplicity we consider electron phonon interaction only, with the coupling  $\lambda = 1$ . Equations similar to Eqs(4.37) can be written for the susceptibility  $\chi^{ab} = \langle o^{a\dagger} o^a o^{b\dagger} o^b \rangle$ . In short notations it reads:

$$\chi = \chi_0 + \chi_0 \tilde{\Gamma} \chi \tag{4.44}$$

where  $\tilde{\Gamma}$  is different from  $\Gamma$  of Eq.(4.38), because now it includes 1D reducible diagrams. The relation between  $\tilde{\Gamma}$  and  $\Gamma$  is simple:

$$\tilde{\Gamma} = \Gamma + \hat{D}_0 \tag{4.45}$$

where  $\hat{D}_0$  is 2 x 2 matrix,  $\hat{D}_0^{GG} = D_0$  and  $\hat{D}_0^{DG} = \hat{D}_0^{GD} = \hat{D}_0^{DD} = 0$ . Using Eq(4.38), Eq(4.44) and Eq(4.45) we can express the self energy  $\Sigma$  through the quantities which are directly computed from the impurity action:

$$\Sigma = [[\chi_{imp}]^{-1} - [\chi_{0imp}]^{-1} + \hat{D}_{0imp} + [\chi_0]^{-1}]^{-1}$$
(4.46)

where  $\chi_{imp}^{ab} = \langle o_a^{\dagger} o_a o_b^{\dagger} o_b \rangle_{imp}$ ,  $\chi_{0imp}^{ab} = \delta_{ab} C_a^2$  and  $D_{0imp}$  is the Weiss field of the impurity action:

$$S_{imp} = \int d\tau d\tau' c_{\sigma}^{\dagger}(\tau) G_{0imp,\sigma}^{-1}(\tau - \tau') c_{\sigma}(\tau')$$

$$+ \frac{1}{2} \phi(\tau) D_{0imp}^{-1}(\tau - \tau') \phi(\tau') + \delta(\tau - \tau') \phi(\tau) c_{\sigma}^{\dagger}(\tau) c_{\sigma}(\tau) \quad (4.47)$$

The described method is exact in the limit  $d \to \infty$ . At finite d it yields a higher  $T_c$  than a naive local approximation  $\Sigma_{ph} = \delta \Phi/\delta D$ . Assuming  $\Sigma_{ph} = \delta \Phi/\delta D$  would be equivalent to taking  $\Gamma_{BK}$  as being local in Eq(4.41), while the correct approach is to take a local approximation on the  $\Phi$  functional only, not on the whole Baym Kadanoff functional.

# Chapter 5

# Parquet EDMFT

# 5.1 Dynamical Mean Field Theories in the Parquet Formalism

The dynamical mean field theory (DMFT) has been very successful in treating non perturbative problems in the domain of strongly correlated electrons such as the Mott transition [30]. In its single site version it becomes exact in the limit of infinite dimensionality [1], but its ideas have been extended to capture the effects that disappear in the infinite dimensional limit, such as the Anderson localization, short range magnetic correlations or long range Coulomb interaction.

In this chapter we present an extension of the single site DMFT using a formalism based on the parquet equations. As first shown by Muller-Hartmann [42] (see also Ref. [43]) this formalism allows a transparent summary of the q dependence of physical quantities in the single site DMFT. Here we use the parquet formalism to analyze various DMFT extensions. The chapter set up as follows: in section 5.2 we review briefly the exact parquet equations (the notations are described in Appendix B.1). In section 5.3 we discuss how different methods emerge from simple approximations to the exact equations, namely DMFT and Extended DMFT (EDMFT). An application of the new equations is presented in section 5.4, where we show how the superconducting fluctuations are fed into the self energy in our extension of the EDMFT.

#### 5.2 Parquet theory

The parquet equations relate a fully irreducible amplitude  $\check{I}$  to the full vertex function  $\check{\Gamma}$ . It can can be written also as a relation between the direct parts I and  $\Gamma$  of those quantities. We state the equations here and refer the reader to the detailed definitions and graphical interpretation in AppendixB.1:

$$\check{I} = \check{\Gamma} - \check{\Gamma} (1 + \frac{1}{2} \mathbf{s} \check{\Gamma})^{-1} \frac{1}{2} \mathbf{s} \check{\Gamma} - \check{\Gamma} (1 + \mathbf{u} \check{\Gamma})^{-1} \mathbf{u} \check{\Gamma} - \check{\Gamma} (1 + \mathbf{c} \check{\Gamma})^{-1} \mathbf{c} \check{\Gamma}$$
(5.1)

or in terms of the direct vertices:

$$I = \Gamma_0 - \Gamma(1 + \mathbf{s}\Gamma)^{-1}\mathbf{s}\Gamma - \Gamma(1 + \mathbf{u}\Gamma)^{-1}\mathbf{u}\Gamma - \Gamma_0(1 + \mathbf{b}\Gamma_0)^{-1}\mathbf{b}\Gamma_0$$
 (5.2)

where

$$\Gamma_0 = (1 + \Gamma \mathbf{l})^{-1} \Gamma (1 + \mathbf{r} \Gamma)^{-1}$$

$$(5.3)$$

In the above equations  $\mathbf{s}$ ,  $\mathbf{u}$  and  $\mathbf{c}$  operations are pairs of Green's functions connecting four point interactions in different channels and  $\mathbf{b}$  is the dressed  $\mathbf{c}$  bubble. The definitions and graphical interpretation of these operations are in AppendixB.1. The equivalence of Eq.(5.1) and Eqs.(5.2,5.3) is presented in AppendixB.3. To complete a parquet scheme we need a relation between  $\Gamma$  (or  $\tilde{\Gamma}$ ) and the one-particle Green's function or its self-energy  $\Sigma = -G^{-1} + G_0^{-1}$ :

$$\Sigma = d(\check{V} + \frac{1}{2}\check{V}\mathbf{s}\check{\Gamma}) \tag{5.4}$$

or in terms of the direct vertices:

$$\Sigma = (d+e)(V+V\mathbf{s}\Gamma) \tag{5.5}$$

where d (e) is the operation that closes a Green's function line in the direct (exchange) channel. They are discussed in AppendixB.1. Assuming that  $\tilde{V} = V$  the self energy formulas can be written in a number of equivalent ways, using the relationships  $d(V\mathbf{s}\Gamma) = d(V\mathbf{u}\Gamma) = e(V\mathbf{c}\Gamma)$  and  $e(V\mathbf{s}\Gamma) = d(V\mathbf{u}\bar{\Gamma}) = e(V\mathbf{c}\bar{\Gamma})$ . It is

convenient to write  $I = V + I_1$  with V the bare interaction vertex. If all graphs for  $I_1$  are kept, this is an exact formula of the many body problem.

### 5.3 DMFT and EDMFT approximations

In this section we introduce DMFT and EDMFT approximations in the parquet formulation. The momentum dependence of the vertices here should be understood as for the purpose of computing local quantities. For example, vertex  $\Gamma$  in DMFT is local for purpose of computing the self energy, but is nonlocal for computing susceptibilities.

The DMFT approximation consists of:

- a) Taking only local graphs for  $I_1 = I_1[G_{ii}, \Gamma_{iiii}]$  and local V in Eqs.(5.1-5.2). The locality of  $I_1$  is understood as locality of  $G_{ii}$  and  $\Gamma_{iiii}$  of which  $I_1$  is a functional [44].  $\Gamma_{iiii}$  is computed from the parquet Eqs.(5.1, 5.2) with local operations  $\mathbf{s}$ ,  $\mathbf{u}$ ,  $\mathbf{c}$  ( $\mathbf{b}$ ).
- b) The self energy  $\Sigma$  is taken to be local. It is computed with local  $\mathbf{s}$ , V and  $\Gamma_{iiii}$  in Eqs.(5.4,5.5). Notice that for the purpose of computing  $\Sigma$  the parquet equations are the set of completely local nonlinear equations for  $G_{ii}$  and  $\Gamma_{iiii}$ .
- c) Nonlocal interactions in DMFT affect the self-energy as a Hartree corrections to the bare dispersion  $\epsilon_k$ .

The graphs for the self-energy  $\Sigma[G_{ii}]$  and for  $I_1(G_{ii}, \Gamma_{iiii})$  can be obtained from an Anderson impurity model, with unrenormalized four point interaction:

$$S_{imp} = \sum_{\sigma} c_{\sigma}^{\dagger} G_{0\sigma imp}^{-1} c_{\sigma} + V n_{\uparrow} n_{\downarrow}$$
 (5.6)

 $G_{0imp}^{-1}$  is adjusted to give the same  $G_{ii}$  as in the lattice model in DMFT, leading to the selfconsistency condition:

$$G_{ii} = \sum_{q} \left[ G_{0q}^{-1} - G_{0imp}^{-1} + G_{ii}^{-1} \right]^{-1}$$
 (5.7)

The idea of the extended DMFT is to allow the momentum dependence of the spin-spin, charge-charge and pair correlations influence the electron self energy. In a most general case the interaction term is:

$$V_{ijkl} = \delta_{ij}\delta_{kl}V_s(i,k) + \delta_{il}\delta_{jk}V_u(i,j) + \delta_{ik}\delta_{jl}V_t(i,j)$$
(5.8)

The EDMFT approximation consists of:

- a) taking local graphs for  $I_1[G_{ii}, \Gamma_{iiii}]$  in Eqs.(5.1,5.2) but keeping the non locality of V. The vertex function  $\Gamma_{ijkl}$  is computed with local  $\mathbf{s}$ ,  $\mathbf{u}$  and  $\mathbf{c}$  but nonlocal V, so  $\Gamma$  has momentum dependence originating in non local V.
- b) The self energy  $\Sigma$  is local, however nonlocality of the interaction in the self energy must be preserved, therefor it is computed as:

$$\Sigma = diag \left\{ d(\check{V}_s + \frac{1}{2}\check{V}_s \mathbf{s}\check{\Gamma}) + d(V_u + \bar{V}_t + V_u \mathbf{u}\check{\Gamma}) + e(V_t + \bar{V}_u + V_t \mathbf{c}\check{\Gamma}) \right\}$$
(5.9)

where operations  $\mathbf{s}$ ,  $\mathbf{u}$  and  $\mathbf{c}$  are taken to be local, keeping nonlocal  $\check{\Gamma}$  and  $\check{V}$ . We use diag to show that only site diagonal terms are retained in  $\Sigma$ .

The local  $\Gamma_{iiii}$  and  $G_{ii}$  can still be obtained from an impurity model, because  $\Sigma$  and  $I_1[\Gamma_{iiii}, G_{ii}]$  are still those of the impurity model. But now the vertex in the impurity model is renormalized:

$$S_{imp} = \sum_{\sigma} c_{\sigma}^{\dagger} G_{0\sigma imp}^{-1} c_{\sigma} + \sum_{\sigma_{1}\sigma_{2}\sigma_{3}\sigma_{4}} V_{imp}^{\sigma_{1}\sigma_{2}\sigma_{3}\sigma_{4}} c_{\sigma_{1}}^{\dagger} c_{\sigma_{2}}^{\dagger} c_{\sigma_{3}} c_{\sigma_{4}}$$
 (5.10)

$$V_{imp} = V_{imp}^s + V_{imp}^u + V_{imp}^t (5.11)$$

$$\check{\Pi} = \sum_{q_s} [\check{\Pi}^{-1} + \frac{1}{2} \check{V}_{imp}^s - \frac{1}{2} \check{V}_{sq_s}]^{-1}$$

$$\check{\Pi} = \sum_{q_u} [\check{\Pi}^{-1} + \check{V}_{imp}^u - V_{uq_u} - \bar{V}_{tq_u}]^{-1}$$

$$\check{\Pi} = \sum_{q_t} [\check{\Pi}^{-1} + \check{V}_{timp}^t - V_{tq_t} - \bar{V}_{uq_t}]^{-1}$$
(5.12)

Usually it is assumed that  $V_s = V_u = 0$  and we need only the last two equations in Eq.(5.12).

#### 5.4 EDMFT2

In this section we attempt to extend further theory to include more momentum dependence in the approximations we make on the parquet equations. Ideally we would like to devise an approximation which included all the diagrams in the next order in 1/d, or in the reducibility of the diagrams which are treated as nonlocal. In the language of reducibility EDMFT retains the momentum dependence in all one particle reducible diagrams (be it a fermion line or an interaction line). The next logical step would be to retain nonlocality in two fermion reducible diagrams. To define this approximation rigorously we introduce the following projection operators:

$$p_s G(x_1, x_2) G(x_3, x_4) = G(x_1, x_2) G(x_3, x_4) \delta_{x_1, x_2} \delta_{x_3, x_4}$$

$$p_u G(x_1, x_2) G(x_3, x_4) = G(x_1, x_2) G(x_3, x_4) \delta_{x_1, x_4} \delta_{x_2, x_3}$$

$$p_t G(x_1, x_2) G(x_3, x_4) = G(x_1, x_2) G(x_3, x_4) \delta_{x_1, x_2} \delta_{x_2, x_4}$$
(5.13)

The projection operators act only on space variables. A projection operator  $p_x$  acts on GG in the corresponding channel x. The projected operators are denoted

 $\dot{\mathbf{s}}$ ,  $\dot{\mathbf{u}}$  and  $\dot{\mathbf{c}}$ :

$$\dot{\mathbf{s}} = p_s \mathbf{s}$$

$$\dot{\mathbf{u}} = p_u \mathbf{u}$$

$$\dot{\mathbf{c}} = p_t \mathbf{c}$$
(5.14)

We can now formulate a new systematic extension of the DMFT, we denote it as EDMFT2:

- a) graphs for  $I_1[G_{ii}, \Gamma_{iiii}]$  are taken to be local, for computing  $\Gamma_{ijkl}$  operations  $\mathbf{s}$ ,  $\mathbf{u}$  and  $\mathbf{c}$  are projected and the interaction V is nonlocal. The momentum dependence of  $\Gamma$  originates in nonlocal V and nonlocal  $\dot{\mathbf{s}}$ ,  $\dot{\mathbf{u}}$  and  $\dot{\mathbf{c}}$ .
- b) The self energy  $\Sigma$  is still local, and computed in the same way as in EDMFT, but with projected  $\mathbf{s}$ ,  $\mathbf{u}$  and  $\mathbf{c}$ :

$$\Sigma = diag \left\{ d(\check{V}_s + \frac{1}{2} \check{V}_s \dot{\mathbf{s}} \check{\Gamma}) + d(V_u + \bar{V}_t + V_u \dot{\mathbf{u}} \check{\Gamma}) + e(V_t + \bar{V}_u + V_t \dot{\mathbf{c}} \check{\Gamma}) \right\}$$
(5.15)

We can also obtain the selfconsistency condition for  $V_{imp}$ , hoping that like in the case of DMFT and EDMFT the impurity model can be used for computing local quantities. From the requirement that  $\Gamma_{iiii} = \Gamma_{imp}$ , we obtain:

$$\dot{\Gamma} = \sum_{q_s} \left[ \dot{\Gamma} \left( 1 + \frac{1}{2} \mathbf{s} \check{\Gamma} \right)^{-1} - \check{V}_{imp}^s + \check{V}_{sq_s} \right] \times$$

$$\left\{ 1 - \frac{1}{2} \dot{\mathbf{s}}_{q_s} \left[ \dot{\Gamma} \left( 1 + \frac{1}{2} \mathbf{s} \check{\Gamma} \right)^{-1} - \check{V}_{imp}^s + \check{V}_{sq_s} \right] \right\}^{-1}$$

$$\dot{\Gamma} = \sum_{q_u} \left[ \dot{\Gamma} \left( 1 + \mathbf{u} \check{\Gamma} \right)^{-1} - \check{V}_{imp}^u + V_{uq_u} + \bar{V}_{tq_u} \right] \times$$

$$\left\{ 1 - \dot{\mathbf{u}}_{q_u} \left[ \dot{\Gamma} \left( 1 + \mathbf{u} \check{\Gamma} \right)^{-1} - \check{V}_{imp}^u + V_{uq_u} + \bar{V}_{tq_u} \right] \right\}^{-1}$$

$$\dot{\Gamma} = \sum_{q_t} \left[ \dot{\Gamma} \left( 1 + \mathbf{c} \check{\Gamma} \right)^{-1} - \check{V}_{imp}^t + V_{tq_t} + \bar{V}_{uq_t} \right] \times$$

$$\left\{ 1 - \dot{\mathbf{c}}_{q_t} \left[ \dot{\Gamma} \left( 1 + \mathbf{c} \check{\Gamma} \right)^{-1} - \check{V}_{imp}^t + V_{tq_t} + \bar{V}_{uq_t} \right] \right\}^{-1}$$
(5.16)

Obtaining the selfconsistency condition is not enough to guarantee that the impurity model is equivalent to the EDMFT2 approximation formulated in terms

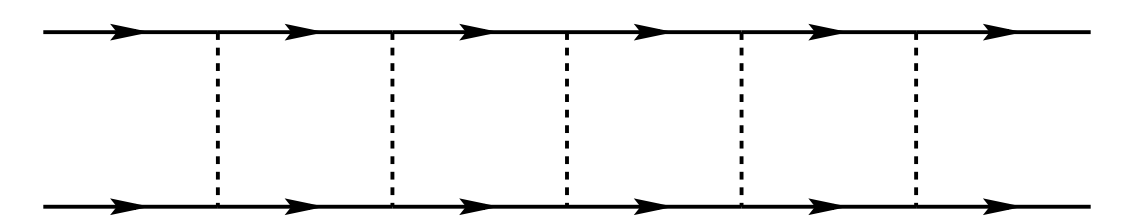


Figure 5.1: Ladder diagram, particle particle channels.

of projected parquet equations. We also have to insure that the local self energy of the lattice model and the impurity model are the same. Using the parquet equations we can show that:

$$\check{V}_{imp}^{s} + \frac{1}{2}\check{V}_{imp}^{s}\mathbf{s}\check{\Gamma}_{imp} - diag\left\{\check{V}_{s} + \frac{1}{2}\check{V}^{s}\dot{\mathbf{s}}\check{\Gamma}\right\} + \frac{1}{2}\check{\Gamma}_{12}^{loc}\left(\mathbf{s}\Gamma_{imp} - diag\{\dot{\mathbf{s}}\Gamma\}\right)$$
(5.17)

Comparing this to the selfenergy expression Eq.(5.15) we see that the impurity model does not reproduce correctly the selfenergy. In the case  $d \to \infty$  when  $\dot{\mathbf{s}} \to \mathbf{s}$ ,  $\dot{\mathbf{u}} \to \mathbf{u}$  and  $\dot{\mathbf{c}} \to \mathbf{c}$  the last term in Eq.(5.17) vanishes and the selfenergy is represented correctly by the impurity model, and we recover the EDMFT approximation. Similar analysis can be done in u and t channels.

# 5.5 Super-conducting fluctuations

To clarify the strength of the nonlocal approximation, which we introduced in the section 5.4, in some simple setting we consider large N limit of the Sp(N) t-J model [45]. The Hamiltonian reads

$$H_{tJ} = -\frac{t}{N} \sum_{ij} c_{i\alpha}^{\dagger} c_{j\alpha} - \frac{J}{N} \sum_{ij} (\epsilon_{\alpha\beta} c_{i\alpha}^{\dagger} c_{j\beta}^{\dagger}) (\epsilon_{\alpha\beta} c_{j\beta} c_{i\alpha})$$
 (5.18)

where  $\epsilon_{\alpha\beta}$  is a generalization of the antisymmetric tensor  $\epsilon$ . A local constraint on the occupation number is enforced to restrict the Hilbert space of the Hamiltonian.

The four point graphs which survive large N limit to the lowest order are ladders in the particle particle and particle hole channels. We concentrate on the particle particle channels which represent super-conducting fluctuations, Fig. (5.1)

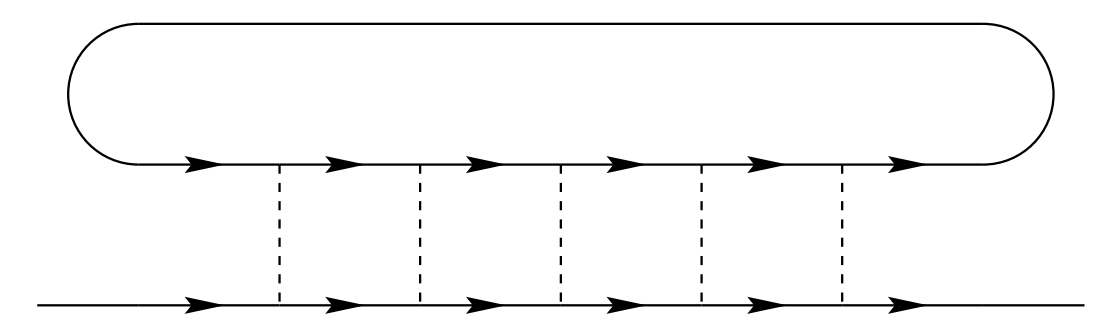


Figure 5.2: Ladder diagram, particle particle channels.

In the usual EDMFT the ladder diagrams are local, while in EDMFT2 they acquire a momentum dependence from a particle particle bubble. Non local superconducting fluctuations are fed back in the self energy in the diagram shown in the Fig.(5.2), which is of order 1/N - the lowest order diagram for t-J model Eq.(5.18).

The improvement of the EDMFT2 over the EDMFT in treating superconducting fluctuations is similar to the improvement of the EDMFT over the DMFT in the the treatment of the charge fluctuations. The EDMFT allows a feedback from nonlocal charge fluctuations, which are omitted in the DMFT, but it skips on the super-conducting fluctuations because there is no pair hopping term in the original Hamiltonian due to the local particle number conservation. EDMFT2 allows nonlocal SC fluctuations that originate from the particle particle bubble. EDMFT2 still omits the momentum dependence of  $J_{ij}$  which is crucial in capturing the d wave super-conductivity. For that one should apply some version of the cluster dynamical mean field theory.

# Chapter 6

### Anderson localization

#### 6.1 Introduction

Understanding the physics of the disordered materials remains a challenging and important problem in the condensed matter field. One reason, why it is important, is that real materials are never perfect and effects caused by disorder must be accounted. If disorder itself or corrections to certain physical quantities due to disorder are small, one usually talks about weak localization, which can be treated successfully by a perturbation theory. More interesting is the case when disorder is strong and essential for some phenomenon to occur. The Anderson localization in 3d is an example of such phenomenon. The mechanism for localization of the noninteracting electrons in the presence of strong disorder, first suggested by Anderson [46] in 1958, has been largely understood both qualitatively and quantitatively. However, the admixture of interaction (even a weak interaction) to the strong disorder significantly complicates the consideration. In the introducting chapter we described many successes of DMFT, showing that it sets up an excellent tool for treating nonperturbative effects in correlated materials. In view of these successes there is little doubt that possibility of including of the efficient disorder treatment in DMFT formalism would be invaluable for the physics community.

And this is possible to some extent. As we already mention one can describe glasses by introduce replicas in DMFT [22]. Yet it has been known that the replica limit is actually ill-defined and does not always work. It definitely fails

to capture the Anderson transition. Alternative to replicas is a super symmetry (SUSY) method, in which the disorder averaging is well defined. It was successfully implemented in nonlinear sigma model devised by Efetov [24], which is a low energy effective model. Also, the use of SUSY is limited to noninteracting systems only, therefore this method is applicable to a limited class of problems.

One is forced to seek new approaches, and there is some progress made. We can name two methods attempting to treat disorder in DMFT fashion: statistical DMFT [26] and typical medium theory [27]. Both methods are uncontrolled at large disorder and confidence in using them relies on intuition and actual qualitatively correct results which these methods produce. In its turn the intuition is usually based on good understanding of the simpler limiting cases, namely the clean limit and noninteracting electrons limit. Understanding these limits is imperative before one can start to think about how to incorporate disorder in DMFT. In the current chapter we study the noninteracting limit.

In section 6.2 we introduce the physical picture of the Anderson transition, describe some peculiarities of the transition and pose the questions we would like to answer in the rest of the chapter. In the next section 6.3 we overview results of numerical simulation of the Anderson localization in the frame of the Anderson model. In section 6.4 we overview a general analysis of the Anderson transition by linearization of the integral equation for the distribution function of the Green's function. In sections 6.5 and 6.6 we consider a toy model of the AL and the exact theory. In section 6.7 we try to reduce exact theory integral equation from two to one variables. In section 6.8 we compare the toy model, exact model and nonlinear sigma model.

#### 6.2 Phenomenon of the Anderson localization

The Anderson localization is the localization of noninteracting electrons due to disorder. The disorder can be modeled, for example, by randomness in the external potential (diagonal disorder). Such randomness is characterized by the disorder strength - a measure of the fluctuations of the potential.

In a translationally invariant system all electron states are extended wave functions. Disordered potential breaks down translational symmetry and some states get localized: electron in that state has finite probability to be found in some region, while everywhere else the wave function is exponentially small. Size of that region defines the localization length  $\xi$ . In the regime, when only a small number of states are localized, corrections to physical quantities, such as conductivity, are small as well, and one talks about weak localization regime. On the contrary, when most of the states or even all states are localized, the corrections are large and of nonperturbative nature, one talks about strong localization.

When all states get localized, conductivity vanishes and system from a metal turns into an insulator. This metal to insulator transition (MIT) is called Anderson transition or Anderson localization. Localization is a quantum effect. It is related to the quantum coherence, which depends strongly on dimensionality. The lower critical dimension for the Anderson transition is d = 2. For  $d \le 2$  an arbitrary small disorder brings about the insulator phase. This is reminiscent of the fact that in  $d \le 2$ , a potential well, however shallow, does always contain a localized state.

In clean interacting systems which exhibit metal to insulator transition the conductivity vanishes due to depletion in the density of states (DOS) around the Fermi level. For example this happens in the Mott transition or when the Coulomb gap forms. The vanishing of the conductivity in the AL is of very different nature. The average DOS actually remains finite, yet conductivity goes

to zero. This can be understood in the following way. In the phase, when all states are localized with some characteristic localization length  $\xi$ , a given state has a wave function which spatially overlaps with approximately  $\xi^d$  other states. This number is finite, so is typical difference between energies corresponding to different states. Such system must be insulating at zero temperature.

As the disorder is introduced to the system, the states get localized, but there typical energies should not change much. For noninteracting electrons it explains an interesting feature of Anderson localization, non-vanishing density of states (DOS). The DOS here is average over all sites local density of states (LDOS). As we explained, two states with close energies are likely to be far apart in real space. Having finite DOS, this may happen only if LDOS is very large on a few sites and small everywhere else. So we see, that while average LDOS is non critical in the transition, the typical (most probable) LDOS is critical: it vanishes in MIT, unlike DOS. So typical LDOS (which can be mathematically defined as the geometrical average LDOS) may be a good candidate for the role of order parameter.

Let us introduce the model which we study. This will be the Anderson tightbinding model described by the following Hamiltonian

$$H = \sum_{i} \epsilon_i c_i^{\dagger} c_i + \sum_{\langle i,j \rangle} t_{ij} c_i^{\dagger} c_j, \quad t_{ij} = t_{ji}^*$$

$$\tag{6.1}$$

where site energies  $\epsilon_i$  are assumed to be random variables and hopping matrix elements  $t_{ij}$  are equal to t for the nearest neighbors and are zero otherwise.

The details of the derivation of the equations are given in the Appendix C.1. The resulting equation reads:

$$-G_i^{-1} = \epsilon_i + t^2 \sum_{j=1}^m G_j$$
 (6.2)

This equation presents relationship between the local Green's function  $G_{ii}$  at zero frequency, the sum is over the nearest neighbors. This equation is only an approximation for real d dimensional lattices, but becomes exact on a model tree

like (loopless) lattice. The Green's function in that case should be understood as computed with one branch of the tree cut off. A tree like lattice with m+1 neighbors near each site is called a Bethe lattice (or Cayley tree) with the coordination number m. This is a lattice we study our model on. One may wonder if considering problem on this lattice is meaningful. In spite of being unrealistic, the Bethe lattice can provide useful insight in the problem. In fact it is very common to be solving physical models using Bethe lattice, due to typical simplicity of equations for it. For the hypercubic lattice number of nearest neighbors is twice the dimensionality of the system. Using this analogy between the dimensionality d and coordination number m we can to some extent consider the Bethe lattice as an approximation to a real lattice. While it is just an approximation for 2 or 3 dimensional lattices, it becomes exact in who limits,  $m \to 1$  and  $m \to \infty$ , we will concentrate particular attention on these limits.

We put t = 1, or in other words we measure frequency E and and potential  $\epsilon$  in terms of t, while Green's functions in terms of  $t^{-1}$ .

We assume that the disorder distribution is symmetric, so the localization at zero frequency corresponds to the system becoming insulating, as we expect for the semicircular DOS of the Bethe lattice the states on the edges of the band to localize first and the states at zero frequency to localize last.

As we already mention, it is not enough to know the first moment of the distribution function  $P_G$ , but rather the whole distribution can be considered as an order parameter. The knowledge of  $P_G$  may also be very useful when one is to decide how to add an interaction to the noninteracting disordered state. This has been partially understood but was not very clearly presented throughout the literature, therefore we would like to clarify it. This and the other main questions which we address are listed below:

1) understanding the form of the distribution function  $P_G(ReG, ImG)$  of the real and imaginary parts of the local greens function, since  $P_G$  is a central quantity

in DMFT, and it is related to a measurable quantity - LDOS. Expression for  $P_G$  in NSM was available before.

- 2) Effects of coordination number, how it enters results on the Bethe lattice. Large coordination number case was already done (Abou Chakra et.al).
- 3) Comparing results to NSM model, and possibility of reduction integral equation describing the problem to one variable equation (like in NSM).

#### 6.3 Overview of numerical results

Our most general goal is to find the distribution function  $P_G(G)$  of local Greens function G. We consider zero frequency case and we put t = 1. Corresponding equation reads (see Appendix. C.1):

$$-G^{-1} = \epsilon + \sum_{j=1}^{m} G_j \tag{6.3}$$

This is a stochastic equation with the independent random variables in the right hand side. We want to find the distribution function  $P_G$ , for a given distribution function  $P_{\epsilon}$ , which would satisfy Eq(6.3). This equation can be written as a nonlinear integral equation for  $P_G$ .

In this section we consider numerical results we obtained. Solving integral equation corresponding to the stochastic equation Eq.(6.3) is a difficult task. It is much easier to use Eq.(6.3) as a recursive equation for computing sets of  $\{G_i\}$  and finding the distribution statistically. In the limiting case of an infinite set the distribution function obtained in this way is a solution of the nonlinear integral equation for  $P_G$ , but for a finite set it is only an approximation. The steps of the algorithm for this procedure are:

1) A set of N values of G is given as an input for this step. From this set of G, m values of G are chosen randomly. A random variable  $\epsilon$  is generated randomly

from the distribution  $P_{\epsilon}$ . These m+1 random variables are plugged in right hand side of Eq.(6.3), and a new  $G_{new}$  value generated.

- 2) Step 1) is repeated N times, so a new set of N values  $G_{new}$  is generated.
- 3) New set is used to built a histogram, which is a discreetized version of the distribution function  $P_G$ .
  - 4) The new set of G is supplied to the step 1) as an input.

In the very beginning a set of N values is chosen arbitrary, with the only restriction that ImG > 0. Steps 1)-2) are repeated until a reasonably smooth histogram  $P_G$  is generated. By analyzing the dependence of the data on the set size N one can interpolate the results to the limit  $N \to \infty$ .

Let us use that kind of simulation to illustrate some features of the Anderson model. Random energies  $\epsilon$  are distributed according to Cauchy distribution

$$P_{\epsilon}(\epsilon) = \frac{1}{\pi} \frac{\gamma}{\gamma^2 + \epsilon^2}$$

First we illustrate the vanishing of the typical LDOS, which can be considered as the order parameter. In Fig.6.1 we plotted  $\exp \langle \ln(ImG) \rangle$  as a function of disorder strength  $\gamma$ .

In Fig.6.2 and Fig.6.3 we plotted the distribution function  $P_{x,y}(x,y)$ , where x = ReG, y = ImG.

In the pure system with no disorder all the lattice sites are equivalent. As a result the G takes the same value  $G_0$  everywhere, so  $P_G$  is just a delta-function:  $P_G(G) = \delta(G - G_0)$ . In the strongly disordered system LDOS is very large on a few sites while tends to zero on most sites. In this case, the distribution  $P_G$  is peaked around small ImG. In Fig.6.2 and Fig.6.3 we illustrated two distinctive regimes: good metal and metal in the critical MIT regime. In the first case  $P_G$  is peaked around  $G_0$ . As disorder increases this peak gets broader and shorter, being centered roughly near the same point. At the same moment  $P_G$  grows at small ImG. At even larger disorder the peak completely vanishes,  $P_G$  becomes

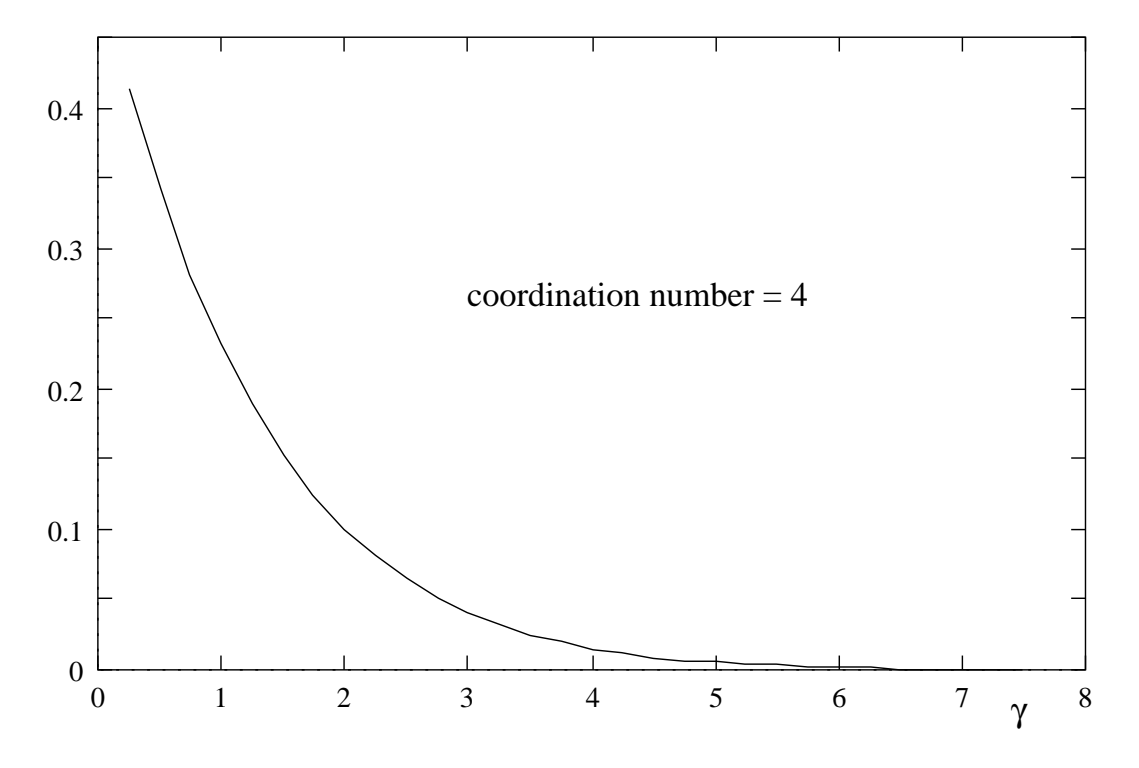


Figure 6.1:  $\langle ImG \rangle_{typical}$  as a function of disorder strength  $\gamma$ 

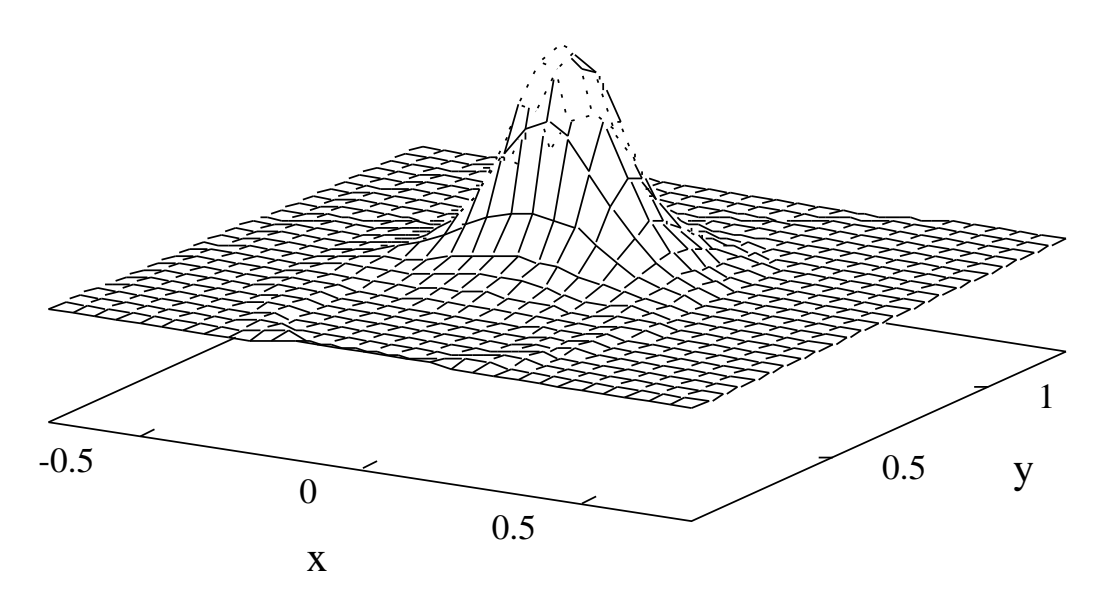


Figure 6.2: Distribution of the onsite Green function G = x + iy at the disorder strength  $\gamma = .05$  obtained in a simulation for the Cauchy distribution of disorder.

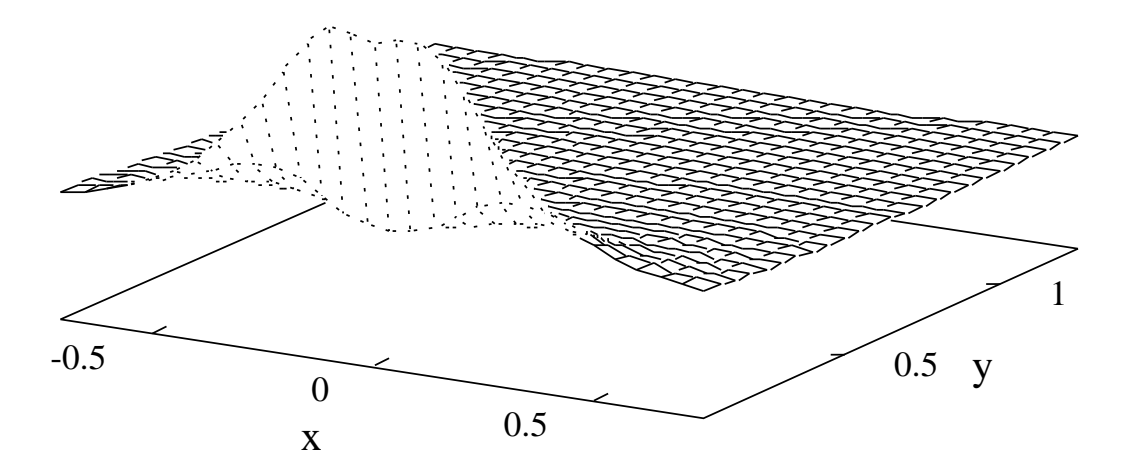


Figure 6.3: The same as above but at the disorder strength  $\gamma = 1$ 

large at very small ImG in some range of ReG. This case is presented in Fig.6.3.

At small disorder  $P_G$  is peaked around the finite  $G_0$ . We tested how well that peak can be fitted by the Gaussian and log-normal distributions. The log-normal distribution is a Gaussian distribution of the logarithm of a variable. In Fig.6.4 and Fig.6.5 we plotted  $\sqrt{\ln(P_y(y)/P_y^{max})}$  as a function of y and y respectively. For Gaussian distribution one would have a linear plot in y variable, and for log-normal - linear plot in y. As one may judge from those plots, the quality of the fitting is limited.

We check the assumption that the distribution function may be written in a special factorizable form:  $P_{x,y}(x,y) = F(x)Q(yf(x))$ . This factorization is exact for NSM [47], but holds only approximately in the other cases that we consider. It is possible to find f(x) analytically by studying the problem in the vicinity of the transition. Under the assumption  $P_{x,y}$  factorizes in variables x and  $\eta = yf(x)$ . We tested this assumption using contour plot of  $P_{x,\ln y}/P_x(x)$  in variables x and  $\ln \eta$  (for convenience, we chose  $P_{x,\ln y}$  rather than  $P_{x,y}$ ; vertical and horizontal axis correspond to x and  $\ln \eta$  respectively). Factorizability of the distribution function in variables x and y should be manifested in the contour plot by contour lines being straight and parallel (see Fig.6.6). As we see it is not quite so. Factorization is not precise, it fails at very small x, especially for small y ( $y \le y_{typical}$ ).

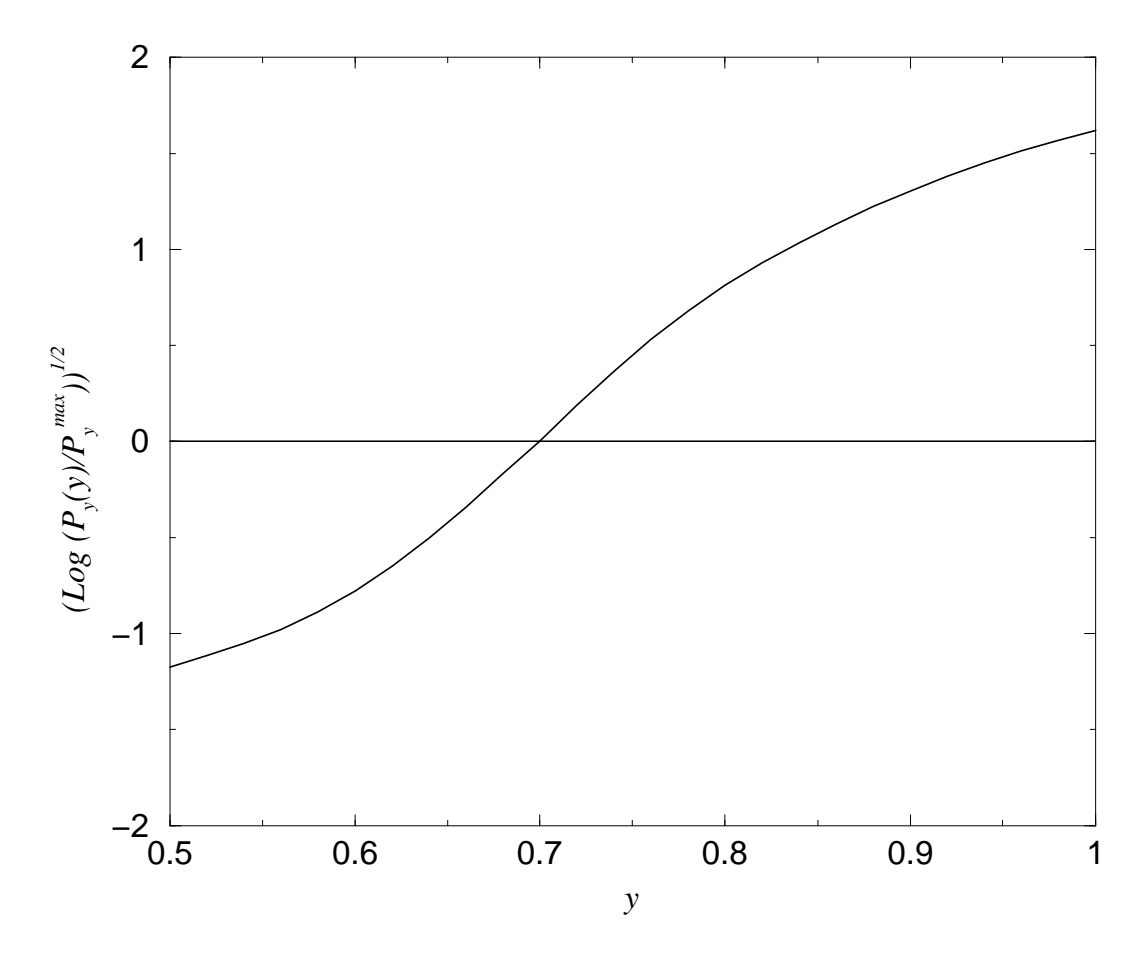


Figure 6.4: In this figure we plotted  $\sqrt{\ln(P_y(y)/P_y^{max})}$  vs. y to check how well  $P_y$  may be fitted in Gaussian distribution. If  $P_y$  were Gaussian, then graph would be a straight line. Disorder strength  $\gamma=.1$ 

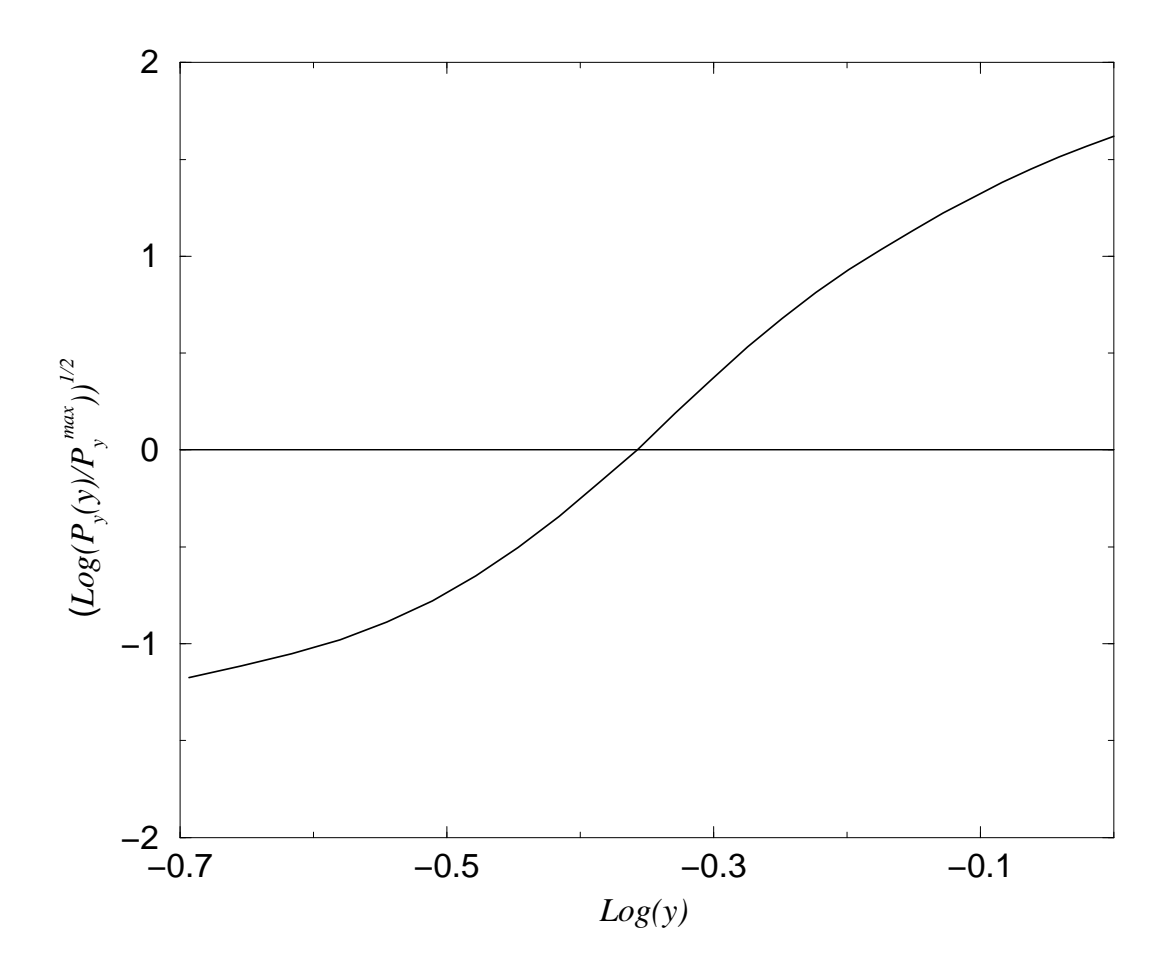


Figure 6.5: In this figure we plotted  $\sqrt{\ln(P_y(y)/P_y^{max})}$  vs.  $\ln y$  to check how well  $P_y$  may be fitted in log-normal distribution. If  $P_y$  were log=normal, then graph would be a straight line. Disorder strength  $\gamma=.1$ 

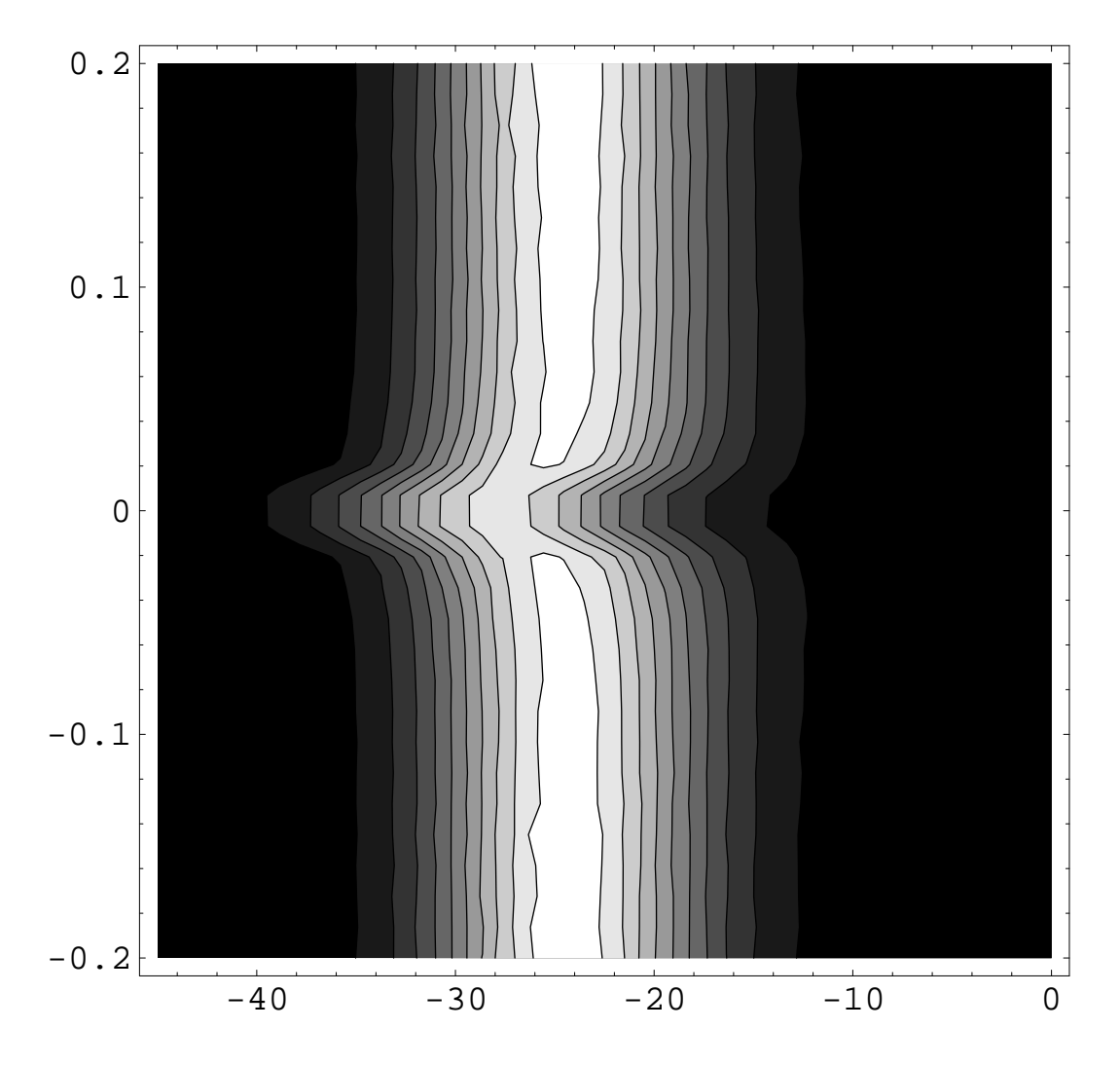


Figure 6.6: Contour plot of the function  $P_{x,\ln y}/P_x(x)$  in variables x and  $\ln \eta = \ln(yf(x))$ ; vertical and horizontal axis correspond to x and  $\ln \eta$  respectively. Simulation done for:  $m=3,\ \gamma=7.81\ (\alpha=0.122),\ N=10000$ 

### 6.4 General Approach

Integral equation corresponding to Eq(6.3) has the following generic form (in Fourier or Laplace-Fourier space), see Appendix C.2:

$$P_G(k,s) = \int_{-\infty}^{+\infty} dk' \int_{0}^{+\infty} \frac{ds'}{s'} Ker(k,s;k',s') P_G(k',s')^m$$
 (6.4)

where k is conjugate to x and s is conjugate to y. The toy model and NSM [48] equations have the same structure. On the insulator side the distribution function  $P_G$  depends on the single variable k:  $P_G(k,s) \equiv P_x(k)$ . By definition,  $P_x(k) = P_G(k,0)$ 

At large s and s' the kernel Ker depends on the ratio s/s'. It implies that  $P_G$  is a scaling function of s near MIT with some characteristic scale  $y_{typical}^{-1}$ . Close to MIT  $P_G(k,s)$  has a soliton-like shape: for  $s \ll y_{typical}^{-1}$   $P_G(k,s) \to P_x(k)$ , and for  $s \gg y_{typical}^{-1}$   $P_G(k,s) \to 0$ . At the scale  $s \sim y_{typical}^{-1}$  there is a smooth kink.

For  $s \ll y_{typical}^{-1}$  deviation  $\delta P_G(k,s) = P_x(k) - P_G(k,s)$  from trivial solution  $P_x(k)$  is small. We expand Eq.(6.4) to the linear order in  $\delta P_G$ :

$$\delta P(k,s) = m \int_{-\infty}^{+\infty} dk' \int_{0}^{+\infty} \frac{ds'}{s'} Ker(k,s;k',s') P_x(k')^{m-1} \delta P(k',s')$$
 (6.5)

We expect the exact  $\delta P_G(k, s)$  to satisfy (approximately) this equation for  $s \ll y_{typical}^{-1}$ , provided Ker(k, s; k', s') decays sufficiently fast for s' > s. We argue that the critical behavior, like the position of the mobility edge, or the scale  $y_{typical}$  close to the transition, can be determined large  $s \gg 1$  asymptotics of the linearized integral equation [25, 48–50]. This will be the case if

$$\int_{-\infty}^{+\infty} dk' \int_{0}^{1} \frac{ds'}{s'} Ker(k, s; k', s') P_G(k', s')^{m-1} \delta P_G(k', s') \ll \delta P_G(k, s)$$

For  $s \gg 1$  the kernel depends on the ratio s/s', therefore the linear equation simplifies to:

$$\delta P(k,s) = m \int_{-\infty}^{+\infty} dk' \int_{0}^{+\infty} \frac{ds'}{s'} \tilde{Ker}(k,k,s/s') P_x(k')^{m-1} \delta P(k',s')$$
 (6.6)

where  $\tilde{Ker}(k, k, s/s')$  is the asymptotic form of Ker(k, k'; s, s').

The eigenfunction of the linear integral operator in Eq.(6.6) which corresponds to the exact solution of the nonlinear integral equation must satisfy the following conditions:

- 1) The eigenfunction should be matching the exact solution where the linearization procedure is not valid, that is at  $s \sim 1$  and  $s \sim y_{typical}^{-1}$ .
- 2) The eigenfunction should be nonegative for all s in the range  $1 \ll s \ll y_{typical}^{-1}$ , since  $P(k,s) \leq 1$ .
- 3) The corresponding eigenvalue  $\hat{\Lambda}$  should be largest in the class of the allowed eigenfunctions and it should be 1, otherwise the eigenfunction of the linearized equation cannot represent a stable solution of the nonlinear equation.

We will study the spectrum of the kernel of the Eq.(6.6), without the prefactor m, that is all eigenvalues are rescaled by m:  $\Lambda = \tilde{\Lambda}/m$ . The kernel of the form f(k, k', s/s')/s' has eigenfunctions of the form  $\psi_z = C(k)s^z$ , where C(k) is a real function and z is a complex number. The corresponding eigenvalue is denoted as  $\Lambda_z$ . Now we have an eigenfunction problem for an equation in one variable:

$$\Lambda_{z}(\gamma, z)C(k) = \int_{-\infty}^{+\infty} dk' \int_{0}^{+\infty} \frac{d\xi}{\xi^{1+z}} \tilde{Ker}(k, k', \xi) P_{x}(k')^{m-1} C(k')$$
 (6.7)

We are interested only real eigenfunctions with real eigenvalues. We denote the real eigenvalue as  $\Lambda(\gamma, \nu(b), b)$ :  $\Lambda(\gamma, \nu(b), b) \equiv \Lambda_{\nu+ib}(\gamma, \nu(b) + ib)$ , where  $\nu(b)$  is a solution of the equation  $Im\Lambda_{\nu+ib} = 0$ . We sketch function  $\nu(b)$  for the Anderson model and the toy model in the Figure.6.7. We also sketch real eigenvalue  $\Lambda(\gamma, \nu(b), b)$  as a function of  $\nu$  in the Figure.6.8. Two upper branches correspond to real z and the lower branch corresponds to complex value z. The kernel of the Eq.(6.7) is real, therefore  $\Lambda_z = \Lambda_{z^*}$ .

The real eigenfunction of the Eq.(6.6) will be denoted as  $\phi(s)$ . There are two ways of constructing  $\phi(s)$ , either as a linear combination of complex valued  $\psi_z$  or as a linear combination of real  $\psi_z$ . In the first case  $\phi(k,s) = C(k)(c_1\psi_z + c_1^*\psi_{z^*})$ 

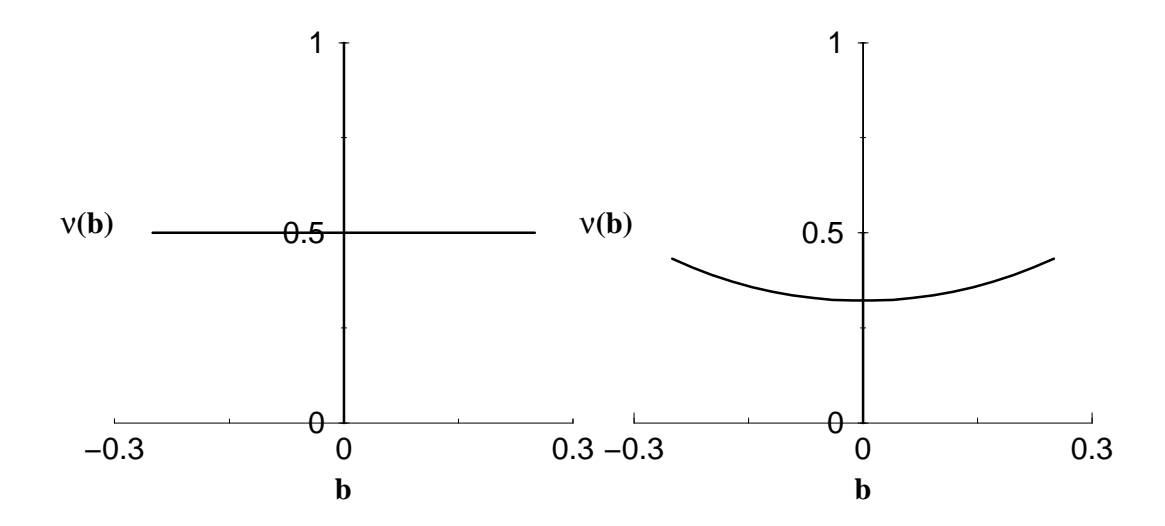


Figure 6.7: Solution of equation  $Im\Lambda_z = 0$  is plotted in  $b,\nu$  axes,  $z = \nu + ib$ , for the Anderson and toy models respectively.

with z satisfying  $Im\Lambda_z = 0$ . In the second case  $\phi(k,s) = C(k)(c_1\psi_{z_1} + c_2\psi_{z_2})$  with  $z_1$  and  $z_2$  satisfying  $\Lambda_{z_1} = \Lambda_{z_2}$ .

Let us consider these two cases in more detail. It is convenient to switch to the logarithmic variable  $\theta = \ln s$  because the kernel is translationally invariant in  $\theta$ . We first consider the eigenfunctions corresponding to the real  $z_1, z_2$ :

$$\phi_1(\theta) = e^{\tilde{\nu}\theta} \sinh(\tilde{b}\theta + c) \quad or \quad \phi_1(\theta) = e^{\tilde{\nu}\theta} \cosh(\tilde{b}\theta + c)$$
 (6.8)

where  $\tilde{\nu} = (z_1 + z_2)/2$  and  $\tilde{b} = (z_2 - z_1)/2$ . We assume that  $z_1 \leq z_2$ . To see how well this function can match the exact solution we compute the logarithmic derivative at  $\theta = 0$  and  $\theta = \theta_k = -\ln y_{typical}$  (that is for s = 1 and  $s = y_{typical}^{-1}$ ). The scale  $\theta_k$  represents the position of the kink in the distribution function. For  $\phi_1 \sim \sinh$  we have:

$$\frac{\phi_1'(\theta)}{\phi_1(\theta)} = \tilde{\nu} + \tilde{b} \coth(\tilde{b}\theta + c) = \begin{cases} \tilde{\nu} + \tilde{b} \coth(c), & \theta = 0\\ \tilde{\nu} + \tilde{b}, & \theta = \theta_k \end{cases}$$
(6.9)

similarly for  $\phi_1 \sim \cosh$ :

$$\frac{\phi_1'(\theta)}{\phi_1(\theta)} = \tilde{\nu} + \tilde{b} \tanh(\tilde{b}\theta + c) = \begin{cases} \tilde{\nu} + \tilde{b} \tanh(c), & \theta = 0\\ \tilde{\nu} + \tilde{b}, & \theta = \theta_k \end{cases}$$
(6.10)

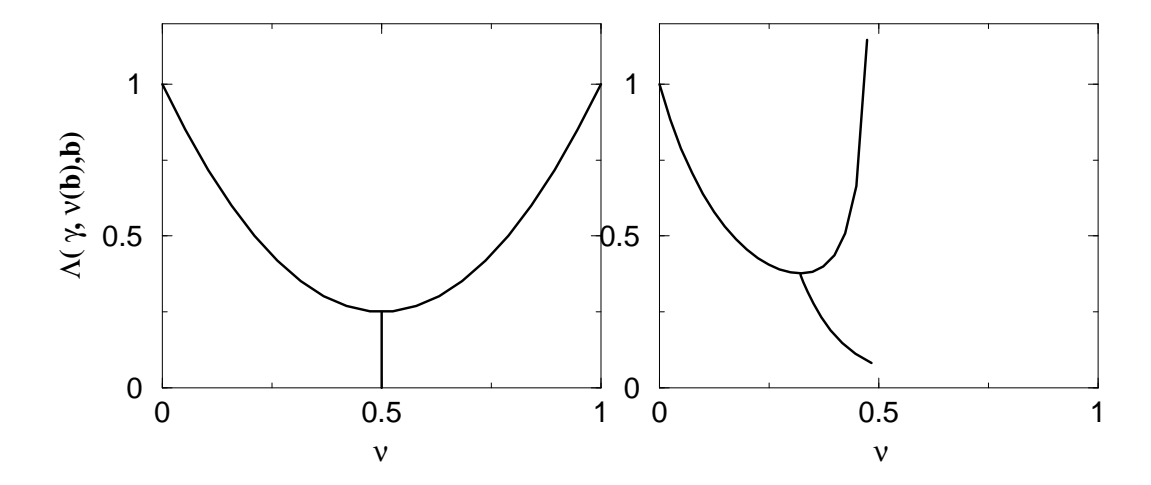


Figure 6.8: Real eigenvalue  $\Lambda(\gamma, \nu(b), b)$  is plotted as a function of  $\nu$  for the Anderson and toy models. In the first case eigenvalue is symmetric function with respect to  $\nu = 1/2$ . Lower branch corresponds to nonzero b, it is a monotonically growing function of b(for b > 0). Two brunches merge at the minimum of the upper branch.

We see that there is some freedom in matching the nonlinear solution of the integral equation, however it is limited, and this is possible only for finite  $\tilde{b}$  and c. Now we show that the eigenfunctions corresponding to the complex z has a significant advantage. The complex z eigenfunction reads:

$$\phi_2(\theta) = e^{\nu(b)\theta} \sin(b\theta + c) \tag{6.11}$$

where  $\nu(b) = \text{Re}z$  and b = Imz. We compute the logarithmic derivative for  $\phi_2$ :

$$\frac{\phi_2'(\theta)}{\phi_2(\theta)} = \nu + \tilde{b}\cot(b\theta + c) = \begin{cases} \nu + b\cot(c), & \theta = 0\\ \nu + \cot(b\theta_k + c), & \theta = \theta_k \end{cases}$$
(6.12)

The crucial difference between  $\phi_1$  and  $\phi_2$  is that  $\phi_2$  has poles at  $b\theta + c = n\pi$  and therefore is somewhat "flexible" in terms of satisfying matching conditions. For  $\phi_2$  these conditions can be meet with b and c of order  $\theta_k^{-1}$ . Since the eigenfunction should be nonnegative for  $0 < \theta < \theta_k$  we must choose n = 0, 1. We argue that  $\phi_1$  cannot be considered matched with the exact solution near the metal to insulator transition, but  $\phi_2$  can. This line of reasoning sets the scale  $\theta_k \sim \pi/b$ . The transition occurs when the kink moves to infinity and  $b \to 0$ .

The transition point can be identified in the Fig.(6.8). In that figure two upper branches correspond to  $\phi_1$  and the lower brunch corresponds to  $\phi_2$ . The lower brunch is doubly degenerate, since  $\Lambda(\nu(-b), -b) = \Lambda(\nu(b), b)$ . The limit  $b \to 0$  is approached at the top of the  $\phi_2$  branch. The three branches meet in the minimum of two upper branches, what follows from the equation  $Im\Lambda(\nu + ib) = 0$ . Indeed,  $Im(\Lambda(\nu) + \Lambda'(\nu)ib + O(b^2)) = 0$ , or  $\Lambda'(\nu) = O(b^2)$ . This proves that the condition for MIT transition can be written as  $m_c \min\{\Lambda(\nu(0), 0) = 1 \text{ or:}$ 

$$m_c \Lambda(\nu_0, 0) = 1 \tag{6.13}$$

where  $\nu_0$  gives the minimum of  $\Lambda_z$  restricted to real z. Near the transition the eigenvalue should satisfy:

$$m\Lambda(\nu(b), b) = 1 \tag{6.14}$$

Expanding this equation near the mobility edge  $\nu = \nu_0$ , b = 0 on the metallic side we have:  $(m - m_c)\Lambda(\nu_0, 0) - m_c/2\Lambda''(\nu_0, 0)b^2 = 0$  or:

$$b = \left(\frac{m - m_c}{m_c}\right)^{\frac{1}{2}} \left(2\frac{\Lambda(\nu_0, 0)}{\Lambda''(\nu_0, 0)}\right)^{\frac{1}{2}}$$
(6.15)

This is a general result [25, 48, 50] which describes the critical behavior of the kink:  $\theta_k \sim (\frac{m-m_c}{m_c})^{-\frac{1}{2}}$ . We see that the eigenvalue  $\Lambda(\nu(b), b)$  is a central quantity determining mobility edge and the dynamics of the kink of  $P_G(k, s)$  near the transition.

# 6.5 Toy Model

Here we consider a simplification of the Anderson model, which we the call toy model. The imaginary part of the AM recursive equation eq(6.3) reads:

$$y = \frac{\sum_{j=1}^{m} y_j}{(\epsilon + \sum_{j=1}^{m} x_j)^2 + (\sum_{j=1}^{m} y_j)^2}$$
(6.16)

In this equation real and imaginary parts of Green's function are not independent on each site J, though near MIT the distribution function of the real part is determined by equation involving  $P_x(x)$  only. If in eq(6.16) x and y variables in rhs are assumed being independent, then this equation will describe the toy model:

$$y = \frac{\sum_{j=1}^{m} y_j}{\epsilon'^2 + (\sum_{j=1}^{m} y_j)^2}$$
 (6.17)

where  $P_{\epsilon'} = P_{\epsilon + \sum_{j=1}^{m} x_j}$  and  $P_{\epsilon'}(k) = P_{\epsilon}(k)P_x(k)^m$ . The assumption that x and y are uncorrelated is reasonable for large m for two reasons: 1) the correlation between the sums  $\sum x_j$  and  $\sum y_j$  becomes weaker as m increases, 2) the width of the distribution of  $\sum x_j$  is much smaller than the width of  $P_{\epsilon}$ , (see Appendix C.3). The validity of the assumption at low m is not clear, and we will see that two models have some differences in the limit  $m \to 1$ .

The TM shares many features with the Anderson model (AM). It is easy to simulate Anderson transition on a finite size "lattice" using recursion relation eq(6.17) and the technique we described in the section 6.4. The toy model, like the AM, has the transition for  $1 < m < \infty$ . If we plot  $y_{typical}$  as a function of disorder strength it will look similar to Fig.6.1, where we plotted  $y_{typical}$  for AM. Vanishing typical density of states is a distinguished feature of the Anderson transition. In Fig.6.9 we compared distribution functions obtained in the simulation for AM and TM. We adjusted the disorder strength to have the same  $y_{typical}$  in two case.

The equation Eq.(6.17) can be written in the form of an integral equation for  $P_y(y)$  (see Appendix C.4):

$$\bar{P}_y(s) = 1 + \int_0^{+\infty} ds' Ker(s, s') \bar{P}_y^{\ m}(s')$$
 (6.18)

where  $Ker(s, s') = Ker_1(s, s') + Ker_2(s, s')$ 

$$Ker_1(s,s') = -\frac{\sqrt{2s}}{\sqrt{s'}} J_1(\sqrt{2ss'}) \tilde{P}_{\epsilon'}(s')$$
(6.19)

$$Ker_2(s,s') = \int_{-s'}^{s'} dk' \frac{s}{2\sqrt{s'^2 - k'^2}} J_1(\sqrt{s(s'+k')}) J_1(\sqrt{s(s'-k')}) \tilde{P}_{\epsilon'}(k') \quad (6.20)$$

In this equation  $\bar{P}_y(s)$  is the Laplace transform of the distribution function. The

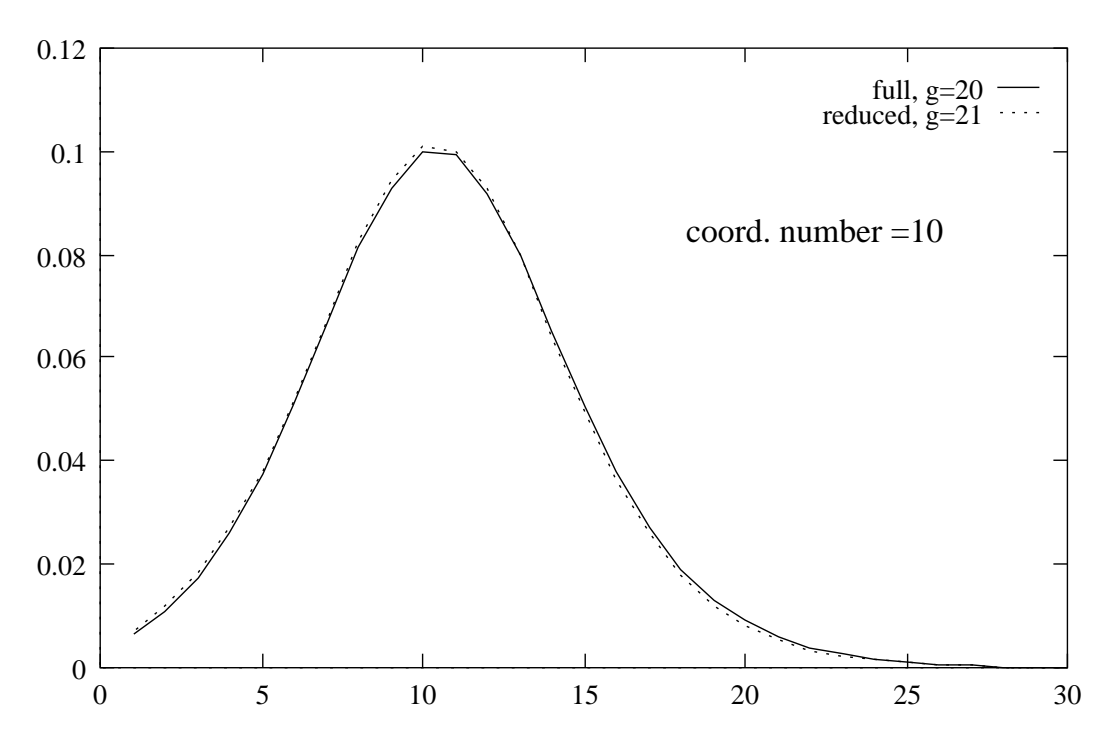


Figure 6.9:  $P_{-\log(y)}$  at coord. number =10

Laplace transform of the distribution function  $P_y(y)$  is necessarily real and positive. Since y is always positive, the Laplace transform is an analytical continuation of the Fourier transform to the imaginary axis. Laplace transformed functions are marked with a bar.

The DOS in the AM is non critical across the MIT. The same is true for the TM. Variable y in the TM plays the role of the LDOS, and the DOS is averaged over sites LDOS:  $\langle y \rangle = \int dy y P_y(y) = \frac{\partial}{\partial s} \bar{P}_y(s)|_{s=0}$ . Differentiating eq(6.18) with respect to s and taking limit  $s \to 0$  we can see that only the term with  $Ker_1$  survives, yielding:

$$\frac{\partial}{\partial s}\bar{P}_y(s)|_{s=0} = \int_0^{+\infty} ds' \tilde{P}_{\epsilon'}(s') \bar{P}_y^{\ m}(s') \approx P_{\epsilon'}(0) = \alpha/\pi$$

 $\alpha$  is finite.

In the previous section we discussed how to analyze an integral equation for a distribution function in two variables. A similar method can be applied to the integral equation of the TM as well. The trivial (insulator phase) solution is now  $P_y(s) \equiv 1$ . Linearized eq(6.18) with the asymptotic kernel reads (this is the analog of eq(6.6)):

$$\delta P(s) = m \int_{0}^{+\infty} \frac{ds'}{s'} \tilde{Ker}(s/s') \delta P(s')$$
 (6.21)

We can drop the bar notation in P(s), keeping in mind that the variable s is used for the Laplace transform only. We will consider the Cauchy distribution of the random potential, because many results can be written in an analytical form for it. For the Cauchy distributed  $\epsilon$  (see Appendix C.4 and Appendix C.7):

$$Ker(\xi) = \sqrt{\xi} P_{\epsilon'}(\sqrt{\xi})$$
 (6.22)

From now on we omit tilde over Ker when it depends on one or three variables, this should be understood as an asymptotic form of the exact kernel. The eigenvalue can be computed explicitly:

$$\Lambda_z(\gamma, z) = \int_0^{+\infty} \frac{d\xi}{\xi^{1+z}} Ker(\xi) = \int_0^{+\infty} \frac{d\xi}{\xi^{\frac{3}{2}+z}} P_{\epsilon}(\sqrt{\xi}) = (\gamma^{2z} \cos \pi z)^{-1}$$
 (6.23)

The second plot in the Fig.6.8(second plot) we plotted real eigenvalues  $\Lambda_z$  for the Cauchy distribution. The upper branch is given by  $\Lambda(\gamma,\nu) = (\gamma^{2\nu}\cos\pi\nu)^{-1}$ .  $\Lambda(\gamma,\nu) \to \infty$ , when  $\nu \to 1/2$  and  $\Lambda(\gamma,\nu) \to 1$  when  $\nu \to 0$ ;  $\Lambda(\gamma,\nu)$  has one minimum at  $\nu_0 = \frac{1}{\pi}\arctan\left(\frac{2}{\pi}\ln\gamma\right) \approx 1/2 - 1/(2\ln\gamma)$ . The lower branch, corresponding to the complex  $z = \nu + ib$ , is given by the equation  $Im\Lambda_z = 0$ . This equation can be written as:

$$\tan \pi \nu \tanh \pi b \cot (2b \ln \gamma) = 1 \tag{6.24}$$

yielding for  $\nu(b)$ 

$$\nu(b) = \frac{1}{\pi} \arctan\left[ (\tanh(\pi b)\cot(2b\ln\gamma))^{-1} \right]$$
 (6.25)

Then from eq(6.23) we have:

$$\Lambda(\gamma, \nu(b), b) = \left[\frac{\gamma^{2\nu(b)}\cos \pi\nu(b)\cosh \pi b}{\cos (2b\ln \gamma)^2}\right]^{-1}$$
(6.26)

where  $\nu(b)$  is given by eq(6.25). It is easy to check that: 1)  $\Lambda(\gamma, \nu(b), b)$  is a monotonically decreasing function and  $\nu(b)$  is a monotonically increasing function of b (for positive b), 2) the minimum of the upper branch coincides with the maximum of the lower branch.

We use eq(6.13) and eq(6.15) to obtain:

$$m_c = \gamma^{2\nu} \cos \pi\nu \tag{6.27}$$

where  $\nu = \frac{1}{\pi} \arctan(\frac{2}{\pi} \ln \gamma)$ . Near the transition:

$$b = \left(\frac{m - m_c}{m_c}\right)^{\frac{1}{2}} \left(\frac{2}{4\ln\gamma^2 + \pi^2}\right)^{\frac{1}{2}} \tag{6.28}$$

In all the above formulas  $\gamma$  enters kernel (see eq(6.22)) in  $P_{\epsilon'}(\xi) = \frac{1}{\pi} \frac{\gamma}{\gamma^2 + \xi^2}$ . This  $\gamma$  is 'renormalized' disorder strength, which is related to the 'bare' strength  $\gamma_0$  as:  $\gamma = \gamma_0 + m\alpha$ .

Mobility edge in limits of the large and small coordination number is:

$$\gamma_0 \to \infty, \quad m_c \to \frac{\pi}{2e} \frac{\gamma_0}{\ln \gamma_0}$$
 (6.29)

$$\gamma_0 \to 0, \quad m_c \to 1 + \frac{2}{\pi^2} \gamma_0^2$$
 (6.30)

We will see that the low m expression for the mobility edge is different for the AM, in which  $m_c$  is linear with  $\gamma_0$  for  $m_c \to 1$ .

#### 6.6 Anderson Model

In this section we study the Anderson model. The disorder potential is Cauchy distributed. The equation determining the eigenvalue  $\Lambda(\gamma, \nu(0))$ , now reads:

$$\Lambda(\gamma,\beta)C_{\beta}(k) = \int_{-\infty}^{+\infty} \frac{dk'}{2\pi} \int_{0}^{+\infty} \frac{d\xi}{\xi^{3/2-\beta}} \cos(k\sqrt{\xi}) \cos(k'\sqrt{\frac{1}{\xi}}) \tilde{P}_{\epsilon'}(k')C_{\beta}(k') \quad (6.31)$$

where  $\tilde{P}_{\epsilon'}(k')$  is the Cauchy distribution with "renormalized" disorder strength  $\gamma' = \gamma + \alpha(m-1)$ , and  $\beta$  is real.

In the AM the eigenvalue has an interesting symmetry [49]:

$$\Lambda(\gamma, \beta) = \Lambda(\gamma, 1 - \beta) \tag{6.32}$$

To see that we multiply equation by  $\tilde{P}_{\epsilon'}(k)$  and switch integration from  $\xi$  to  $1/\xi$ :

$$\Lambda(\gamma,\beta)(\tilde{P}_{\epsilon'}(k)C_{\beta}(k)) = \int_{-\infty}^{+\infty} \frac{dk'}{2\pi} \int_{0}^{+\infty} \frac{d\xi}{\xi^{1/2+\beta}} \cos(k'\sqrt{\xi}) \cos(k\sqrt{\frac{1}{\xi}}) \tilde{P}_{\epsilon'}(k) (\tilde{P}_{\epsilon'}(k')C_{\beta}(k'))$$
(6.33)

In eq(6.31)  $C_{\beta}(k)$  is an eigenvector of  $Ker_{\beta}$  with eigenvalue  $\Lambda_{\beta}$ . In eq(6.33)  $\tilde{P}_{\epsilon'}(k)C_{\beta}(k)$  is an eigenvector of the kernel adjoint to  $Ker_{1-\beta}$ , corresponding to the same eigenvalue. By this we prove the symmetry relation eq(6.32). From this symmetry follows that the physical solution corresponds to  $\beta = 1/2$ , so from now on we will consider only this case and will drop the index  $\beta$ :  $C(k) \equiv C_{\beta=1/2}(k)$ . For  $\beta = 1/2$ ,  $Ker_{\beta} = Ker_{1-\beta}$  and  $g(k) = \tilde{P}_{\epsilon'}(k)C(k)$  is the adjoint of C(k).

The kernel  $\int_{-\infty}^{+\infty} \frac{dk'}{2\pi} \int_{0}^{+\infty} \frac{d\xi}{\xi} \cos(k'\sqrt{\xi}) \cos(k\sqrt{\frac{1}{\xi}})$  reads in real space:  $\int_{-\infty}^{+\infty} dy \frac{1}{|x|} \delta(y - \frac{1}{x})$ . From eq(6.31) we immediately have  $\Lambda C(x) = \frac{1}{|x|} g(\frac{1}{x})$ , and since we are interested in the case  $\Lambda m = 1$ :

$$mg(x) = \frac{1}{|x|}C(\frac{1}{x})$$
 (6.34)

We use variables x or y is an argument of a function to denote the function in real space; if k is used as an argument, it is a Fourier transform of a function. For example C(k) is the Fourier transform of C(x).

In general C(x) cannot be found analytically, but we can construct an approximation for C(x) which becomes exact in the limit  $\gamma \to \infty$  (C(x) for both large and small disorder is studied numerically in Appendix C.6). We want to show that at large  $\gamma'$  in the region  $k/\gamma' \ll 1$ :  $C(k) \approx \mathbf{C}_{eul} + \ln \frac{|k|}{\gamma'} + O(1/\ln \gamma')$ . Due to presence of the exponentially decaying function  $\tilde{P}_{\epsilon'}(k) = \exp(-\gamma'|k|)$  in the kernel, knowledge of C(k) at  $k/\gamma' \ll 1$  is sufficient to determine the whole function C(x). We plug  $C(k) = \mathbf{C}_{eul} + \ln \frac{|k|}{\gamma'} + O(1/\ln \gamma')$  into the rhs of eq(6.31)

and show that this is approximately an eigenfunction. We perform integration:

$$\Lambda(\gamma,\beta)C_{\beta}(k) = \int_{-\infty}^{+\infty} \frac{dk'}{2\pi} \int_{0}^{+\infty} \frac{d\xi}{\xi^{3/2-\beta}} \cos(k\sqrt{\xi}) \cos(k'\sqrt{\frac{1}{\xi}}) e^{-\gamma'|k'|} \times \left(\mathbf{C}_{eul} + \ln\frac{|k'|}{\gamma'} + O(1/\ln\gamma')\right) = \int_{0}^{+\infty} \frac{d\xi}{\xi} \cos(k\sqrt{\xi}) \frac{1}{\pi} \frac{\gamma'}{\gamma'^2 + \frac{1}{\xi}} \times \left[2\ln\gamma' + \frac{1}{2}\ln(1 + \frac{1}{\xi\gamma'^2}) + \frac{1}{\sqrt{\xi}\gamma'} \arctan\frac{1}{\sqrt{\xi}\gamma'} + O(1/\ln\gamma')\right] = \frac{4\ln\gamma'}{\pi\gamma'} \left(-\frac{1}{2} \left[e^{-\frac{k}{\gamma'}} \mathbf{Ei}(\frac{k}{\gamma'}) + e^{\frac{k}{\gamma'}} \mathbf{Ei}(\frac{-k}{\gamma'})\right] + O(1/\ln\gamma')\right) \tag{6.35}$$

We have used the formula:

$$\int_0^{+\infty} dy y \cos(xy) \frac{1}{1+y^2} = -\frac{1}{2} [e^{-x} \mathbf{Ei}(x) + e^x \mathbf{Ei}(-x)]$$
 (6.36)

where  $\mathbf{Ei}(x)$  is exponential integral. Using the expansion:

$$\frac{1}{2}\left\{e^{-x}\mathbf{Ei}(x) + e^{x}\mathbf{Ei}(-x)\right\} \to (\mathbf{C}_{eul} + \ln|x|), \quad x \to 0$$
(6.37)

we find lhs of eq(6.31) at small  $k/\gamma'$ :

$$\Lambda(\gamma)C(k) = \frac{4\ln\gamma'}{\pi\gamma'}(\mathbf{C}_{eul} + \ln\frac{|k|}{\gamma'} + O(1/\ln\gamma'))$$
(6.38)

We can make two conclusions here: 1) at large coordination number transition occurs at  $m = \pi \gamma'/(4 \ln \gamma')$ ; 2) the function C(x) is given by:

$$C(x) = \frac{1}{\pi} \frac{\gamma'^{-1}|x|}{\gamma'^{-2} + x^2} \left[ 2\ln\gamma' + \frac{1}{2}\ln(1 + \frac{1}{x^2\gamma'^2}) + \frac{1}{x\gamma'}\arctan\frac{1}{x\gamma'} + O(\frac{1}{\ln\gamma'}) \right]$$
(6.39)

it follows from eq(6.35). We know the small k asymptotics of C(k) at small k and can also find asymptotics for large k (it comes from Fourier transformation of the first term in eq(6.39)):

$$C(k) \to \begin{cases} -(\mathbf{C}_{eul} + \ln \frac{|k|}{\gamma'}), & \frac{k}{\gamma'} \ll 1\\ \propto \frac{\gamma'^2}{k^2}, & \frac{k}{\gamma'} \gg 1 \end{cases}$$

$$(6.40)$$

The limits for C(k) were obtained for the case of large  $\gamma'$ . From eq(6.39) we clearly see that  $1/\gamma'$  is a characteristic scale for C(x) ( $\gamma'$  is characteristic scale for C(k)). This is different for small  $\gamma'$ , see e.g. Fig.C.1. Let us try to extend

the result for the region of small  $\gamma'$ . The following arguments are not rigorous, but hopefully we explain the qualitative picture. In eq(6.31)  $\gamma'$  plays the role of a cut off, which arises from  $\tilde{P}_{\epsilon'}(k)$ . Function C(k), as wee can see in eq(6.40) has an "effective cut off"  $1/\gamma'$  (in the real space). We can say, that the cut off  $\Lambda$  in the rhs of eq(6.31) generates the cut off  $\Lambda^{-1}$  in the lhs. Let us also assume that convolution of two functions with characteristic scales  $\Lambda_1$  and  $\Lambda_2$  has a new characteristic scale  $\Lambda_1 + \Lambda_2$ . Let  $\kappa$  be the cut off (characteristic scale) for C(k), then  $\kappa + \gamma'$  is a cut off for  $\tilde{P}_{\epsilon'}(k)C(k)$ , what results in the cut off  $(\kappa + \gamma')^{-1}$  in the rhs of the equation. From where follows:

$$(\kappa + \gamma')^{-1} = \kappa \tag{6.41}$$

Recalling that

$$\gamma' = \gamma + \alpha(m-1) \tag{6.42}$$

and

$$\alpha^{-1} = \gamma + \alpha m \tag{6.43}$$

one gets  $\kappa = \alpha = (-\gamma + \sqrt{\gamma^2 + 4m})/(2m)$ . The limits of C(k) for large and small k become:

$$C(k) \to \begin{cases} -(\mathbf{C}_{eul} + \ln|k|\alpha), & k\alpha \ll 1\\ \propto \frac{1}{k^2\alpha^2}, & k\alpha \gg 1 \end{cases}$$
(6.44)

Eq(6.44) reduces to eq(6.40) in the limit of large  $\gamma$  since  $\alpha \to 1/\gamma$  as  $\gamma \to \infty$ . Apparently  $\alpha$  is a quantity correctly defining scale in the whole range of coordination number. It is a scale in very relaxed sense: when  $\alpha$  is small (large  $\gamma$ ) C(x) is given by eq(6.39), when  $\alpha \to 1$  ( $\gamma \to 0$ ) C(x) tends to some function. Precise form of that limiting function can be found only numerically. Some details are discussed in Appendix C.6.

We made an ansatz that distribution function near MIT can be written in the following form:

$$P_{x,y}(x,y) = P_x(x)Q(yf(x))f(x)$$
 (6.45)

where function  $Q(\xi)$  is normalized to 1:  $\int d\xi Q(\xi) = 1$ . This is true for NSM. How well this formula works for AM can be tested numerically (see Fig.6.6). From expansion  $P_{x,y}(k,s) = P_x(k) + C(k)\sqrt{s}$  we conclude that at large y ( $y_{typical} \ll y \ll 1$ ):

$$P_{x,y}(x,y) \propto C(x)y^{-3/2}$$
 (6.46)

Form of  $P_G$  given by eq(6.45) is quite restrictive, so from eq(6.46) and eq(6.45) follows  $Q(\xi) \propto \xi^{-3/2}$  and:

$$f(x) = (P_x(x)/C(x))^2 (6.47)$$

In NSM [48]  $f(x) = 1/(\alpha^2 + x^2)$ . In AM f(x) has similar behavior:  $f(x) \sim const$  as  $x \to 0$ ,  $f(x) \sim 1/x^2$  as  $x \to \infty$ , f(x) has scale  $\alpha$ . Indeed,  $C(x) \sim const$  and  $P_x(x) \sim const$  at small x,  $C(x) \sim 1/x$  and  $P_x(x) \sim 1/x^2$  at large x, and both functions have  $\alpha$  as a characteristic scale.

The equation yf(x) = const should determine the position of the kink in the x - y plain. Solution,  $y_k = f(x)^{-1} = (C(x)/P_x(x))^2$ , more or less agrees with simulation (see Fig.6.6). Deviation from the scaling form at small x can likely be attributed to the presence of the long tails in the Cauchy distribution.

### 6.7 Integral Equation Reduction

We would like to reduce number of variables in the integral equation from two to one by getting rid of the variable k, which is auxiliary, because the distribution of x variable is non critical. First we switch to variables, in which  $P_G$  factorizes. Expanding  $P(k,s) = P_x(k)H(\eta)$  an comparing this expansion to  $P(k,s) = P_x(k) + C(k)\sqrt{s}$  we find new variables:

$$P(k,s) = P_x(k)H(\eta), \quad \eta = sh^{-2}(k), \quad h(k) = \frac{P_x(k)}{C(k)}$$
 (6.48)

For h(k) at small and large k we have (from eq(6.44)):

$$\frac{P_x(k)}{C(k)} \to \begin{cases}
-e^{-\alpha|k|} (\mathbf{C}_{eul} + \ln|k|\alpha)^{-1}, & k\alpha \ll 1 \\
\propto e^{-\alpha|k|} k^2 \alpha^2, & k\alpha \gg 1
\end{cases}$$
(6.49)

In the new variables  $(k \text{ and } \eta)$  the integral equation reads:

$$P(k,\eta) = \int_{-\infty}^{+\infty} \frac{dk'}{2\pi} \int_{0}^{+\infty} \frac{d\eta'}{\eta'} \sqrt{\frac{\eta}{\eta'}} \frac{h(k)}{h(k')}$$

$$\times \cos\left(k \frac{h(k')}{h(k)} \sqrt{\frac{\eta'}{\eta}}\right) \cos\left(k' \frac{h(k)}{h(k')} \sqrt{\frac{\eta}{\eta'}}\right) P_{\epsilon}(k') P^{m}(k',\eta') \quad (6.50)$$

To reduce number of variables in the integral equation we act on the rhs of eq(6.50) with some projection operator  $\hat{\Pi}$ :  $\hat{\Pi}P(k,\eta) = \Psi(k) \int dk \Phi(k) P(k,\eta)$ . Equation then reduces to:

$$H(\eta) = \int_{-\infty}^{+\infty} dk \Phi(k) \int_{-\infty}^{+\infty} dk' \int_{0}^{+\infty} \frac{d\eta'}{\eta'} Ker(k, k', \eta/\eta') \Psi(k')^m H(\eta')^m$$
 (6.51)

where  $Ker(k, k', \xi) = \sqrt{\xi} \frac{h(k)}{h(k')} \cos(k \frac{h(k')}{h(k)} \frac{1}{\sqrt{\xi}}) \cos(k' \frac{h(k)}{h(k')} \sqrt{\xi}) P_{\epsilon}(k')$ . To make eq(6.51) equivalent to eq(6.50) one has to choose  $\Psi(k)$  and  $\Phi(k)$ :  $\Psi(k) = P_x(k)$ ,  $\Phi(k) = N^{-1}\phi(k)$ , where  $N = \int dk P_x(k) \phi(k)$  and  $\phi(k)$  is quite arbitrary.

If we also want to preserve symmetry of the eigenvalue  $\Lambda_{\beta} = \Lambda_{1-\beta}$ , we need to choose  $\phi(k)$  being adjoint eigenfunction of the linearized eq(6.50):  $\phi(k) = P_{\epsilon}(k)P_x(k)^m/h^2(k)$ . Then eigenvalue is given by:

$$\Lambda_{\beta} = \int_{-\infty}^{+\infty} \frac{dk dk'}{2\pi} \int_{0}^{+\infty} \frac{d\xi}{\xi^{3/2-\beta}} (h(k)h(k'))^{-1} \times \cos(k \frac{h(k')}{h(k)} \sqrt{\frac{1}{\xi}}) \cos(k' \frac{h(k)}{h(k')} \sqrt{\xi}) P_{\epsilon}(k) P_{\epsilon}(k') P(k, \eta)^{m} P(k', \eta')^{m}$$
(6.52)

to see that the expression is symmetrical with respect to change  $\beta \to 1 - \beta$ , we have to switch simultaneously  $\xi \to 1/\xi$  and exchange k and k'.

Finally, equation reduced to one variable reads:

$$H(\eta) = \frac{1}{N} \int_0^{+\infty} \frac{d\eta'}{\eta'} \sqrt{\frac{\eta}{\eta'}} \frac{1}{2\pi} dk dk'$$

$$\times \cos(k \frac{h(k')}{h(k)} \sqrt{\frac{\eta'}{\eta}}) \cos(k' \frac{h(k)}{h(k')} \sqrt{\frac{\eta}{\eta'}}) g(k) g(k') H^m(\eta') \quad (6.53)$$

where  $N = \int dk C(k)g(k)$ 

For more discussion see Appendix C.8.

### 6.8 Comparison of NSM, TM and AM

In this section we compare critical behavior in three models: TM, NSM and AM. We study dependence of mobility edge on disorder at large and small m.

For TM we obtained:

$$m_c \to 1 + \frac{2}{\pi^2} \gamma^2, \qquad \gamma \to 0$$
 (6.54)

$$m_c \to \frac{\pi}{2e} \frac{\gamma}{\ln \gamma}, \qquad \gamma \to \infty$$
 (6.55)

In NSM mobility edge is given by [48]:

$$\frac{1}{m_c} = \alpha (K_0(\alpha) I_{\frac{1}{2}}'(\alpha) - K_0'(\alpha) I_{\frac{1}{2}}(\alpha))$$
 (6.56)

from where we find: at small  $\alpha$ ,  $m_c \to -\sqrt{\frac{\alpha}{2\pi}} \ln \alpha$ ; at large  $\alpha$ ,  $m_c \to 1 + \frac{1}{8\alpha}$ . In NSM  $\alpha$  should be treated like  $1/\gamma^2$  in TM. So:

$$m_c \to 1 + \frac{\gamma^2}{8}, \qquad \gamma \to 0$$
 (6.57)

$$m_c \to \frac{\sqrt{\pi}\gamma}{\sqrt{2}\ln\gamma}, \qquad \gamma \to \infty$$
 (6.58)

We see that TM and NSM have similar behavior in what concerns the mobility edge position.

Finding the mobility edge in AM with Cauchy distributed disorder mounts to determining the largest eigenvalue (which corresponds to the only positive eigenfunction) of the integral operator with the kernel:

$$K(t,u) = \frac{1}{\pi} \frac{1}{|u|} \frac{\gamma}{\gamma^2 + (\frac{1}{u} + t)^2}$$
(6.59)

Just from the form of the kernel we may guess that corrections to the eigenfunction and eigenvalue at small  $\gamma$  are linear with  $\gamma$ , since the kernel has long tails  $\propto \gamma$ .

It also clearly follows from numerical solving eigenvector problem. We obtained the following set of numbers:  $\{m_c - 1, \gamma\} = \{0.061, 0.3; 0.10, 0.5; 0.21, 1\}$ . It is difficult to approach very small  $\gamma$ . But even these numbers reveals linear law with good accuracy, we have:  $(m_c - 1)/\gamma = 0.205 + 0.005$ . We also applied a variational approach (see Appendix C.5) which yielded:  $(m_c - 1)/\gamma = 2/\pi^2 = 0.2026$ , what is surprisingly close to the numerical result. So, for AM we get:

$$m_c \to 1 + c_1 \gamma, \quad c_1 \sim \frac{2}{\pi^2}, \qquad \gamma \to 0$$
 (6.60)

$$m_c \to \frac{\pi \gamma}{4 \ln \gamma}, \qquad \gamma \to \infty$$
 (6.61)

We see that, while at large disorder AM resembles TM and NSM (cf. eq(6.55-6.54, 6.58-6.57)), at small disorder it is different.

We also want to compare expansion in the parameter b defining kink scale. We showed that in general  $\Lambda(\gamma, \nu, b) = \Lambda(\gamma, \nu, 0) + \#b^2$ . We want to make sure that nothing extraordinary happens at  $m \to 1$ . We start with the toy model. As we derived before

$$\Lambda(\nu, b) = (\gamma'^{2\nu} \cos \pi\nu \cosh \pi b / \cos (2b \ln \gamma'))^{-1}$$

where  $\nu = \frac{1}{\pi} \arctan\left(\frac{2}{\pi} \ln \gamma'\right) + O(b^2)$ . In our case  $\gamma' \to 1$  and  $\nu \to O(b^2)$ . We see that  $b^2$  term arises only from  $\cosh \pi b$ . Finally from expansion of  $1/\cosh \pi b$  and eq(6.54) we have:

$$\Lambda \to 1 - \frac{\gamma^2}{2\pi^2} - \frac{\pi^2}{2}b^2 \tag{6.62}$$

In the NSM, the role of  $\Lambda$  is played by some function  $\Gamma_{0\rho}(\alpha)$  [48]:

$$\Gamma_{0\rho}(\alpha) = \alpha (K_{\rho}(\alpha) I_{\frac{1}{2}}'(\alpha) - K_{\rho}'(\alpha) I_{\frac{1}{2}}(\alpha))$$
(6.63)

where  $\rho$  is equivalent to b. We will expand  $\Gamma_{0\rho}(\alpha)$  in  $\alpha^{-1}$  and  $\rho$  around  $\alpha = \infty$  and b = 0.  $\alpha^{-1}$  is equivalent to  $\gamma^2$ . It is not hard to find that

$$\frac{\partial}{\partial \alpha^{-1}} \Gamma_{00}(\infty) = -\frac{1}{8} \tag{6.64}$$

and

$$\frac{\partial^2}{\partial \rho^2} \Gamma_{0\rho=0}(\infty) = 1 \tag{6.65}$$

To obtain last formula we used that  $\frac{\partial^2}{\partial \rho^2} K_{\rho=0}(z) \to K_i(z)$  when  $z \to \infty$ . So the expansion is:

$$\Gamma_{0\rho}(\gamma^{-2}) = 1 - \frac{1}{8}\gamma^2 + \frac{1}{2}\rho^2$$
(6.66)

To estimate coefficient in the expansion for the full model we use the same approach (see Appendix C.5) as for the expansion in  $\gamma$  only. But kernel in eq(6.59) now is slightly modified:

$$K(t,u) = \frac{1}{\pi} \frac{1}{|u|} \frac{\gamma}{\gamma^2 + (\frac{1}{u} + t)^2} \frac{|u|^{ib} + |u|^{-ib}}{2}$$
(6.67)

Then instead of eq(C.37) we have:

$$\Lambda_{l} = \max\{\frac{1}{\pi^{2}} \int_{0}^{+\infty} dk c^{ib} \mathbf{G}_{13}^{21} \left(\frac{k^{2}}{4c^{2}} \Big|_{\frac{ib}{2}, 0, \frac{1}{2}}^{\frac{1}{2} + \frac{ib}{2}}\right) K_{0}(kc) e^{-\gamma k} + C.C.\}$$
(6.68)

Further calculations were performed numerically. We found that coefficient near  $b^2$  is finite when  $\gamma \to 0$ . So we found:

$$\Lambda(\gamma, b) = 1 - \frac{2}{\pi^2}\gamma + constb^2$$
(6.69)

where  $const \approx -1.1$ . As for  $b^2$  term in the expansion, all three model exhibit similar behavior.

# Chapter 7

### Conclusion

We have performed a semiclassical analysis of the E-DMFT equations for a simple Fermion Boson model. Comparison with earlier QMC treatments of the same problem reveals that this method reproduces semiquantitatively all the trends found in the previous study [28]. It can be used therefore in the study of more complicated systems, such as fermions interacting with spin fluctuations. We also investigated this approach in the order phase revealing some inadequacies of the approach which are closely related to the existence of anomalous dimensions in finite dimensional systems. Since this non trivial k dependence which is characteristic of low dimensional systems cannot be generated by a local theory, EDMFT produces spurious results such as the existence of a first order phase transition in d < 4. Since at zero temperature the dynamical critical exponent is such that in two dimensions an ansatz without anomalous dimensions is internally consistent, [31] a continuation of the disordered state, beyond the first order phase transition, might be useful to study this system. In this spirit we pointed out that a continuation of the E-DMFT, at finite temperatures, suitably interpreted, gives improved estimates of the critical temperature compared to the simplest mean field treatment or the Bloch Langer method [37]. It could be used to obtain better estimates of ferromagnetic transition temperatures where spatial fluctuations of the order parameter substantially decrease the Curie temperature below the DMFT estimates. This is the case of bcc Iron [51], a problem which will require a more realistic investigation of EDMFT. Further investigation of the quantum problem will require zero temperature methods which go beyond the semiclassical approximation.

We derive a general criterion for the disordered phase instability in EDMFT. Our analysis elucidates the signuture of the second order transition when approached from the disordered side. This result is a reminder of a known fact [42], that no precursor effect of the instability toward a symmetry breaking can be observed at the one-particle level. This result also casts some doubt on the validity of the EDMFT description of the local quantum criticality [52] in terms of the Bose Fermi Kondo model, at least in the way it was formulated in Ref. [31].

We took a different perspective on the DMF theories, by considering equations for two body vertices - parquet equations. Local approximations leading to DMFT and EDMFT can be concisely formulated using parquet equation. The local approximation can be extended to include 1/d corrections, arising in particle particle and particle hole channels. This allows to feed back to the local selfenergy nonlocal superconducting fluctuations, for example. This can also be viewed as an extension alternative to a cluster DMFT, which requires much more computing power for solving. The downside is that one has to deal with matrix inversion in the selfconsistency conditions. Yet this can be considered as a starting point for simplifying approximations.

Finally, we performed detailed analysis of the Anderson model of localization and compared it to the non linear sigma model description.

# Appendix A

### **EDMFT**

#### A.1 Critical Temperature

The transition to the ordered state for a classical model in BL method is signaled by the divergence in the zero momentum term in the sum:

$$G_2 = \sum_{q} \frac{J_q}{1 - J_q M_2} \tag{A.1}$$

This equation is analogous to the selfconsistency equation of the EDMFT, it arises when summing ring diagrams.  $M_2$  is a vertex and  $J_{ij}$  is a line in the ring diagram.  $G_2(i)M_2$  is the sum of all ring diagrams which cover the site i.  $M_2$  and  $G_2$  are related to D in EDMFT:

$$D = M_2 + M_2 G_2 M_2 \tag{A.2}$$

Below we are explicitly summing ring graphs on a Bethe lattice to express  $G_2$  through  $M_2$ .

We are introducing notations:  $\tilde{G}_2(i)$  and Q(i).  $\tilde{G}_2(i)$  equals  $G_2(i)$  when the latter is computed on a lattice with all but one bonds cut out from the site i. the sum of ring graphs with only one vertex belonging to the site i.  $Q(i)M_2$  includes those diagrams from  $\tilde{G}_2(i)M_2$  which have only one vertex belonging to the site i.

The following relations can be established:

$$G_2 = z\tilde{G}_2 + z\tilde{G}_2(z-1)M_2\tilde{G}_2 + z\tilde{G}_2(z-1)M_2\tilde{G}_2(z-1)M_2\tilde{G}_2 + \dots$$
 (A.3)

$$\tilde{G}_2 = Q + QM_2Q + QM_2QM_2Q + \dots (A.4)$$

$$Q = JM_2J + JM_2(z-1)\tilde{G}_2M_2J + JM_2(z-1)\tilde{G}_2M_2(z-2)\tilde{G}_2M_2J$$
$$+JM_2(z-1)\tilde{G}_2M_2(z-2)\tilde{G}_2M_2(z-2)\tilde{G}_2M_2J + \dots$$
(A.5)

where z is the number of nearest neighbors, J is a bond on the lattice.

Summing geometrical series, we obtain:

$$G_2 = \frac{z\tilde{G}_2}{1 - (z - 2)M_2\tilde{G}_2} \tag{A.6}$$

$$\tilde{G}_2 = \frac{Q}{1 - M_2 Q} \tag{A.7}$$

$$Q = J^2 M_2 \frac{1 + M_2 \tilde{G}_2}{1 - (z - 2)M_2 \tilde{G}_2}$$
(A.8)

Solving these equations we get:

$$G_2 = \frac{zQ}{1 - zM_2Q} \tag{A.9}$$

$$Q = \frac{1 - \sqrt{1 - (z - 1)(2M_2J)^2}}{(z - 1)2M_2}$$
 (A.10)

Eq(A.9) and eq(A.10) solve  $G_2$  for  $M_2$ .

Curves  $J_c$  vs z for BL and EDMFT, together with MFT solution  $J_c = 1/z$  are presented in Fig(4.4) and compared to the exact solution:

$$J_c = \frac{1}{2} \ln \frac{z}{z - 2} \tag{A.11}$$

#### A.2 Order of the phase transition

Here we are proving that the EDMFT equations give a transition of the first order for d < 4 and of the second order in the higher dimensions. For classical phonons EDMFT equations read:

$$m(r - J_{q=0}) = -\frac{\delta\Phi[m,D]}{\delta m}$$

$$D = \sum_{q} \left[r + 2\frac{\delta\Phi[m,D]}{\delta D} - J_{q}\right]^{-1}$$
(A.12)

It is easily seen that

$$\frac{\delta^2 \Phi[m, D]}{\delta m^2} \bigg|_{m=0} = 2 \frac{\delta \Phi[0, D]}{\delta D} \tag{A.13}$$

Solving Eq.A.12 for r using the above relation for derivatives, up to the second order in m we have:

$$-\frac{m^2}{2}D''|_{m=0} = D|_{m=0} - \sum_{q} \left[ \left( 2\frac{\delta^2}{\delta D^2} - \frac{1}{6}\frac{\delta^4}{\delta m^4} \right) \Phi[m, D]|_{m=0} m^2 + J_{q=0} - J_q \right]^{-1}$$
(A.14)

The coefficient in front of  $m^2$  in the rhs is positive. The left hand side of Eq.(A.14) is  $\propto m^2$ ; while the right hand side has two contributions, one  $\propto m^{d-2}$  and the other  $\propto \delta \beta$ , where  $\delta \beta = \beta - \beta_c$ . For d < 4 the term  $\propto m^{d-2}$  is dominant and  $\delta \beta \propto -m^{d-2} < 0$ . A negative  $\delta \beta$  implies the first order transition. For d > 4 the term  $m^2$  from lhs becomes dominant and  $\delta \beta \propto m^2 > 0$ . This is the usual mean field behavior resulting in a second order transition.

We showed that in a classical model the transition is of the first order below the upper critical dimension. The same is true for a quantum transition as well. We show it in the appendix A.3 considering large N limit.

As discussed earlier in connection with the order of the transition, this artifact of the EDMF results from the inability of a local theory to capture physics that requires the introduction of anomalous dimensions. In spite of this shortcoming, when properly interpreted, EDMFT results in improved estimates of the critical temperature relative to DMFT.

### A.3 Quantum phase transition

In this appendix we investigate the phase transition in the quantum version of  $\phi^4$  model. We compare EDMFT and a full lattice model using large N technique. We will show that above the upper critical dimension  $d > d_{uc} = 4 - z$  the exact critical exponents and the critical exponents obtained in EDMFT coincide. Below  $d_{uc}$  the EDMFT and the lattice model exhibit different critical exponents. In the EDMFT the transition is of the first order for  $\frac{1}{2}d_{uc} < d < 2$  and of the second order otherwise. The transition is of the second order in the lattice case. Moreover, in EDMFT the exponents have universal value for  $d < \frac{1}{2}d_{uc}$  and a non universal value for  $\frac{1}{2}d_{uc} < d < d_{uc}$ .

The lattice model is described by the action:

$$S = \frac{1}{2}D_0^{-1}\phi^2 + \frac{U}{4}(\phi^2)^2 \tag{A.15}$$

where  $D_{0\omega,q}^{-1}=r+|\omega|^{\frac{2}{z}}+q^2$ ,  $\phi^2=\sum_{a=1}^N\phi_a^2$ , U=u/N, r is a variable parameter which drives the phase transition. Corresponding EDMFT equations are:

$$mD_{0\omega,q=0}^{-1} + \frac{\delta\Phi[m,D]}{\delta m} = 0$$
 (A.16)

$$D = \sum_{q} \left[ D_{0q}^{-1} + 2 \frac{\delta \Phi[m, D]}{\delta D} \right]^{-1}$$
 (A.17)

The functional  $\Phi[m, D]$  includes all two particle irreducible diagrams which are constructed from the magnetization m (dot), the particle propagator D (line) and the interaction term U (four legged vertex).  $\Phi$  satisfies the following equation:

$$\Gamma$$
 = x +  $\times$  +  $\times$  +  $\times$  +  $\times$  +

Figure A.1: 1/N expansion of  $\Gamma$ . All diagrams are of the order 1/N

$$\frac{\delta^2 \Phi[m, D]}{\delta m^2} \bigg|_{m=0} = 2 \frac{\delta \Phi[0, D]}{\delta D} \tag{A.18}$$

Expanding  $\Phi$  in small m and using Eq.(A.18) we write EDMFT equations as:

$$D_{0\omega,q=0}^{-1} + 2\frac{\delta\Phi[0,D]}{\delta D} + \frac{1}{6}\frac{\delta^4\Phi[m,D]}{\delta m^4}|_{m\to 0}m^2 = 0$$
 (A.19)

$$D_{\omega} = \int_{0}^{\Lambda} dq^{d} [|\omega|^{\frac{2}{z}} + q^{2} + \{2\Gamma - \frac{1}{6} \frac{\delta^{4} \Phi[m, D]}{\delta m^{4}}|_{m \to 0}\} m^{2}]^{-1}$$
 (A.20)

where  $\Gamma = \frac{\delta^2 \Phi[0,D]}{\delta D^2}$ .

Let  $D_{0c}$ ,  $D_c$ ,  $r_c$  be values of  $D_0$ , D, r in the transition point. Subtracting  $D_{0c\omega,q=0}^{-1} + 2\frac{\delta\Phi[0,D_c]}{\delta D} = 0$  from Eq.(A.19) and keeping lowest order terms we have:

$$\delta r + 2\Gamma \delta D + \frac{1}{6} \frac{\delta^4 \Phi}{\delta m^4} m^2 = 0 \tag{A.21}$$

where  $\delta r = r - r_c$ ,  $\delta D = D - D_c$ . This equation provides a relation between the variation of the driving term r and the order parameter m. We will show that for  $d > d_{uc}$  the last term in the left hand side wins over the second term, the transition is mean field like. The second term becomes important and determines the character of the transition for  $d < d_{uc}$ .

We will consider the large N limit up to the order of 1/N. Diagrams which enter  $\Gamma$  are chains of bubbles (see Fig.A.1), which can be summed up as geometrical series:

$$\Gamma = \frac{1}{N} \left( \frac{u}{2} + \frac{u}{1 + \frac{u}{2}\chi} \right) \tag{A.22}$$

where  $\chi_{\omega} \sim \int d\nu D_{\nu} D_{\nu+\omega}$  in the quantum problem or  $\chi = D^2$  in the classical problem. The only term of the order 1/N which enters  $\delta^4 \Phi/\delta^4 m$  is 6u/N. All other terms are of order  $O(1/N^3)$ .

Eq.(A.21) and Eq.(A.22) hold in case of a lattice as well, but D now depends on both momentum and frequency, and summations now run over wave vectors as well.

The upper and lower critical dimensions are determined by the convergence of integrals  $Tr\delta D$  and TrD in the ultraviolet and infrared limits respectively:

$$Tr\delta D \sim \int d\omega dq \frac{q^{d-1}}{(|\omega|^{\frac{2}{z}} + q^2)^2}$$
 (A.23)

$$TrD \sim \int d\omega dq \frac{q^{d-1}}{(|\omega|^{\frac{2}{z}} + q^2)}$$
 (A.24)

These equations are the same for the mean field and lattice models, they yield the upper critical dimension  $d_{uc} = 4 - z$  and the lower critical dimension  $d_{lc} = 2 - z = d_{uc} - 2$ .

We first consider EDMFT. In a crude way one can estimate:

$$d > 2, D_{\omega} \sim \int d^{d}q (|\omega|^{\frac{2}{z}} + q^{2})^{-1} \sim (d-2)^{-1} (\Lambda_{q}^{(d-2)} - |\omega|^{\frac{d-2}{z}}) (A.25)$$

$$d < 2, D_{\omega} \sim -(d-2)^{-1} |\omega|^{\frac{d-2}{z}} (A.26)$$

and

$$d > 2,$$
  $\chi_{\omega} \sim \int d\nu D_{\nu} D_{\nu+\omega} \sim (d-2)^{-2} |\omega|^{\frac{d-2}{z}+1}$  (A.27)

$$d < 2,$$
  $\chi_{\omega} \sim -(d-2)^{-2} (2\frac{d-2}{z} + 1)^{-1} |\omega|^{2\frac{d-2}{z} + 1}$  (A.28)

 $\Lambda_q$  is a momentum cutoff. We see from Eq.(A.28) that for  $d < d_{uc}/2$  the susceptibility  $\chi_{\omega}$  is divergent at low frequency, it leads to a universal critical behavior for  $d < d_{uc}/2$ , as follows from the self energy calculation below. The self energy

in large N limit is  $\delta \Sigma \sim 2\Gamma D$ :

$$\frac{d_{uc}}{2} < d < d_{uc}, \quad \Sigma_{\omega} \sim \frac{1}{N} (d-2)^{-1} u |\omega|^{\frac{d-2}{z}+1}$$
(A.29)

$$d_{lc} < d < \frac{d_{uc}}{2}, \quad \Sigma_{\omega} \sim \frac{1}{N} \int d\nu \frac{D_{\nu+\omega}}{\chi_{\nu}} \sim \frac{1}{N} (d-2) (2\frac{d-2}{z} + 1) |\omega|^{-\frac{d-2}{z}}$$
 (A.30)

In a similar way we can calculate a contribution from m to  $\Gamma \delta D$ 

$$\frac{d_{uc}}{2} < d < d_{uc}, \qquad \Gamma \delta D \sim \frac{1}{N} (d-2)^{-1} u m^{d-2+z}$$
(A.31)

$$d_{lc} < d < \frac{d_{uc}}{2}, \qquad \Gamma \delta D \sim \frac{1}{N} (d-2) (2\frac{d-2}{z} + 1) m^{-d+2}$$
 (A.32)

This result together with Eq.(A.21) suggests that the transition is the first order for  $\frac{1}{2}d_{uc} < d < 2$ .

Now we consider the lattice model.

$$\chi_{\omega,q} \sim \int d\nu d^d p (|\nu + \omega|^{\frac{2}{z}} + (p+q)^2)^{-1} (|\nu|^{\frac{2}{z}} + p^2)^{-1} \sim (d+z-4)^{-1} (|\omega|^{\frac{2}{z}} + q^2)^{\frac{d+z}{2}-2}$$
(A.33)

$$\Sigma_{\omega,q} \sim \frac{1}{N} \int d\nu dp \chi_{\nu,p}^{-1} D_{\nu+\omega,p+q} \sim \frac{1}{N} (d+z-4) (|\omega|^{\frac{2}{z}} \ln|\omega| + q^2 \ln q) \qquad (A.34)$$

In this case the frequency dependent part of the self energy can be conveniently exponentiated to yield:  $D \sim [|\omega|^{\frac{2}{\tilde{z}}} + q^{2-\eta}]^{-1}$  with  $\tilde{z} = 2 - N^{-1}(d - d_{uc})c_1(d)$  and  $\eta = -N^{-1}(d - d_{uc})c_2(d)$ , where  $c_1(d)$  and  $c_2(d)$  are some smooth functions of d.

We also calculate a contribution from m to  $\Gamma \delta D \sim N^{-1}(d-d_{uc})m^2 \ln m$ . It yields  $\delta r \sim m^{\frac{1}{\beta}}$  with  $\beta = \frac{1}{2} + (d-d_{uc})\frac{1}{N}c_3(d)$ . The transition is the second order in this case.

## Appendix B

## Parquet EDMFT

#### **B.1** Definitions

For a detailed derivation of the parquet theory equations one should refer to Ref [53]. Below we summarize notations and write out established equations without derivations.

Any two-body vertex diagram  $\alpha \equiv \alpha(1,2;3,4)$  has two incoming legs (indices 1 and 2) and two outgoing legs (indices 3 and 4), see Fig.B.1. The exchange of a diagram  $\alpha$  is defined as  $\bar{\alpha}(1,2;3,4) = \alpha(1,2;4,3)$ . The left-right flip of a diagram  $\alpha$  is defined as  $\tilde{\alpha}(1,2;3,4) = \alpha(2,1;4,3)$ . A diagram called direct if incoming particles propagate from leg 1 to leg 3 and from leg 2 to leg 4.

A sum of diagrams contributing to a two-body vertex is denoted by upper case letters. The sum  $\check{X}$  includes both direct graphs X and exchange graphs  $\hat{X}$ . If  $X = \hat{X}$  the vertex is antisymmetric:  $\check{X} = X + \bar{X}$ . This is the case we consider.

Two direct graphs  $\alpha$  and  $\beta$  can be connected by two one-particle Green's functions G to form a direct two-body graph in exactly five topologically distinctive ways:

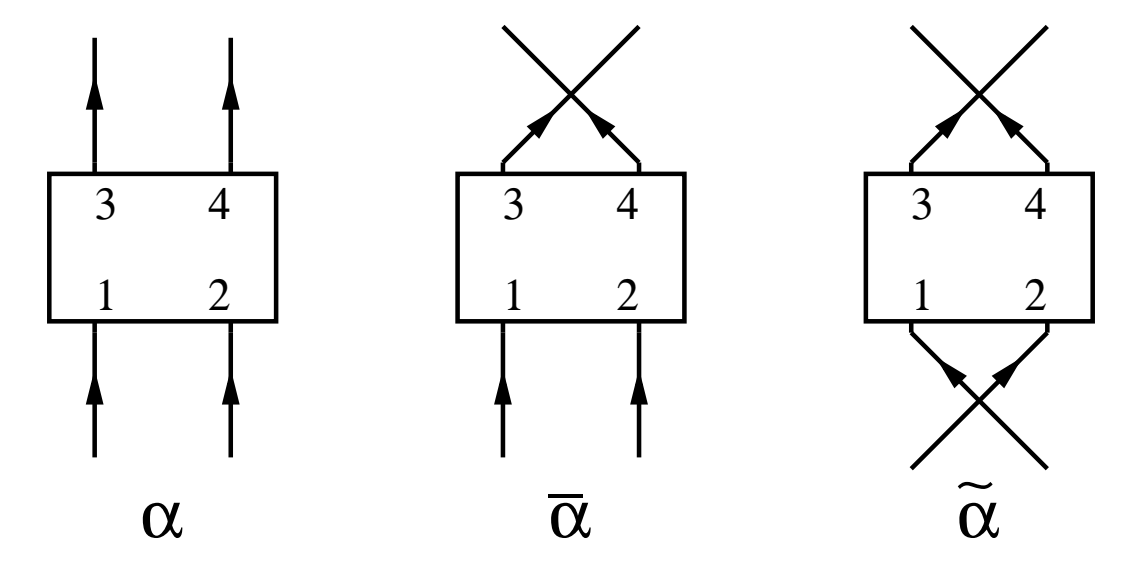


Figure B.1: Two-body diagram  $\alpha$ . Legs 1 and 2 are incoming particles, legs 3 and 4 are outgoing particles. Diagrams  $\bar{\alpha}$  and  $\tilde{\alpha}$  are exchange of  $\alpha$  and a flip of  $\alpha$  respectively

$$(\alpha \mathbf{s}\beta)(1,2;3,4) = \alpha(1,2;5,6)G(5,7)G(6,8)\beta(7,8;3,4)$$

$$(\alpha \mathbf{u}\beta)(1,2;3,4) = \alpha(1,5;6,4)G(6,7)G(8,5)\beta(7,2;3,8)$$

$$(\alpha \mathbf{c}\beta)(1,2;3,4) = \alpha(1,5;3,6)G(6,7)G(8,5)\beta(7,2;8,4)$$

$$(\alpha \mathbf{l}\beta)(1,2;3,4) = \alpha(1,5;6,3)G(6,7)G(8,5)\beta(7,2;8,4)$$

$$(\alpha \mathbf{r}\beta)(1,2;3,4) = \alpha(1,5;3,6)G(6,7)G(8,5)\beta(7,2;4,8)$$
(B.1)

All other connections can be obtained from these five by applying left-right flip to  $\alpha$  or  $\beta$ . Five basic operations are shown in Fig.(B.2). Any diagram is two particle reducible in one (and only one) of three channels: s, u or t. If legs 1, 2 can be separated from legs 3, 4 by cutting two lines the diagram is reducible in s channel. Separability of 1, 4 from 2, 3 and 1, 3 from 2, 4 corresponds to channels u and t respectively. The s operation is an s channel operation, the u is a u channel operation.

A two-body graph can be closed off with a Green's function to form a one-body graph. This can be done in the direct (d operation) or exchange (e operation)

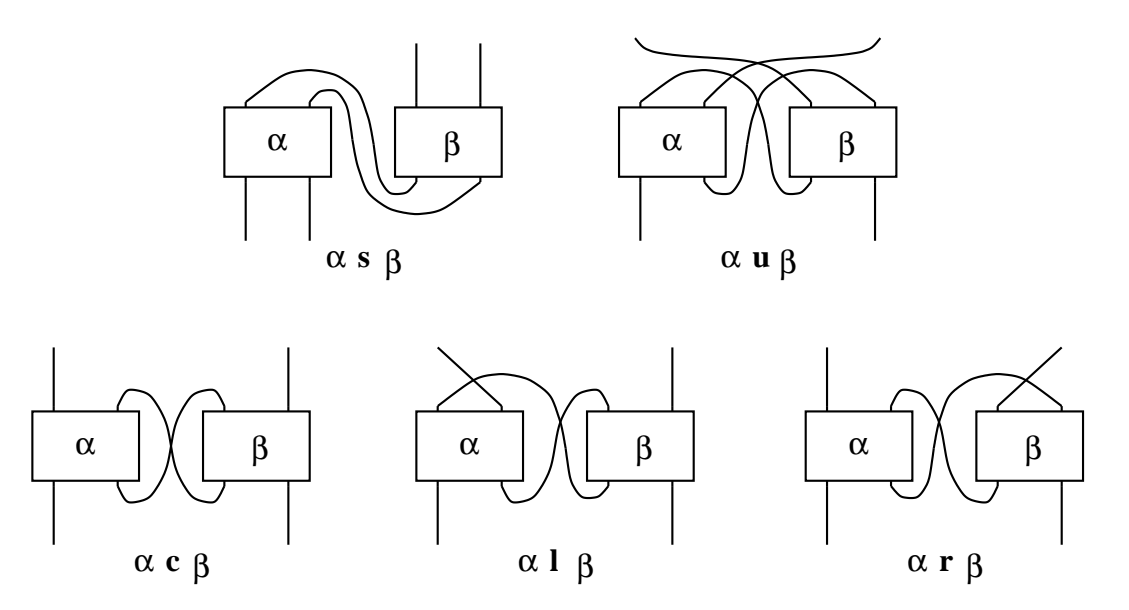


Figure B.2: Five distinctive ways to connect two diagrams  $\alpha$  and  $\beta$ .

channel:

$$d(\alpha)(1,2) = \alpha(1,3;2,4)G(4,3)$$
  

$$e(\alpha)(1,2) = \alpha(1,3;4,2)G(4,3)$$
(B.2)

 $G^{II}$  is the two-body Green's function. The two-body vertex  $\Gamma$  is closely releted to  $G^{II}$  and defined by:

$$G^{II}(1,2;3,4) = G(1,3)G(2,4) - G(1,4)G(2,3) + G(1,5)G(2,6)\Gamma(5,6;7,8)G(7,3)G(8,4)$$
(B.3)

Green's function G is related to the bare Green's function  $G_0$  throug the Dyson equation

$$\Sigma = G_0^{-1} - G^{-1} \tag{B.4}$$

The self energy  $\Sigma$  can be expressed in terms of  $\Gamma$  and the bare interaction vertex V:

$$\Sigma = d(\check{V} + \frac{1}{2}\check{\Gamma}\mathbf{s}\check{V}) = (d+e)(V + \Gamma\mathbf{s}V)$$
 (B.5)

### B.2 Exact parquet theory

The parquet theory solves the problem of generating all two-body reducible graphs from a set of two-body irreducible graphs  $\check{I}$ . If  $\check{I}$  is antisymmetric, the parquet equations can be written in terms of direct graphs only [53, 54]:

$$\Delta_{S} = I + U + B + L + R + A$$

$$\Delta_{U} = I + S + B + L + R + A$$

$$\Delta_{B} = I + S + U$$

$$S = \Delta_{S} \mathbf{s} (\Delta_{S} + S)$$

$$U = \Delta_{U} \mathbf{u} (\Delta_{U} + U)$$

$$B = \Delta_{B} \mathbf{b} (\Delta_{B} + B)$$

$$\Gamma_{0} = I + S + U + B$$

$$L = \Gamma \Gamma_{0}$$

$$R = \Gamma_{0} \mathbf{r} \Gamma$$

$$A = \Gamma \Gamma_{0} \mathbf{r} \Gamma$$

$$\Gamma = \Gamma_{0} + L + R + A$$
(B.6)

The set of equations Eqs.(B.6) can alternatively be written as:

$$\Delta_{S} = \Gamma - S$$

$$\Delta_{U} = \Gamma - U$$

$$\Delta_{B} = \Gamma_{0} - B$$

$$S = \Delta_{S} \mathbf{s} \Gamma$$

$$U = \Delta_{U} \mathbf{u} \Gamma$$

$$B = \Delta_{B} \mathbf{b} \Gamma$$

$$\Gamma_{0} = I + S + U + B$$

$$\Gamma = (1 + \Gamma \mathbf{l}) \Gamma_{0} (1 + \mathbf{r} \Gamma)$$
(B.7)

or

$$\Gamma_{12} = \Gamma - \Gamma_{12} \mathbf{s} \Gamma$$

$$\Gamma_{14} = \Gamma - \Gamma_{14} \mathbf{u} \Gamma$$

$$\Gamma_{13} = \Gamma - \Gamma_{13} \mathbf{b} \Gamma$$

$$\Gamma_{0} = I + \Gamma_{12} \mathbf{s} \Gamma + \Gamma_{14} \mathbf{u} \Gamma + \Gamma_{13} \mathbf{b} \Gamma$$

$$\Gamma = (1 + \Gamma \mathbf{l}) \Gamma_{0} (1 + \mathbf{r} \Gamma)$$
(B.8)

where  $\Gamma_{12} \equiv \Delta_S$ ,  $\Gamma_{14} \equiv \Delta_U$  and  $\Gamma_{13} \equiv \Delta_B$ .

The parquet equations can be formally solved for I, see Eq.(5.2).

The parquet equations can also be written for full vertices, which include both direct and exchange parts:

$$\dot{\Delta}_{S} = \dot{\Gamma} - \dot{S}$$

$$\dot{\Delta}_{U} = \dot{\Gamma} - \dot{U}$$

$$\dot{\Delta}_{C} = \dot{\Gamma} - \dot{C}$$

$$\dot{S} = \frac{\dot{1}}{2} \Delta_{S} \dot{\mathbf{s}} \dot{\Gamma}$$

$$\dot{U} = \dot{\Delta}_{U} \mathbf{u} \dot{\Gamma}$$

$$\dot{C} = \dot{\Delta}_{C} \dot{\mathbf{c}} \dot{\Gamma}$$

$$\dot{\Gamma} = \dot{I} + \dot{S} + \dot{U} + \dot{C}$$
(B.10)

or

$$\dot{\Gamma}_{12} = \dot{\Gamma} - \frac{1}{2} \dot{\Gamma}_{12} \mathbf{s} \dot{\Gamma} 
\dot{\Gamma}_{14} = \dot{\Gamma} - \dot{\Gamma}_{14} \mathbf{u} \dot{\Gamma} 
\dot{\Gamma}_{13} = \dot{\Gamma} - \dot{\Gamma}_{13} \mathbf{c} \dot{\Gamma} 
\dot{\Gamma} = \dot{I} + \frac{1}{2} \dot{\Gamma}_{12} \mathbf{s} \dot{\Gamma} + \dot{\Gamma}_{14} \mathbf{u} \dot{\Gamma} + \dot{\Gamma}_{13} \mathbf{c} \dot{\Gamma}$$
(B.11)

 $\check{S}$ ,  $\check{U}$  and  $\check{C}$  include all graphs reducible in s, u and t channels respectively.  $\check{\Gamma}_{12} \equiv \check{\Delta}_S$ ,  $\check{\Gamma}_{14} \equiv \check{\Delta}_U$  and  $\check{\Gamma}_{13} \equiv \check{\Delta}_B$ .

Formal solution for I is Eq.(5.1).

Systems Eq.(B.7) and Eq.(B.10) are equivalent and the following relationships can be established (the only requirement might be  $\check{\Gamma} = \tilde{\check{\Gamma}}$  or  $\check{I} = \tilde{\check{I}}$ ):

$$\check{S} = S + \bar{S} \tag{B.12}$$

$$\check{U} = U + \bar{B} + \bar{L} + \bar{R} + \bar{A} \tag{B.13}$$

$$\check{C} = \bar{U} + B + L + R + A \tag{B.14}$$

Given I (or I) including all two-body irreducible vertex diagrams constructed from the propagator G and the bare interaction vertex V, Eq(5.1) (or Eq.(5.2,5.3)),

the Dyson equation Eq.(B.4) and the expression for self energy Eq.(B.5) form a closed set of equations:

$$\check{\Gamma} = \check{I}[G, V] + \frac{1}{2}\check{\Gamma}(1 + \frac{1}{2}\mathbf{s}\check{\Gamma})^{-1}\mathbf{s}\check{\Gamma} + \check{\Gamma}(1 + \mathbf{u}\check{\Gamma})^{-1}\mathbf{u}\check{\Gamma} + \check{\Gamma}(1 + \mathbf{c}\check{\Gamma})^{-1}\mathbf{c}\check{\Gamma}$$
(B.15)

$$G = [G_0^{-1} - \Sigma]^{-1} \tag{B.16}$$

$$\Sigma = d(\check{V} + \frac{1}{2}\check{\Gamma}\mathbf{s}\check{V}) \tag{B.17}$$

Below we show that the exact parquet theory is a natural starting point for deriving DMFT, EDMFT and other possible extensions of DMFT.

### B.3 Two parquet scheme equivalence

We start by showing the equivalence of Eq.(5.2) and Eq.(5.1) to the lowest order in perturbation theory, proceeding later with proving the general case. Up to the second order Eq.(5.2) and Eq.(5.1) read:

$$I = \Gamma - \Gamma I \Gamma - \Gamma r \Gamma - \Gamma s \Gamma - \Gamma u \Gamma - \Gamma c \Gamma$$
(B.18)

$$\check{I} = \check{\Gamma} - \frac{1}{2} \check{\Gamma} \mathbf{s} \check{\Gamma} - \check{\Gamma} \mathbf{u} \check{\Gamma} - \check{\Gamma} \mathbf{c} \check{\Gamma}$$
(B.19)

Then we add Eq.(B.18) and exchange of itself, transforming any diagram of the type  $\overline{\alpha \mathbf{x} \beta}$  into  $\gamma \mathbf{y} \delta$ , using associativity relations:  $\overline{\Gamma l \Gamma} = \Gamma \mathbf{u} \overline{\Gamma}$ ,  $\overline{\Gamma r \Gamma} = \overline{\Gamma} \mathbf{u} \Gamma$ ,  $\overline{\Gamma s \Gamma} = \Gamma \mathbf{s} \overline{\Gamma}$ ,  $\overline{\Gamma u \Gamma} = \overline{\Gamma} \mathbf{c} \overline{\Gamma}$ ,  $\overline{\Gamma c \Gamma} = \overline{\Gamma} \mathbf{u} \overline{\Gamma}$ . Collecting terms with  $\mathbf{s}$ ,  $\mathbf{u}$  and  $\mathbf{c}$  operations we arrive to Eq.(B.19).

Let us now consider all orders of perturbation theory. It is convenient to rewrite Eq.(5.2) and Eq.(5.1) as:

$$I = -\Gamma(1 + \mathbf{s}\Gamma)^{-1}\mathbf{s}\Gamma - \Gamma(1 + \mathbf{u}\Gamma)^{-1}\mathbf{u}\Gamma + \Gamma_0(1 + \mathbf{b}\Gamma_0)^{-1}$$
(B.20)

$$\check{I} = -\check{\Gamma}(1 + \frac{1}{2}\mathbf{s}\check{\Gamma})^{-1}\frac{1}{2}\mathbf{s}\check{\Gamma} - \check{\Gamma}(1 + \mathbf{u}\check{\Gamma})^{-1}\mathbf{u}\check{\Gamma} + \check{\Gamma}(1 + \mathbf{c}\check{\Gamma})^{-1}$$
(B.21)

Three terms in rhs of Eq.(B.20) and Eq.(B.21) are correspondingly -S, -U,  $\Gamma_0 - B$  and  $-\check{S}$ ,  $-\check{U}$ ,  $\check{\Gamma} - \check{C}$ .

Since for each operation  $\mathbf{s}$ ,  $\mathbf{u}$  or  $\mathbf{c}$  the usual associativity relation holds  $\alpha \mathbf{x}(\beta \mathbf{x} \gamma) = (\alpha \mathbf{x} \beta) \mathbf{x} \gamma$ , it would be convenient to write all equations using only these three operations. Using relations  $\alpha \mathbf{c} \beta = \bar{\alpha} \mathbf{l} \beta = \alpha \mathbf{r} \bar{\beta}$  we can write (cf Eq.(5.3)):

$$\Gamma_0 = (1 + \bar{\Gamma}\mathbf{c})^{-1}\Gamma(1 + \mathbf{c}\bar{\Gamma})^{-1} = \sum_{n=0}^{\infty} \sum_{k=0}^{k=n} (-1)^n (\Gamma\mathbf{c})^k \Gamma(\mathbf{c}\bar{\Gamma})^{n-k}$$
(B.22)

Composite operation  $\mathbf{b} = \mathbf{c} + (\mathbf{r}\Gamma)\mathbf{c}$  can be written as  $\mathbf{c} + \mathbf{c}\bar{\Gamma}\mathbf{c}$ , so:

$$\mathbf{b}\Gamma_0 = \mathbf{c}\Gamma(1+\mathbf{c}\bar{\Gamma})^{-1} = \sum_{n=0} (-1)^n \mathbf{c}\Gamma(\mathbf{c}\bar{\Gamma})^n$$
 (B.23)

We write the last term of Eq.(B.20) in powers of  $\Gamma$ :

$$\Gamma_{0}(1+\mathbf{b}\Gamma_{0})^{-1} = \sum_{n=0}^{\infty} (-1)^{n} \Gamma_{0}(\mathbf{b}\Gamma_{0})^{n}$$

$$= \sum_{i=2}^{\infty} \sum_{\substack{n_{1}=0\\n_{2}=0\\n_{i}=0}} (-1)^{p} (\bar{\Gamma}\mathbf{c})^{n_{1}} \Gamma(\mathbf{c}\bar{\Gamma})^{n_{2}} \mathbf{c} \Gamma(\mathbf{c}\bar{\Gamma})^{n_{3}} ... \mathbf{c} \Gamma(\mathbf{c}\bar{\Gamma})^{n_{i}} \quad (B.24)$$

where  $p = \sum_{i} n_{i} + i - 1$  is the order of the corresponding term. One can notice that all terms in the sum in Eq.(B.24) are different and the sum contains all terms in the expansion of  $\check{\Gamma}(1 + \mathbf{c}\check{\Gamma})^{-1}$  except for terms of the type  $\bar{\Gamma}\mathbf{c}\bar{\Gamma}\mathbf{c}...\bar{\Gamma}$ . Summing up these unaccounted terms we obtain:

$$\sum_{n=0} (-1)^n \bar{\Gamma} (\mathbf{c}\bar{\Gamma})^n = \bar{\Gamma} (1 + \mathbf{c}\bar{\Gamma})^{-1} = \overline{\Gamma (1 + \mathbf{u}\Gamma)^{-1}} = \overline{\Gamma - U}$$
 (B.25)

We used the relationship  $\overline{\alpha \mathbf{u}\beta} = \bar{\alpha} \mathbf{c}\bar{\beta}$ . From Eq.(B.24), Eq.(B.25) and the expansion of  $\check{\Gamma}(1+\mathbf{c}\check{\Gamma})^{-1}$  it follows  $\Gamma_0(1+\mathbf{b}\Gamma_0)^{-1} + \bar{\Gamma}(1+\mathbf{c}\bar{\Gamma})^{-1} = \check{\Gamma}(1+\mathbf{c}\check{\Gamma})^{-1}$ . This can be written as  $\Gamma_0 - B + \bar{\Gamma} - \bar{U} = \check{\Gamma} - \check{C}$  or finally as:

$$\check{C} = \bar{U} + B + L + R + A \tag{B.26}$$

In a similar way we derive:

$$\check{U} = U + \bar{B} + \bar{L} + \bar{R} + \bar{A} = \bar{\check{C}} \tag{B.27}$$

Using associtiviaty in s channel and the relation  $\overline{\Gamma s \Gamma} = \Gamma s \overline{\Gamma}$ , it is not difficult to check that  $\check{S} = S + \overline{S}$ . For that we write S and  $\check{S}$  in series:

$$S = -\sum_{n=1}^{\infty} (-1)^n \Gamma(\mathbf{s}\Gamma)^n$$
 (B.28)

$$\check{S} = -\sum_{n=1} (-\frac{1}{2})^n \check{\Gamma}(\mathbf{s}\check{\Gamma})^n \tag{B.29}$$

Each term of the n+1th order in  $\Gamma$  in Eq.(B.29) equals to  $S/2^n$  if it has even number of  $\bar{\Gamma}$  and equals to  $\bar{S}/2^n$  otherwise. Number of terms of each kind is  $2^n$ , so it proves that

$$\dot{S} = S + \bar{S} \tag{B.30}$$

Writing the fully irreducible part in two representations:

$$I = \Gamma - S - U - B - L - R - A$$

$$\check{I} = \check{\Gamma} - \check{S} - \check{U} - \check{C}$$
(B.31)

and using Eqs.(B.26,B.27,B.30) we show that  $\check{I} = I + \bar{I}$ . This proves the equivalence of direct and antisymmetric parquet equations.

## Appendix C

### Anderson Localization

### C.1 Anderson model equation

Let us now derive the equation describing the problem. We use the Anderson tight-binding model described by a Hamiltonian

$$H = \sum_{i} \epsilon_i c_i^{\dagger} c_i + \sum_{\langle i,j \rangle} t_{ij} c_i^{\dagger} c_j, \quad t_{ij} = t_{ji}^*$$
 (C.1)

where site energies  $\epsilon_i$  are assumed to be random variables and hopping matrix elements  $t_{ij}$  are equal to t for the nearest neighbors and to zero otherwise.

To derive the equation we expand around the atomic limit, that is in the hopping amplitude t. The bare on-site Green's function on a site subscribed with 0 is

$$G_0^{0-1}(E) = E - \epsilon_0$$
 (C.2)

and the dressed Green's function is

$$G_0^{-1}(E) = E - \epsilon_0 - \Sigma_0(E)$$
 (C.3)

where the self energy is

$$\Sigma_0(E) = t^2 \sum_{ij} G_{ij}^{(0)}(E)$$
 (C.4)

Green's functions appearing under the sum are those calculated for the lattice with the site 0 being removed. We would like to close the system of eq(C.3) and eq(C.4). For that we argue that first, at large dimensionality  $G_{ij}^{(0)} \approx G_{ij}$ , that is removing one site produces little effect on a Green's function, and second, if  $i \neq j$ 

than Gij is of higher order with the respect to a local Green's function (i = j). After that simplifications, plugging selfenergy from eq(C.4) into eq(C.3) we get:

$$G_0^{-1}(E) = E - \epsilon_0 - t^2 \sum_i G_i(E) - i\varepsilon \tag{C.5}$$

Here the Green's functions are local Green's functions and the sum is over the nearest neighbors. We introduce also an infinitesimal positive  $\varepsilon$  to tackle possible singularities. Later we wont write it explicitly, still recalling it where necessary.

On an artificial lattice with no loops (a tree like lattice) the derivation would be just exact provided we sum over all but one nearest neighbors. Indeed, on a loopless lattice  $G_{ij}^{(0)} = 0$  for the different i and j, and summing over all but one neighbors in the right hand side we have just  $G^{(0)}$  in the left hand side of eq(C.5). Such a tree like lattice with m being number of neighbors near every site is called a Bethe lattice (or Cayley tree) with the coordination number m. And this is a lattice we are going to solve the problem on. This is a quite unrealistic lattice, one would wonder how it relates to a reallife lattices. For the hypercubic lattice number of nearest neighbors is twice the dimensionality. By this analogy we can say that the coordination number m kind of plays a role of the dimensionality and we can hope to obtain a qualitatively correct picture for the large dimensionality, where hopefully presence of loops is less important than at  $d \leq 2$ . Neglecting of loop correlations decreases the lower critical dimension (or rather coordination number) to 1. Exactly at m=1 the Bethe lattice is just a one dimensional system, so this limit is also of interest. So, we will concentrate our attention on two limits: large  $(m \gg 1)$  and small  $(m \to 1)$  coordination number.

We put t = 1, or in other words we measure frequency E and and potential  $\epsilon$  in terms of t, while Green's functions in terms of  $t^{-1}$ .

If the distribution of the random potential is an even function of  $\epsilon$  then eq(C.5) is symmetrical under the change  $E \to -E$ ,  $G \to -G$  and the following complex conjugation. This is assumed everywhere later. In that case E = 0 is the middle

of the band. DOS on a Bethe lattice is a semicircle. It is natural to expect states first to localize where DOS is small and last to localize where DOS is large, that is right in the middle of the band. That is why we will particularly interested in results for E=0. In that case recursion relation describing Anderson localization in the Anderson model reads:

$$-G^{-1} = \epsilon + \sum_{j=1}^{m} G_j \tag{C.6}$$

#### C.2 Green's function distribution function

We want to study a distribution function. In general we call it  $P_{\xi}(z)$ .  $P_{\xi}(z)$  is a distribution function of a random variable  $\xi$ , where the distribution assumed to be over different sites on a lattice. It shows probability to find value of  $\xi = z$  on a randomly chosen site. Strictly speaking, we define distribution function as:

$$P_{\xi}(z) = \lim_{\Delta z \to 0, \, \Delta N_{\xi} \to \infty} \frac{\Delta N_{\xi}/N}{\Delta z}$$

where  $\Delta N_{\xi}$  is a number of sites on which variable  $\xi$  takes values between z and  $z + \Delta z$ ; N is total number of sites in the lattice, and it is implied of course that  $N \to \infty$ .  $\xi$  may also be a vector, in that case in the above definition we change  $\Delta z$  for  $\mu(\mathbf{z}) \prod_i \Delta z_i$ , where measure  $\mu$  in our case will be just 1.

Recursive eq(6.3) can be brought in the form of an integral equation. In eq(6.3) all the variables in the right hand side are independent, and so the distribution function in the lhs is simply related to the distribution function in the rhs:

$$P_{G^{-1}}(G^{-1}) = \int d\epsilon P_{\epsilon}(\epsilon) \prod_{i=1}^{m} dG_{i} P_{G}(G_{i}) \delta(G^{-1} + \epsilon - E + \sum_{i=1}^{m} G_{i})$$
 (C.7)

In the rhs we have a convolution type integral and hence it is convenient to go to Fourier transform (FT) of the equation. Fourier transformed quantities are marked with a tilde:  $\tilde{P}_G(z)$ . We will not go in the details of derivation right now, we just need to realize a general form of the Fourier transformed equation, and this

is an easy part. First we note that the FT of a distribution function of a sum of several independent quantities is simply a product of FTs of distribution functions of those quantities:  $\tilde{P}_{A+B} = \tilde{P}_A \tilde{P}_B$ . Second we notice that FT of the distribution function of an inverse quantity is related to FT of the distribution function of the quantity itself through some linear integral operator  $\hat{L}$ :  $\tilde{P}_G = \hat{L} \tilde{P}_{G^{-1}}$ . Then the integral equation is of the following form:

$$\tilde{P}_G = \hat{K}\tilde{P}_G^m \tag{C.8}$$

where  $\hat{K}$  is the integral operator:  $\hat{K} = \hat{L}\tilde{P}_{\epsilon}$ 

## C.3 Real part of the Green's function, Cauchy distribution

When transition is approached,  $\langle y \rangle_{typical}$  tends to 0 while  $\langle x \rangle_{typical}$  remains finite. Keeping this in mind one can drop y from the real part of eq(6.3) to find distribution of x in the critical region:

$$x^{-1} = \epsilon - \sum_{j}^{m} x_j \tag{C.9}$$

In the case of the Cauchy distribution of the random variable  $\epsilon$   $P_{\epsilon}(\epsilon) = \frac{1}{\pi} \frac{\gamma}{\gamma^2 + \epsilon^2}$  eq(C.9) has a simple solution. One can note that the distribution of the sum of several random variables  $x_i$  distributed with Cauchy distribution is a Cauchy distribution as well and width  $\gamma$  of this distribution is just sum of  $\gamma_i$ ; inverse of the Cauchy distribution with width  $\gamma$  is a Cauchy distribution width width  $\gamma^{-1}$ . Then from eq(C.9) it follows immediately that

$$labela2P_x(x) = \frac{1}{\pi} \frac{\alpha}{\alpha^2 + x^2}, \quad \alpha = \frac{-\gamma + \sqrt{\gamma^2 + 4m}}{2m}$$
 (C.10)

We see that distribution of the real part of the Green's function is a non critical at the transition. At large  $\gamma$ ,  $\alpha \approx \gamma^{-1}$  and  $Re[\sum_{j=1}^{m} G_j] \approx m/\gamma$ . But in the transition  $m_c \propto \gamma/\ln \gamma$ , so width of the distribution of  $\epsilon$  increases faster than that of  $Re[\sum_{j=1}^{m} G_j] \approx m/\gamma$  by  $\ln \gamma$ .

### C.4 Fourier Laplace transormed integral equation

Integral equation corresponding to eq(6.17) in the real space reads:

$$P_y(y) = \int d\epsilon P_{\epsilon}(\epsilon) \prod_{i=1}^m dy_i P_y(y_i) \delta(y - \frac{\sum_{i=1}^m y_i}{\epsilon^2 + (\sum_{i=1}^m y_i)^2})$$
 (C.11)

Introducing dummy variable x we can rewrite the equation:

$$P_{y}(y) = \int dx d\epsilon \frac{1}{(x^{2} + y^{2})^{2}} P_{\epsilon}(\epsilon) \prod_{i=1}^{m} dy_{i} P_{y}(y_{i}) \delta(\frac{x}{x^{2} + y^{2}} + \epsilon) \delta(\frac{-y}{x^{2} + y^{2}} + \sum_{i=1}^{m} y_{i})$$
(C.12)

Or in terms of Fourier and Laplace transforms of distribution functions (Fourier transform:  $\tilde{f}(k) = \int dx f(x) e^{-ikx}$ ; Laplace transform:  $\bar{f}(s) = \int_0^{+\infty} dx f(x) e^{-sx}$ ):

$$\bar{P}_{y}(s) = \int \frac{dx dy dk_{1} dk_{2}}{(2\pi)^{2}}$$

$$\tilde{P}_{\epsilon}(k_{1}) \tilde{P}_{y}^{m}(k_{2}) \frac{1}{(x^{2} + y^{2})^{2}} \exp\left(-ik_{1} \frac{x}{x^{2} + y^{2}} + ik_{2} \frac{y}{x^{2} + y^{2}} - sy\right) \quad (C.13)$$

Changing variables:  $x = \frac{U}{U^2 + V^2}$ ;  $y = \frac{V}{U^2 + V^2}$ :  $\bar{P}_y(s) = \frac{V}{V^2 + V^2}$ 

$$\int \frac{dU dV dk_1 dk_2}{(2\pi)^2} \tilde{P}_{\epsilon}(k_1) \tilde{P}_y^{\ m}(k_2) \exp\left(-ik_1 V + ik_2 U - s \frac{V}{U^2 + V^2}\right)$$
 (C.14)

$$-s\frac{V}{U^2 + V^2} = -\frac{is}{2}(\frac{1}{U + iV} - \frac{1}{U - iV})$$
 (C.15)

$$\exp\left(-\frac{is/2}{U+iV}\right) = -2i(U+iV) \int_0^{+\infty} RdR J_0(R\sqrt{2s}) \exp\left(i(U+iV)R^2\right) \quad (C.16)$$

and formally complex conjugate equation:

$$\exp\left(\frac{is/2}{U - iV}\right) = 2i(U - iV) \int_0^{+\infty} RdR J_0(R\sqrt{2s}) \exp\left(-i(U - iV)R^2\right) \quad (C.17)$$

Using eq(C.15), eq(C.16) and eq(C.17) we get:

$$\exp(-isV/(U^2+V^2)) = 4(U^2+V^2) \int_0^{+\infty} dR_1 \int_0^{+\infty} dR_2 \cdot R_1 R_2 J_0(R_1\sqrt{2s}) J_0(R_2\sqrt{2s}) \exp(i(U+iV)R_1^2 - i(U-iV)R_2^2)$$
 (C.18)

$$(U^2 + V^2) \rightarrow -\left(\frac{\partial^2}{\partial k_1^2} + \frac{\partial^2}{\partial k_2^2}\right) \exp\left(-ik_1V + ik_2U\right) \tag{C.19}$$

Changing variables:  $\xi=R_1^2-R_2^2,\,\eta=R_1^2+R_2^2,$  corresponding Jacobian:

$$J = \frac{1}{4} \frac{1}{\sqrt{\eta^2 - \xi^2}} = \frac{1}{8R_1 R_2} \tag{C.20}$$

Then using eq(C.18-C.20) we rewrite eq(C.14) as:

$$\bar{P}_y(s) = -\frac{1}{2} \int_{-\infty}^{+\infty} dU \int_0^{+\infty} dV \int_{-\infty}^{+\infty} \frac{dk_1}{2\pi} \int_{-\infty}^{+\infty} \frac{dk_2}{2\pi} \int_{-\infty}^{+\infty} d\xi \int_0^{+\infty} d\eta$$

$$\cdot \tilde{P}_{\epsilon}(k_1) \tilde{P}_y^m(k_2) \left(\frac{\partial^2}{\partial k_1^2} + \frac{\partial^2}{\partial k_2^2}\right) \exp\left(-ik_1V + ik_2U + i\xi U - \eta V\right) \cdot \\
\cdot J_0(\sqrt{s(\eta + \xi)}) J_0(\sqrt{s(\eta - \xi)}) \Theta(\eta^2 - \xi^2) \tag{C.21}$$

Integrating over U we have:

$$\int_{-\infty}^{+\infty} dU \exp\left(-ik_1 U + iU\xi\right) = 2\pi\delta(-k_1 + \xi) \tag{C.22}$$

Integrating over V we have:

$$\int_{0}^{+\infty} dV \int_{-\infty}^{\infty} dk_2 \tilde{P}_y^{\ K}(k_2) \exp(ik_2 V - \eta V) = 2\pi \int_{0}^{+\infty} dk_2 \tilde{P}_y^{\ K}(-ik_2) \delta(k_2 - \eta)$$
(C.23)

So applying eq(C.22) and eq(C.23) to eq(C.21) we get:

$$\bar{P}_{y}(s) = -\frac{1}{2} \int_{-\infty}^{+\infty} \frac{dk_{1}}{2\pi} \int_{0}^{+\infty} \frac{dk_{2}}{2\pi} \int_{-\infty}^{+\infty} d\xi \int_{0}^{+\infty} d\eta \tilde{P}_{\epsilon}(k_{1}) \tilde{P}_{y}^{m}(-ik_{2}) \cdot (\frac{\partial^{2}}{\partial k_{1}^{2}} - \frac{\partial^{2}}{\partial k_{2}^{2}}) J_{0}(\sqrt{s(\eta + \xi)}) J_{0}(\sqrt{s(\eta - \xi)}) \Theta(\eta^{2} - \xi^{2}) \delta(k_{1} - \xi) \delta(k_{2} - \eta) \quad (C.24)$$

or

$$\bar{P}_{y}(s) = -\frac{1}{2} \int_{-\infty}^{+\infty} \frac{dk_{1}}{2\pi} \int_{0}^{+\infty} \frac{dk_{2}}{2\pi} \tilde{P}_{\epsilon}(k_{1}) \bar{P}_{y}^{m}(k_{2}) \left(\frac{\partial^{2}}{\partial k_{1}^{2}} - \frac{\partial^{2}}{\partial k_{2}^{2}}\right)$$

$$J_{0}(\sqrt{s(k_{2} + k_{1})}) J_{0}(\sqrt{s(k_{2} - k_{1})}) \Theta(k_{2}^{2} - k_{1}^{2})$$

$$\left(\frac{\partial^{2}}{\partial k_{1}^{2}} - \frac{\partial^{2}}{\partial k_{2}^{2}}\right) g(k_{2} + k_{1}) h(k_{2} - k_{1}) =$$
(C.25)

$$\left(\frac{\partial}{\partial k_1} + \frac{\partial}{\partial k_2}\right)\left(\frac{\partial}{\partial k_1} - \frac{\partial}{\partial k_2}\right)g(k_2 + k_1)h(k_2 - k_1) = -4g'(k_2 + k_1)h'(k_2 - k_1)$$

SO

$$(\frac{\partial^{2}}{\partial k_{1}^{2}} - \frac{\partial^{2}}{\partial k_{2}^{2}}) J_{0}(\sqrt{s(k_{2} + k_{1})}) J_{0}(\sqrt{s(k_{2} - k_{1})}) \Theta(k_{2}^{2} - k_{1}^{2}) =$$

$$- \frac{s}{\sqrt{k_{2}^{2} - k_{1}^{2}}} J_{1}(\sqrt{s(k_{2} + k_{1})}) J_{1}(\sqrt{s(k_{2} - k_{1})}) \Theta(k_{2}^{2} - k_{1}^{2}) +$$

$$\frac{2\sqrt{s}}{\sqrt{k_{2} + k_{1}}} J_{1}(\sqrt{s(k_{2} + k_{1})}) J_{0}(\sqrt{s(k_{2} - k_{1})}) \delta(k_{2} - k_{1}) \Theta(k_{2} + k_{1}) +$$

$$\frac{2\sqrt{s}}{\sqrt{k_{2} + k_{1}}} J_{0}(\sqrt{s(k_{2} + k_{1})}) J_{1}(\sqrt{s(k_{2} - k_{1})}) \delta(k_{2} + k_{1}) \Theta(k_{2} - k_{1}) -$$

$$-4J_{0}(\sqrt{s(k_{2} + k_{1})}) J_{0}(\sqrt{s(k_{2} - k_{1})}) \delta(k_{2} + k_{1}) \delta(k_{2} - k_{1})$$

$$(C.26)$$

$$-\int_{0}^{+\infty} dk_{2} \int_{-\infty}^{+\infty} dk_{1} \frac{\sqrt{s}}{\sqrt{k_{2} \pm k_{1}}} J_{1}(\sqrt{s(k_{2} \pm k_{1})}) J_{0}(\sqrt{s(k_{2} \mp k_{1})}) \delta(k_{2} \mp k_{1}) \cdot \Theta(k_{2} \pm k_{1}) = -\int_{0}^{+\infty} dk_{2} \frac{\sqrt{s}}{\sqrt{2k_{2}}} J_{1}(\sqrt{2sk_{2}}))$$
(C.27)

$$2\int_{0}^{+\infty} dk_{2} \int_{-\infty}^{+\infty} dk_{1} J_{0}(\sqrt{s(k_{2}+k_{1})}) J_{0}(\sqrt{s(k_{2}-k_{1})}) \delta(k_{2}+k_{1}) \delta(k_{2}-k_{1}) =$$

$$4\int_{0}^{+\infty} dk_{2} J_{0}(\sqrt{2sk_{2}}) \delta(2k_{2}) = 4\int_{0}^{+\infty} dk_{2} \delta(2k_{2}) = 1 \qquad (C.28)$$

From eq(C.26-C.28), eq(C.25) becomes:

$$\bar{P}_{y}(s) = 1 - \int_{0}^{+\infty} dk_{2} \frac{\sqrt{s}}{\sqrt{2k_{2}}} J_{1}(\sqrt{2sk_{2}}) \tilde{P}_{\epsilon}(+k_{2}) \bar{P}_{y}^{m}(k_{2}) - \int_{0}^{+\infty} dk_{2} \frac{\sqrt{s}}{\sqrt{2k_{2}}} J_{1}(\sqrt{2sk_{2}}) \tilde{P}_{\epsilon}(-k_{2}) \bar{P}_{y}^{m}(k_{2}) + \int_{0}^{+\infty} dk_{2} \int_{-k_{2}}^{k_{2}} dk_{1} \cdot \frac{s}{2\sqrt{k_{2}^{2} - k_{1}^{2}}} J_{1}(\sqrt{s(k_{2} + k_{1})}) J_{1}(\sqrt{s(k_{2} - k_{1})}) \tilde{P}_{\epsilon}(k_{1}) \bar{P}_{y}^{m}(k_{2})$$
(C.29)

If the function  $P_{\epsilon}(\epsilon)$  is an even function, then the final equation reads:

$$\bar{P}_y(s) = 1 + \int_0^{+\infty} ds' (Ker_1(s, s') + Ker_2(s, s')) \bar{P}_y^m(s')$$
 (C.30)

where

$$Ker_{1}(s,s') = -\frac{\sqrt{2s}}{\sqrt{s'}}J_{1}(\sqrt{2ss'})\tilde{P}_{\epsilon}(s')$$

$$Ker_{2}(s,s') = \int_{-s'}^{s'} dk' \frac{s}{2\sqrt{s'^{2} - k'^{2}}}J_{1}(\sqrt{s(s'+k')})J_{1}(\sqrt{s(s'-k')})\tilde{P}_{\epsilon}(k')$$

We can show that eq(C.30) near MIT reduces translationally invariant (in logarithmic variables) equation:

$$\bar{P}_{y}(s) = \int_{0}^{+\infty} ds' \sqrt{s/s'^{3}} P_{\epsilon'}(\sqrt{s/s'}) \bar{P}_{y}^{\ m}(s')$$
 (C.31)

To show how this we rewrite eq(C.30) in equivalent form:

$$\bar{P}_{y}(s) = 1 + \int_{0}^{+\infty} ds' Ker'(s, s') \bar{P}_{y}^{\ m}(s') + \int_{0}^{+\infty} ds' \sqrt{s/s'^{3}} P_{\epsilon}(\sqrt{s/s'}) \bar{P}_{y}^{\ m}(s')$$
(C.32)

where

$$Ker'(s, s') = Ker_1(s, s') + Ker_2(s, s') - \sqrt{s/s'^3}P_{\epsilon}(\sqrt{s/s'})$$
 (C.33)

Idea is simple. We know that insulator solution  $(\bar{P}_y(s) \equiv 1)$  satisfies eq(C.32) and eq(C.31) as well. Then if  $\bar{P}_y(s) = 1$ , two first terms in eq(C.32) cancel out. But we can show that Ker'(s,s') consists of two terms: one falls off quickly and another oscillates highly at large s and  $k_2$ . It means that this kernel takes contribution only from the distribution function at small argument, where  $\bar{P}_y(s) \approx 1$  close to transition.  $Ker_1(s,s')$  and  $Ker_2(s,s') - \sqrt{s/s'^3}P_{\epsilon}(\sqrt{s/s'})$  are the terms we referred to above.

#### C.5 Variational method

We want to estimate largest eigenvalue of the operator K using variational approach:

$$K(t,u) = \frac{1}{\pi} \frac{1}{|u|} \frac{\gamma}{\gamma^2 + (\frac{1}{u} + t)^2}$$
 (C.34)

As a trial function we will take the function which corresponds to the NSM distribution function (in the sense  $P^{NSM}(k,s) \approx P_x(k) - \psi(k)\sqrt{s}$ ):  $\psi(x) = 1/\sqrt{1+c^2x^2}$ ; then the lower limit for the eigenvalue of K operator will be:

$$\Lambda_l = \max\{\frac{\int_{-\infty}^{+\infty} dt du \psi(t) K(t, u) \psi(u)}{\int_{-\infty}^{+\infty} du \psi(u) \psi(u)}\}$$
 (C.35)

or after some manipulations:

$$\Lambda_l = \max\left\{\frac{4}{\pi^2} \int_0^{+\infty} dk K_0(\frac{k}{c}) K_0(kc) e^{-\gamma k}\right\}$$
 (C.36)

where  $K_0$  is the modified Bessel function. The expression is symmetrical with respect to change  $c \to 1/c$ . So at c = 1 we have either maximum or minimum of  $\Lambda_l$ . Not difficult to check that it is a maximum. At c = 1 the integral can be done analytically:

$$\frac{4}{\pi^2} \int_0^{+\infty} dk K_0(k)^2 e^{-\gamma k} = \frac{1}{\pi^2} (2\mathbf{K}(\frac{\gamma^2}{4}) - \gamma \mathbf{F}_{32}(1, 1, 1; \frac{3}{2}, \frac{3}{2}; \frac{\gamma^2}{4}))$$
 (C.37)

where **K** is the elliptic integral, and  $\mathbf{F}_{32}$  is the generalized hypergeometric function. Expanding in  $\gamma$  we have:

$$\Lambda_l = 1 - \frac{2}{\pi^2} \gamma + O(\gamma^2) \tag{C.38}$$

## $C.6 \quad C(x) \text{ function}$

In this appendix we explain behavior of the function C(x) (see eq(6.31)). We are looking for the largest eigenvalue.

From the expansion  $P_G(x,y) \sim C(x)y^{-3/2}$  follows that C(x) is everywhere positive. Since the kernel of the integral operator is everywhere positive, it has only one positive eigenfunction which corresponds to the largest eigenvalue. So the approximate eigenvector we found (see eq(6.39)) does indeed corresponds to the largest eigenvalue. We will compare that analytical formula to numerically obtained eigenfunctions.

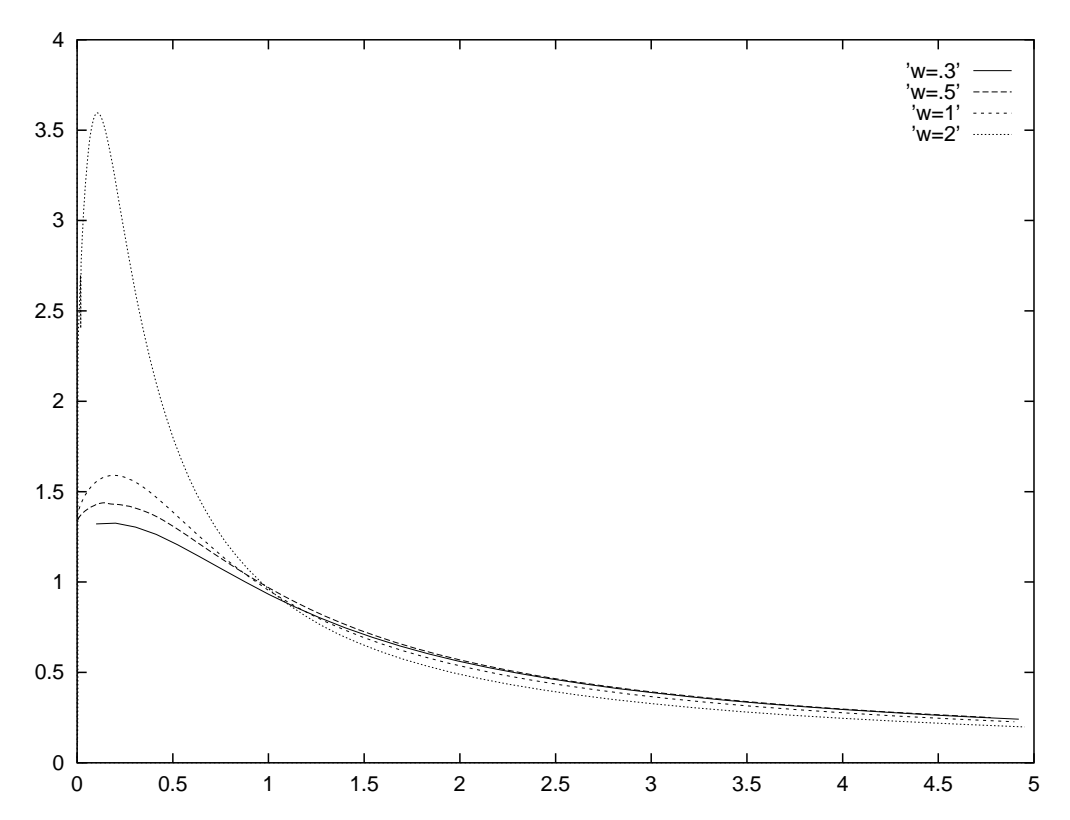


Figure C.1: Eigenfunction C(x) for small values of  $\gamma'$  ('w' on the plot).

Function C(x) has different behavior at large and low coordination. For  $\gamma' \ll 1$  (or  $m-1 \ll 1$ ) to the first order C(x) is independent of scale  $\gamma'$ , it tends to some function. Fig.C.1 illustrates this tendency.

For  $\gamma' \gg 1$  (or  $m \gg 1$ ) C(x) is approximately given by the formula eq(6.39). There are two terms in eq(6.39), each of which is scaling invariant, that is a function of  $x/\gamma'$ . But these two terms enter with different weights, so the whole expression is not scaling invariant. In Fig.(7) we plotted function proportional to

$$C^{numer}(\frac{\xi}{\gamma'})[2\ln\gamma' + \frac{1}{2}\ln(1+\frac{1}{\xi^2}) + \frac{1}{\xi}\arctan\frac{1}{\xi}]^{-1}$$
 (C.39)

where  $C^{numer}(x)$  a function found solving eq(6.31) numerically at different values of  $\gamma'$ . If eq(6.39) correctly describes C(x) at large  $\gamma'$ , then the function in Fig.C.2 should tend to  $\frac{\xi}{\xi^2+1}$ . This is demonstrated in the plot.

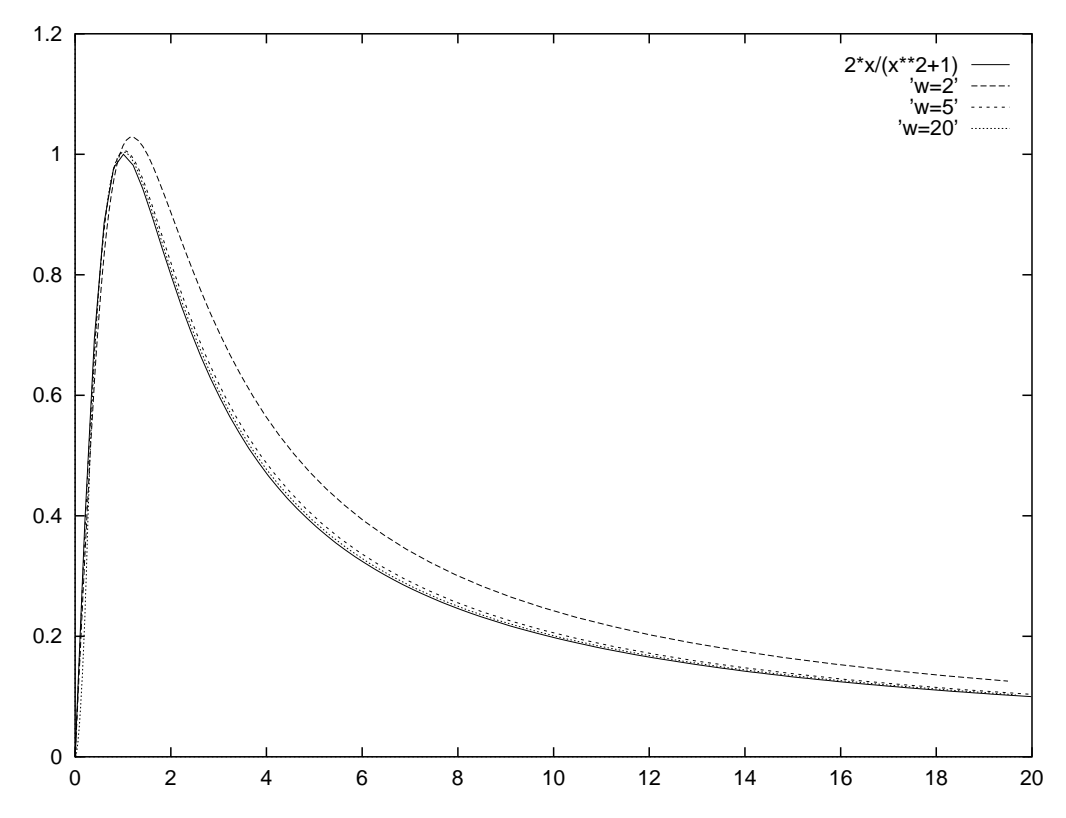


Figure C.2: Function  $C(\frac{\xi}{\gamma'})[2\ln\gamma' + \frac{1}{2}\ln(1+\frac{1}{\xi^2}) + \frac{1}{\xi}\arctan\frac{1}{\xi}]^{-1}$  is plotted for large values of  $\gamma'$  ('w' on the plot). If analytical expression given by eq(6.39) is correct, than graphs should tend to asymptotic function  $2\xi/(\xi^2+1)$  (full line).

### C.7 Limits of the integral equation kernel

Let us consider different limits of  $Ker_2(s, s')$  in eq(6.20), to which we refer in many cases. We can rewrite  $Ker_2(s, s')$  as:

$$Ker_2(s,s') = \int_{-1}^1 dx \frac{s}{2\sqrt{1-x^2}} J_1(\sqrt{ss'(1+x)}) J_1(\sqrt{ss'(1-x)}) \tilde{P}_{\epsilon}(xs') \quad (C.40)$$

Depending on how ss' and  $\gamma s'$  compare to 1 we can extract different asymptotes.

Case 1):  $ss' \gg 1$ ,  $\gamma s' \gg 1$ . First we notice that integrand in eq(reff1) is nonsingular at  $x = \pm 1$ . Due to presence of an exponential function  $\tilde{P}_{\epsilon}(xs') = \exp(-\gamma |xs'|)$  an important region of integration is  $x \ll 1$ . We use asymptotes of Bessel functions and expansion of the arguments of the Bessel functions in x (but not expansion of Bessel functions themselves, since  $s/\gamma$  is not necessarily small). Then

$$Ker_{2}(s,s') \approx \int_{-1}^{1} dx \frac{1}{2\pi} \frac{2\sqrt{s}}{\sqrt{s'}}$$

$$\times \cos(\sqrt{ss'}(1+x/2) + \pi/4) \cos(\sqrt{ss'}(1-x/2) + \pi/4) \tilde{P}_{\epsilon}(xs')$$

$$= \int_{-1}^{1} dx \frac{1}{2\pi} \frac{1}{s'} \sqrt{\frac{s}{s'}} (\cos(x\sqrt{ss'}) - \sin(2\sqrt{ss'})) \tilde{P}_{\epsilon}(xs')$$

$$\approx \int_{-\infty}^{+\infty} dk' \frac{1}{2\pi} \sqrt{\frac{s}{s'^{3}}} (\cos(k'\sqrt{\frac{s}{s'}}) - \sin(2\sqrt{ss'})) \tilde{P}_{\epsilon}(k')$$

$$= \sqrt{\frac{s}{s'^{3}}} P_{\epsilon}(\sqrt{\frac{s}{s'}}) - \sqrt{\frac{s}{s'^{3}}} P_{\epsilon}(0) \sin(2\sqrt{ss'}) \quad (C.41)$$

The second term oscillates highly and we can ignore it:

$$Ker_2(s, s') \approx \sqrt{\frac{s}{s'^3}} P_{\epsilon}(\sqrt{\frac{s}{s'}}); \quad ss' \gg 1, \quad \gamma s' \gg 1$$
 (C.42)

Case 2):  $ss' \gg 1$ ,  $\gamma s' \ll 1$ . This case is not much of interest as we will consider more general limit:  $s \gg \gamma$ .

Case 3):  $ss' \ll 1$ ,  $\gamma s'$  any. Using expansion of Bessel functions at small argument we have:

$$Ker_2(s,s') \approx \frac{s^2}{4} \int_0^{s'} dk_1 \tilde{P}_{\epsilon}(k'); \quad ss' \ll 1$$
 (C.43)

Let us consider two more general limits:

Case 4):  $s \ll \gamma$ , s' any. In this case there are two overlapping possibilities  $\gamma s' \gg 1$  or  $ss' \ll 1$ , but in any way the following formula works:

$$Ker_2(s, s') \approx \frac{s}{s'} J_1^2(\sqrt{ss'}) \int_0^{s'} dk_1 \tilde{P}_{\epsilon}(k'); \quad s \ll \gamma$$
 (C.44)

Case 5):  $s \gg \gamma$ . If  $s' \gg 1$ , this is just the case(1) if  $1/s \ll s' \ll 1$  then the integrand is the product of two incoherently oscillating functions. Using asymptotes of Bessel functions we can estimate result of integrating x as  $\sim 1/s'$ . Recalling that  $\delta \bar{P}_y(s')$  is the sum of two functions  $\propto s'^{\nu}$  we can estimate integral:  $\int_{1/s}^1 \delta \bar{P}_y(s')/s' ds' \sim \delta \bar{P}_y(s')|_{s'=1} \sim \delta \bar{P}_y(1)$ . When s' < 1/s,  $Ker_2(s,s') \sim s^2 s'$  and we estimate integral  $\int_0^{1/s} \delta \bar{P}_y(s') s^2 s' ds' \sim \delta \bar{P}_y(s') s^2 s'^2|_{s'=1/s} \sim \delta \bar{P}_y(1/s)$ .  $\delta \bar{P}_y(1/s) \ll \delta \bar{P}_y(1) \ll \delta \bar{P}_y(s)$ , this is important to justify the statement: distribution at large y does not define distribution at small y. We of course should not forget about  $Ker_1(s,s')$  of eq(6.19), but it gives even a smaller contribution.

## C.8 Integral equation reduction

As we see (eq(6.49)), h(k) is a relatively slowly varying function, so it may be tempting to forget about it entirely. Then integrations over k and k' in eq(6.53) are just Fourier transformations, so the integral equation becomes:

$$H(\eta) \int_{-\infty}^{+\infty} dk C(k) g(k) = \int_{0}^{+\infty} 2\pi \frac{d\eta'}{\eta'} \sqrt{\frac{\eta}{\eta'}} g(\sqrt{\frac{\eta'}{\eta}}) g(\sqrt{\frac{\eta}{\eta'}}) H^{m}(\eta')$$
 (C.45)

The kernel is a function of  $\xi = \eta'/\eta$ :  $Ker(\xi) = \xi^{-3/2}g(\xi^{1/2})g(\xi^{-1/2})$ . Limits of the kernel are:  $Ker(\xi) \propto \xi^{-2}$ , as  $\xi \to \infty$ ,  $Ker(\xi) \propto \xi^{-1}$ , as  $\xi \to 0$ . Linearized eq(C.45) has a symmetry  $\nu_{\beta} = \nu_{1-\beta}$ , and surprisingly, even yields a numerically exact value for  $\nu_{1/2}$ . Indeed, the linear equation for  $\beta = 1/2$  is:

$$\int_{-\infty}^{+\infty} dk C(k) g(k) = m \int_{0}^{+\infty} 2\pi \frac{d\xi}{\xi} g(\xi^{1/2}) g(\xi^{-1/2})$$
 (C.46)

And by virtue eq(6.34) this is a correct identity. However, something is quite bad in eq(C.45): insulator solution does not satisfy it, because integral is logarithmically divergent at small  $\xi$ .

Let us check limit  $\xi \to 0$  more accurately. In this case  $k \sim \xi^{-1/2} \gg 1$  and  $k' \sim \xi^{1/2} \ll 1$ . Then  $h(k) \approx const$ ,  $h(k') \approx 1/\ln k'$ .  $g(x) \to const$ , as  $x \to 0$ , so only integration over k' is important. Function g(k) has a logarithmic singularity at small k. To take care of it we change variable of integration to  $t = -k' \ln k'$ , then  $dt = -dk' (\ln k' + 1) \approx dk' \ln k'$ .  $g(k') \approx -\ln k' \tilde{P}_{\epsilon'}(k')$ , so  $\cos(k' \frac{h(k)}{h(k')} \frac{1}{\sqrt{\xi}}) g(k') \to \cos(t/\sqrt{\xi}) \tilde{P}_{\epsilon'}(t/\ln t)$  Function  $\tilde{P}_{\epsilon'}(k)$  is a smooth function at small k, so it is probably ok to put  $\ln t \equiv \ln \sqrt{\xi}$ . Now integration over t yields  $P_{\epsilon'}(1/(\sqrt{\xi} \ln \xi))$ , and  $Ker(\xi) \to \ln \xi^2/\sqrt{\xi}$ , as  $\xi \to 0$ .

### References

- [1] W. Metzner and D. Vollhardt, Phys. Rev. Lett. **62**, 324 (1989).
- [2] A. Georges and G. Kotliar, Phys. Rev. B 45, 6479 (1992).
- [3] A. Georges, G. Kotliar, and Q. Si, Int. J. Mod. Phys. B 6, 705 (1992).
- [4] A. M. Sengupta and A. Georges, Phys. Rev. B **52**, 10295 (1995).
- [5] U. Brandt and C. Mielsch, Z. Phys. **75**, 365 (1989).
- [6] U. Brandt and C. Mielsch, Z. Phys. **79**, 295 (1990).
- [7] U. Brandt and C. Mielsch, Z. Phys. 82, 37 (1991).
- [8] J. K. Freericks, M. Jarrell, and D. J. Scalapino, Phys. Rev. B 48, 6302 (1993).
- [9] J. K. Freericks, M. Jarrell, and D. J. Scalapino, Europhys. Lett. 25, 37 (1994).
- [10] H. Kajueter, *Ph.D. thesis* (PUBLISHER, Rutgers University, 1996), available at URL http://www.physics.rutgers.edu/~kotliar/thesis/kajueter.ps.gz.
- [11] Q. Si and J. L. Smith, Phys. Rev. Lett. 77, 3391 (1996), Phys. Rev. B, 61, 5184 (2000).
- [12] M. H. Hettler et al., Phys. Rev. B 58, 7475 (1998).
- [13] G. Kotliar, S. Y. Savrasov, G. Palsson, and G. Biroli, Phys. Rev. Lett. 87, 186401 (2001).
- [14] G. Biroli and G. Kotliar, Phys. Rev. B 65, 155112 (2002).
- [15] K. Aryanpour, T. A. Maier, and M. Jarrell, http://xxx.lanl.gov/abs/cond-mat/0301460 (unpublished).
- [16] G. Biroli, O. Parcollet, and G. Kotliar, http://xxx.lanl.gov/abs/cond-mat/0307587 (unpublished).
- [17] T. Maier, M. Jarrell, T. Pruschke, and J. Keller, Phys. Rev. Lett. 85, 1524 (2000).
- [18] O. Parcollet, G. Biroli, and G. Kotliar, http://xxx.lanl.gov/abs/cond-mat/0308577 (unpublished).

- [19] S. Savrasov, G. Kotliar, and E. Abrahams, Nature 410, 793 (2001).
- [20] S. Biermann, F. Aryasetiawan, and A. Georges, Phys. Rev. Lett. 90, 086402 (2003).
- [21] A. M. Finkelshtein, Sov. Phys. JETP **57**, 97 (1983).
- [22] V. Dobrosavljevic and G. Kotliar, Phys. Rev. B 50, 1430 (1994).
- [23] J. J. Verbaarschot and M. R. Zirnbauer, J. Phys. A: Math. Gen. 17, 1093 (1985).
- [24] K. B. Efetov, Adv. Phys. **32**, 53 (1983).
- [25] A. Mirlin and Y. Fyodorov, Nucl. Phys. B **366**, 507 (1991).
- [26] V. Dobrosavljevic and G. Kotliar, Phys. Rev. Lett. 78, 3943 (1997).
- [27] V. Dobrosavljevic, A. A. Pastor, and B. K. Nikolic, Europhys. Lett. **62**, 76 (2003).
- [28] Y. Motome and G. Kotliar, Phys. Rev. B bf 62, 12800 (2000).
- [29] R. Chitra and G. Kotliar, Phys. Rev. B 63, 115110 (2001).
- [30] A. Georges, G. Kotliar, W. Krauth, and M. J. Rozenberg, Rev. Mod. Phys. 68, 13 (1996), and references therein.
- [31] Q. Si, S. Rabello, K. Ingersent, and L. Smith, Nature 413, 804 (2001).
- [32] R. Chitra and G. Kotliar, Phys. Rev. Lett. 84, 3678 (2000).
- [33] A. Georges, R. Siddharthan, and S. Florens, http://xxx.lanl.gov/abs/cond-mat/0106517 (unpublished).
- [34] H. Attias, and Y. Alhassid, Nucl. Phys. A625 565 (1997).
- [35] J. K. Freericks, M. Jarrell, and D. J. Scalapino, Phys. Rev. B 48, 6302 (1993).
- [36] A. J. Millis, R. Mueller, and B. I. Shraiman, Phys. Rev. B 54, 5389 (1996).
- [37] C. Bloch and J. Langer, J. Math. Phys. 6, 554 (1965).
- [38] T. Holstein, Ann. Phys. 8, 325 (1959).
- [39] J. Hubbard, Proc. R. Soc. London A 281, 401 (1964).
- [40] M. J. Rozenberg, X. Y. Zhang, and G. Kotliar, Phys. Rev. Lett. 69, 1236 (1992).
- [41] G. Baym and P. R. L. P. Kadanoff, Phys. Rev. **124**, 287 (1961).

- [42] E. Muller-Hartmann, Int. J. Mod. Phys. B 3, 2169 (1989).
- [43] V. Janis, Phys. Rev. B **64**, 115115 (2001).
- [44] C. D. Dominicis and P. C. Martin, J. Math. Phys. 5, 31 (1964).
- [45] S. Sachdev and N. Read, Int. J. Mod. Phys. 5, 219 (1991).
- [46] P. W. Anderson, Phys. Rev. **109**, 1492 (1958).
- [47] A. Mirlin and Y. Fyodorov, J. de Physique I 4, 655 (1994).
- [48] K. B. Efetov and O. Viehweger, Phys. Rev. B 45, 11546 (1992).
- [49] R. Abou-Chacra, P. W. Anderson, and D. J. Thouless, J. Phys. C 6, 1734 (1973).
- [50] I. A. Gruzberg and A. D. Mirlin, J. Phys. A: Math. Gen. 29, 5333 (1996).
- [51] S. Lichtenstein, M. Katsnelson, and G. Kotliar, Phys. Rev. Lett. 87, 067205 (2001).
- [52] P. Sun and G. Kotliar, Phys. Rev. Lett. **91**, 037209 (2003).
- [53] A. Lande and R. A. Smith, Phys. Rev. A 45, 913 (1992).
- [54] R. A. Smith, Phys. Rev. A 46, 4586 (1992).

# Vita

# Sergey Pankov

1992-98	Moscow Institute of Physics and Technology, M. S. in Physics.
1996-03	Graduate study, Dept. of Physics, Rutgers University
2002	Semiclassical Analysis of Extended Dynamical Mean Field Equations, Sergey Pankov, Gabriel Kotliar and Yukitoshi Motome. Phys. Rev. B <b>66</b> , 045117 (2002); preprint cond-mat/0112083
2003	Structural Transition of Wigner Crystal on Liquid Substrate, Masudul Haque, Indranil Paul and Sergey Pankov. Phys. Rev. B 68, 045427 (2003); preprint cond-mat/0211648
2003	Non-Fermi liquid behavior from two-dimensional antiferromagnetic fluctuations: a renormalization-group and large-N analysis, Sergey Pankov, Serge Florens, Antoine Georges, Gabriel Kotliar and Subir Sachdev. Accepted for publication in Phys. Rev. B; cond-mat/0304415
2003	Ph.D. in Physics, Rutgers University. Thesis written under the supervision of Professor Gabriel Kotliar.